Title

Modeling Lithospheric Delamination on Venus

Author

Adams, Andrea

Publication Date

2023

Peer reviewed|Thesis/dissertation

UNIVERSITY OF CALIFORNIA SAN DIEGO

Modeling Lithospheric Delamination on Venus

A dissertation submitted in partial satisfaction of the
requirements for the degree Doctor of Philosophy

in

Earth Sciences

by

Andrea C. Adams

Committee in charge:

David Stegman, Chair
James Day
Quinn Konopacky
David May
David Sandwell
Suzanne Smrekar

2023

The Dissertation of Andrea C. Adams is approved, and it is acceptable in quality and form for publication on microfilm and electronically.

University of California San Diego

2023

DEDICATION

For Colby

TABLE OF CONTENTS

LIST OF FIGURES

LIST OF TABLES

ACKNOWLEDGEMENTS

I would first like to acknowledge my advisor, Dave Stegman, who has never failed to support me as a person first and then as a scientist, even when none of my models worked. I've loved my time at Scripps, and our weekly meetings, corn dog lunches, and skeletor references were a big part of it. I'd do it all over again if I could. I would also like to thank all of the members of my committee. Thank you, Sue, for our invaluable discussions about Venus. Thank you to Dave May for making me feel like my technical issues were solve-able, and to David Sandwell for including me in tea time and not stealing all of Colby's toys.

My time at Scripps would not have been nearly as enjoyable without the friendship of our entire 2017 cohort - Hugh, Roz, Margaret, Dorian, Zeyu, and Nic. I am especially grateful for Hugh, founding member of the Jazz Legends: Legends of Jazz, for being my office mate for 6 years. I would also like to acknowledge the entire SIO Marine EM lab for giving me so many opportunities to go to sea. Jake - thank you for teaching me how to drive a forklift and knowing how hard it is for me to say no to field work. Lastly, thank you to my parents and to Michael and Colby for your unwavering support. Grad school was a joint effort with Colby, the self-appointed guardian of Revelle 1000, who put in his hours every day, attended every meeting, and did most of the work.

Portions of this dissertation are published or expected to be published in peer-reviewed journals.

Chapter 2, in full, is a reprint of the material as it appears in Journal of Geophysical Research: Planets: Adams, A. C., Stegman, D. R., Smrekar, S. E., Tackley, P. J. (2022). Regional-scale lithospheric recycling on Venus via peel-back delamination. Journal of Geophysical Research: Planets, 127, e2022JE007460. https://doi.org/10.1029/2022JE007460. The dissertation author was the primary investigator and author of this paper.

Chapter 3, in full, is a reprint of the material as it appears in Journal of Geophysical Research: Planets: Adams, A. C., Stegman, D. R., Mohammadzadeh, H., Smrekar, S.

E., Tackley, P. J. (2023). Plume-induced delamination initiated at rift zones on Venus. Journal of Geophysical Research: Planets, 128, e2023JE007879. https://doi.org/10.1029/2023JE007879. The dissertation author was the primary investigator and author of this paper.

Chapter 4, in part is currently being prepared for submission for publication of the material as: Adams, A. C., Stegman, D. R., Smrekar, S. E., Tackley, P. J. Modeling Peel-Back Delamination on Venus in Three Dimensions. The dissertation author is the primary investigator and author of this material.

VITA

2015 B.S. Mechanical Engineering, The Ohio State University

2017 M.S. Experimental Geosciences, Universität Bayreuth, Germany

2023 Ph.D. Earth Sciences, University of California San Diego

PUBLICATIONS

Adams, A. C., Stegman, D. R., Smrekar, S. E., Tackley, P. J. (2022). Regional-scale lithospheric recycling on Venus via peel-back delamination. Journal of Geophysical Research: Planets, 127, e2022JE007460. https://doi.org/10.1029/2022JE007460

Adams, A. C., Stegman, D. R., Mohammadzadeh, H., Smrekar, S. E., Tackley, P. J. (2023). Plume-induced delamination initiated at rift zones on Venus. Journal of Geophysical Research: Planets, 128, e2023JE007879. http://doi.org/10.1029/2023JE007879

Adams, A. C., Stegman, D. R., Smrekar, S. E., Tackley, P. J. Modeling Peel-Back Delamination on Venus in Three Dimensions, *in prep.*

ABSTRACT OF THE DISSERTATION

Modeling Lithospheric Delamination on Venus

by

Andrea C. Adams

Doctor of Philosophy in Earth Sciences

University of California San Diego, 2023

David Stegman, Chair

Thousands of kilometers of possible subduction sites have been identified on Venus near certain quasi-circular surface features called corona and near branches of rift zone trenches called chasmata. Subduction on Earth is driven by negative plate buoyancy with respect to the underlying mantle, however lithosphere on Venus may be significantly more buoyant than on Earth. On Earth, only 6-7 km of positively buoyant crust compete with the negative thermal buoyancy of the lithospheric mantle, but on Venus the enhanced positive buoyancy from 30 km of globally-averaged crust would significantly inhibit subduction initiation. Plume-lithosphere interactions have been proposed as a mechanism for subduction initiation, but the relatively high bending moments and elastic thicknesses

near subduction sites indicate the lithosphere is thick and may not be easily penetrated by thermal upwellings. The following chapters present a series of 2D and 3D numerical models using the code, StagYY, to investigate the dynamics of regional-scale lithospheric recycling initiated at chasmata trenches on Venus with realistic crustal densities. Rather than subduction, a tectonic regime called "peel-back delamination" (PBD) was observed in which the lithospheric mantle decouples and peels away from the overlying positively buoyant crust. Though net-negative lithospheric buoyancy is not a requirement for delamination, PBD is driven by the negative thermal buoyancy of the lithospheric mantle and resisted by the positive compositional buoyancy of the crust and the strength of the lithosphere. Aided by the pre-existing lithospheric weakness at chasmata, plume-rift interactions may accelerate timescales of delamination initiation. A thermal upwelling is shown to destabilize even thinner, more positively buoyant rift-adjacent lithosphere than in models without plume-rift interactions. Plume-induced PBD may require a minimum lithospheric thickness of approximately 150-200 km, and therefore may be most applicable to the inferred thick lithosphere near the Dali-Diana chasmata system. 3D delamination models show a radial retrograde migration of a trench and flexural bulge, compatible with the style of surface deformation observed at Artemis Corona in the Dali-Diana chasmata region of Venus.

Chapter 1

Introduction

From a distance, there is no planet more similar to Earth than Venus. Located approximately 56 million kilometers closer to the sun, Venus is Earth's closest planetary neighbor in our solar system. Venus and Earth formed concurrently approximately 4.5 billion years ago. They are relatively similar in size - Venus has an average radius of 6052 km and Earth has a somewhat larger radius of 6371 km. Similarities in size and density indicate that like Earth, Venus is comprised of a thin layer of crust at the surface, a deep mantle, and an iron-rich core.

Given their similarities in formation, it would be reasonable to think that Venus and Earth would follow a similar path of evolution. Yet, at their surface it seems their histories could not be more different. Venus is enveloped in a dense CO_2-rich atmosphere with surface pressures approximately 90 times greater than on Earth. While it is believed that there may have once been liquid water at the surface, a runaway greenhouse effect likely evaporated all surface H_2O. Combined with high surface temperatures of nearly 500 degrees Celsius, Venus is extremely uninhabitable for human life. The question of why the evolutions of Venus and Earth, despite their initial similarities, have diverged with such striking differences has mystified scientists for decades.

In the early 1990s, NASA's Magellan mission massively propelled our understanding of Venus forward through its acquisition of global gravity, radar topography, and synthetic

aperture radar (SAR). Previously, all radar images of the surface were low resolution or regionally-focused. Magellan mapped nearly 98% of the surface with approximately 100 m resolution, revealing a complex and highly deformed surface [1]. The radar images showed vast volcanic plains punctuated by dynamically-supported volcanic rises, ancient crustal plateaus, mountain ranges, wrinkle ridges, and nearly 1000 impact craters. Approximately 500 nearly-circular features called corona cover the surface of Venus with most diameters ranging from 60-1100 km, several of which are thought to be the signature of plume-lithosphere interactions [2, 3]. The largest is Artemis Corona with a diameter of 2600 km, though it's tectonic or volcanic origins are still not fully understood. Additional volcanic features include large shield volcanoes and flattened "pancake domes". An extensive system of rift zones cover the surface, many of which contain networks of deep, branching trenches called chasmata.

Although there are clear indicators of surface deformation and tectonic activity, a major finding of Magellan was that Venus does not have Earth-like plate tectonics [1]. On Earth, the lithosphere is divided into a number of different plates moving across the surface relative to each other. Plate tectonics are an important regulator of convective heat loss on Earth - heat is lost when new plates are formed at mid-ocean ridges, and cold, negatively buoyant lithosphere is continuously recycled into the mantle at subduction zones. Continuous lithospheric recycling at large networks of subduction zones appears to be unique to Earth, perhaps being facilitated by the presence of water and sediments on the downgoing plate. It is possible that planets such as Venus with no surface water or sediments may be unable to undergo the same style of lithospheric recycling.

The acceptance of plate tectonics theory in the 1960s revolutionized the way we understand Earth's interior convective motion and how it is directly linked to plate motion at the surface. Currently no such framework exists for Venus. However, the theory of plate tectonics is merely a kinematic description of the plate motion at the surface alone, incapable of providing a dynamical description of the underlying mantle convection;

however, the governing equations of mantle dynamics may be used to predict surface motions that can be compared to observed plate kinematics. In order to better understand the observed surface features of Venus, we must first understand the coupling between Venus' surface and interior.

1.1 Lithospheric Stability on Venus

The lithosphere of any terrestrial planet refers to the rigid outermost layer consisting of crust and the uppermost mantle. Although different definitions of lithosphere exist (mechanical, thermal, elastic), the following chapters refer to the thermal lithosphere which is the uppermost thermal boundary layer of mantle convection where heat from the warmer interior is transported to the atmosphere via conduction. The base of the thermal boundary layer is typically defined by $T_s + 0.9(T_m - T_s)$, where T_s is the surface temperature and T_m is the characteristic mantle temperature. By this definition, the thermal lithosphere typically includes a cold upper portion which experiences brittle deformation and a warm lower portion which undergoes ductile deformation. Generally, the crust is contained within the uppermost rigid portion of the thermal lithosphere, and the lithospheric mantle overlying the asthenosphere contains both brittle and ductile components. If we assume a homogeneous mantle composition, the major differences between the lithospheric and asthenospheric mantle stem from the lithospheric mantle having a colder temperature.

The stability of the lithosphere is directly related to its viscosity. Viscosity is strongly temperature-dependent as described by the Arrhenius equation (equation 2.1), and a relatively cool lithosphere is expected to be several orders of magnitude stronger than the underlying asthenosphere. Yet owing to Venus' high surface temperature and possibly higher mantle temperature [4, 5, 6], lithosphere on Venus is expected to be warmer and therefore lower viscosity than on Earth. Lithospheric viscosity is also dependent on its stress state, where stresses that exceed its material yield strength are accompanied

by a reduction in viscosity. On Earth, the yield strength of the lithosphere increases linearly with depth according to its material cohesion and friction coefficient until reaching a maximum of 400-800 MPa near the brittle-ductile transition [7]. Experimental data using a dry diabase crust and olivine mantle composition thought to be representative of Venus [8] with 6 K/km thermal gradient gives a similar maximum yield strength of nearly 600 MPa [9]. Despite being unable to measure the viscosity structure of Venus directly, it appears lithosphere in some areas is weak enough to bend but strong enough to sustain a flexural response to plate bending similar to Earth. Lithosphere near certain coronae and rift zone chasmata exhibit plate bending moments and elastic thicknesses comparable to retrograde subduction zones on Earth, in which the trench migrates away from the overriding plate as the sinking slab rolls back [2, 3, 10].

On Earth, lithospheric instability is primarily driven by the negative buoyancy of the cold lithosphere with respect to the underlying mantle. Net lithospheric buoyancy is effectively a competition between the negative thermal buoyancy of the lithospheric mantle and the positive compositional buoyancy of the crust; due to thermal diffusion, as oceanic lithospheric mantle cools and thickens, it becomes increasingly negatively buoyant until it eventually outweighs the positive buoyancy of the 6-7 km of oceanic crust and can subduct. Subduction on Venus, however, is inhibited by a globally-thick crust (approx. 25-30 km) which adds significant positive buoyancy to the plate [11, 12]. The paradox of lithospheric recycling on Venus is that negative plate buoyancy requires even thicker lithosphere than on Earth, but due to the strong temperature dependence of viscosity, the plates become stiffer and less conducive to forming instabilities.

If Venus has no obvious system of plate boundaries, how do lithospheric instabilities form? Subduction initiation on Earth is highly contentious, with theories including passive margin collapse [13], continent spreading [14], polarity reversal at faults [15], and plume-lithosphere interactions [16, 17]. The plume-induced retrograde subduction model has also been applied to Venus as a way to explain lithospheric flexure near coronae and

chasmata. This conceptual model describes a mantle plume fracturing the lithosphere from below, rising to the surface, and pushing the plate edges downward until buoyant crust reaches P-T conditions of its higher density phase, eclogite [2, 18]. On one hand, eclogite formation associated with surface loading may solve the issue of positively buoyant plates; yet, it is unclear how the plume could penetrate strong, thick lithosphere representative of the proposed rollback subduction sites on Venus. The stability of the lithosphere in the presence of a pre-existing rift has not previously been systematically investigated, and would help understand the fate of non-uniformly thick lithosphere that includes a weak and positively buoyant crust. It is also unclear for which conditions this mechanism could operate on Venus and over what timescales.

1.2 Geodynamic Modeling in StagYY

Geodynamics is the study of how internal forces within a planet continuously shape its surface. Computational methods, specifically numerical modeling, can be a powerful tool to study geodynamics across a diverse range of spatial and temporal scales. A numerical model can be designed to study nearly any geodynamic process, including continental collision, ice sheet dynamics, crust formation at mid-ocean ridges, subduction, strain localization in seismogenic zones, planetary accretion, and many others. Numerical models may compliment other more data-driven methods to provide a holistic approach to understanding a complex system. They may be designed to reflect specific locations on Earth or other planets, or they may be more general to better understand a certain concept. Models can be made to be as simple or as complex as necessary to target a specific process.

One example of a useful numerical modeling code that can be adapted for various planetary convection problems is StagYY [19]. Like most numerical modeling approaches, StagYY involves discretization of large systems of equations designed to represent certain

physical processes. Written in Fortran 90, it uses a finite difference/finite volume technique to solve the equations of highly viscous flow on a staggered grid.

$$\nabla \cdot v = 0 \tag{1.1}$$

$$\nabla \cdot \sigma + \rho g = 0 \tag{1.2}$$

$$\rho C_p(\frac{\partial T}{\partial t} + v \cdot \nabla T) - \nabla \cdot (k \nabla T) = \rho H + S \tag{1.3}$$

Where v is the velocity vector, σ is the stress tensor, ρ is density, g is gravitational acceleration, C_p is heat capacity, T is temperature, k is thermal conductivity, H is a volumetric heat production term, and the term S corresponds to viscous dissipation, adiabatic heating, and latent heat associated with phase transitions. Equations 1.1-1.3 represent the conservation of mass, momentum, and energy equations, respectively. Over short timescales with minimal expected thermal diffusion, the energy equation can be neglected and only the Stokes conservation equations (1.1-1.2) are required to describe viscous flow. These partial differential equations solve for velocity, pressure, stress, and their derivatives with respect to space and time at various points on the grid cell (Fig. 1.2). A model domain is a mesh consisting of a specific layout of grid cells, where increasing the number of grid cells increases the model resolution.

Several grid geometries are possible in StagYY, including a 2D or 3D cartesian box, 2D spherical annulus, 3D spherical grid, and 3D Yin Yang grid. Choices for model geometry and boundary conditions have the potential to affect results. For example, a cartesian box model that is too shallow or not sufficiently wide may alter mantle flow dynamics and lead to unrealistic surface effects. Alternatively, a full or partial spherical annulus from surface to core may be the most realistic geometry that can be used in

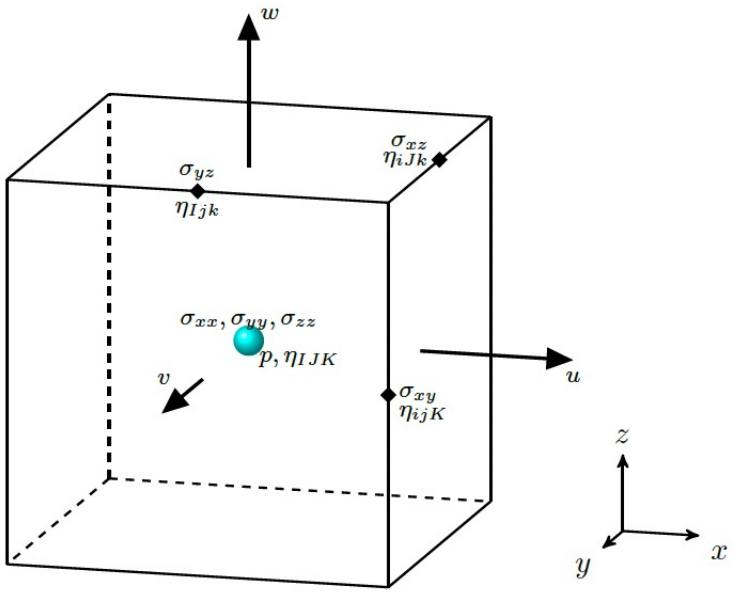

Figure 1.1. A three dimensional staggered grid cell indicating where pressure, velocity, and viscosity are solved. Pressure and temperature are defined at the cell centers, and the three components of velocity are defined at the center of the cell wall perpendicular to each respective direction. Image taken from the StagYY user manual.

2D, provided the sidewall boundaries are sufficiently far from the area of interest. A no-slip sidewall boundary condition would typically not be used for Earth models due to the nature of plate tectonics and individual plate motions, but may be applicable for an effectively single-plate planet such as Venus. In both Earth and Venus models, it is important to use either a free surface or a pseudo-free surface layer as an upper boundary condition to allow realistic development of topography [20].

Material properties can be tracked using tracer particles that carry information about composition, temperature, and composition-dependent viscosity and yield parameters. Each grid cell contains a minimum number of particles which are advected through space and time unconfined to their original grid cell. A 2nd or 4th order Runge Kutta scheme utilizes the velocity field to advect tracers through space. The tracer method allows the user to construct a model setup of various compositional layers with defaults including basalt and harzburgite. Tracer particles with properties of air allow the use of a

pseudo-free surface boundary condition referred to as "sticky-air". Another major benefit of using tracers is that phase changes can be implemented by creating new tracer types to represent new material compositions. In Chapters 2-4, a depth-dependent relative density approach is used to approximate phase changes in the crust and mantle. For example, when a crust tracer reaches the eclogite transition depth, it is converted to an eclogite tracer type with otherwise the same properties as basalt except for an increase in density, $B_{eclogite}$, with respect to the reference mantle density, ρ_0.

The equations can be solved using either a direct or iterative solver, though the iterative technique requires less memory and is generally more appropriate for 3D and larger 2D models. Beginning with an initial guess, iterations are performed until the error is sufficiently small for the solution to be acceptable. Multigrid methods may be used to accelerate convergence by performing V-cycles to switch from fine to coarse grids. Once solved on a coarse grid, the solution is effectively passed back to the fine grid. However, switching back to the fine grid may be problematic if the model contains large viscosity contrasts that are difficult to represent in the coarse grid; therefore it is important to restrict the viscosity range to $\sim$5-8 orders of magnitude.

These large systems of equations are best solved using high performance computing (HPC) techniques to access a higher number of processors. MPI-based parallelization works by splitting the full model domain into subdomains which can be computed synchronously. The number of nodes and tasks per node can be varied by the user to reduce wall time and achieve optimal code performance. All models discussed in Ch. 2-4 were calculated using resources at the San Diego Supercomputer Center (SDSC). Chapter 2 was performed using NSF-funded supercomputer, *Comet*, and the models of Chapters 3-4 were run using its successor, *Expanse*.

1.3 Assumptions and Uncertainties in Modeling Venus

Every model includes a number of assumptions due to our incomplete knowledge of planetary interiors, but for Venus, this is especially true. On Earth we have multiple types of geophysical, geochemical, and observational techniques to put constraints on parameters such as mantle potential temperature, lithospheric thickness, and water content in the mantle. However for Venus, the most relevant data to inform our model design comes from the few surface composition samples from Venera and Vega and Magellan's revolutionary, but still relatively low resolution gravity and topography compared to Earth. Until new missions are able to reach Venus, caution must be used when selecting parameters for model design. However, this also means that numerical models have an important place in studies of Venus due to their usefulness in systematic explorations of large parameter spaces. With numerical models, it is possible to study a range of potential parameters and their effects on the surface and mantle dynamics of Venus in a way that is not possible using traditional geophysical methods.

The work in the following chapters addresses the questions of whether regional-scale lithospheric recycling can be initiated at chasma rift zones on Venus, how this process may operate, and the conditions where it is most likely to occur. Already, a wide range of tectonic regimes have been modeled for Venus, including the widely popular global "catastrophic" overturn occurring on geologically-short timescales [21, 22, 23, 24, 25], a stagnant-lid [26, 27], a sluggish-lid [28, 29], plume-induced subduction [18], a heat-pipe [30], and a plutonic squishy-lid [31, 32]. Many of these models were run with different codes and were built with different assumptions, for example whether they implemented melting and volcanic processes, how they parameterized yielding, and whether viscosity was both temperature and pressure-dependent. Important questions to consider when designing a model are what are the most important aspects for modeling a specific process

on Venus? What features can be added or changed to expand our knowledge from previous studies? Which parameters can be neglected and how do they affect the model results?

Lithospheric recycling is inherently driven by gravitational instabilities; only something that is negatively buoyant with respect to the underlying mantle can sink. The models of Ch. 2-4 focus on the effects of positive buoyancy of crustal basalt on lithospheric recycling, which is typically neglected or underestimated in studies of Venus [21, 22, 23, 24, 25]. Many previous Venus models also use a low maximum yield stress to facilitate large-scale lithospheric recycling [21, 22, 23, 24]. However, the models presented here use a custom yield stress parameterization which may more accurately reflect the higher bending moments observed at potential subduction sites on Venus. Regional-scale plume-induced subduction has been previously modeled for Venus, but for a model setup with a spherical plume embedded in very thin lithosphere with significant melt weakening [18]. The models presented in Ch. 2-4 study thicker lithosphere which is characteristic of the observed lithospheric flexure at proposed subduction zones on Venus. Plume-lithosphere interactions are studied in Ch. 3-4, but the plume is initialized at mid-mantle depths to allow the development of plume flattening and a realistic lithospheric stress state due to uplift. The models avoid boundary condition interactions by utilizing a 180 degree spherical annulus and a "sticky-air" pseudo-free surface upper boundary [33]. Previous global catastrophic overturn models have used a free-slip upper boundary condition, which has been shown to significantly affect plate bending dynamics by restricting topography [20]. Lastly, the 2D models of Ch. 2-3 use a relatively high grid resolution (2048x512 in a half spherical annulus) compared to previous 2D global overturn models (512x64 in a full spherical annulus) in order to accurately calculate the stress state in the lithosphere which controls material yielding and plate bending.

Although the following models improve upon the existing Venus modeling studies in a number of ways, certain assumptions must be made in order to target specific processes. For example, melting features are excluded in order to prevent crust formation and keep

the crustal buoyancy variable constant for each model through time - this allows a clearer understanding of how crustal buoyancy and net plate buoyancy affect lithospheric recycling. However it is important to be aware that melting would have an effect on topography and crust production, so these aspects of the model results should be viewed with caution. It may also be appropriate to neglect heating across the core-mantle boundary, as this could produce numerous thermal upwellings that could interfere with the rift zone dynamics. Instead, there is an option to control the size, temperature, and position of a mantle upwelling by turning off bottom heating and prescribing the plume as part of the initial condition. Finally, the models use a yield strength parameterization which assumes the crust is relatively weak ($C_0 = 10$ MPa). There is currently no definitive consensus in the Venus community for whether the crust is relatively strong or weak, though a strong crust would likely affect the model results [8, 34, 35, 36]. Details are discussed further in section 2.4.4.

With these considerations in mind, 2D and 3D numerical models were built using StagYY to further investigate regional-scale lithospheric recycling on Venus. Chapter 2 uses 2D models to propose a new mechanism of buoyancy-driven lithospheric recycling for Venus called "peel-back delamination". In Chapter 3, a rising thermal upwelling is added to the model setup to determine the effect of plume-rift interactions on the development of lithospheric delamination. Chapters 2 and 3 systematically explore large parameter spaces using computationally inexpensive 2D models to identify the conditions where delamination is most likely to occur. Finally, Chapter 4 will use the results of the parameter studies in Chapters 2 and 3 to design a three dimensional model of peel-back delamination on Venus.

Chapter 2

Regional-Scale Lithospheric Recycling on Venus via Peel-Back Delamination

2.1 Introduction

We currently lack an understanding of the global tectonic and convective framework that has governed Venus throughout its evolution. On Earth, resurfacing occurs via plate tectonics, where new crust is formed at mid-ocean ridges and old lithosphere is continuously recycled at subduction zones. Despite being Earth's closest neighbor in the solar system and having similarities in size and composition, Venus shows no evidence of Earth-like plate tectonics [1, 37]. Since NASA's Magellan mission in the early 1990s, two key observations related to impact craters have guided our insight into how the surface of Venus may have evolved over time: approximately 975 total craters suggest a relatively young surface age (250-750 Myr) [38, 39, 40, 41] and the crater population has a near spatially random distribution [42, 43, 44]. In the decades since Magellan, these observations have divided ideas about Venus' surface evolution into two hypotheses: (1) the catastrophic/episodic resurfacing hypothesis and (2) the regional equilibrium resurfacing hypothesis.

The catastrophic resurfacing (CR) model describes a tectonic regime where the cooling and thickening of Venus' lithosphere is interrupted by at least one, but perhaps

multiple global-scale overturns over the last 4.5 billion years [41, 45, 46, 47]. These events are thought to occur over relatively short geologic timescales (<100 Myr) and are followed by a period of resurfacing [44, 48]. This theory rose in popularity because the post-overturn uniform surface age is a simple explanation for the spatially random crater distribution on Venus. The young surface age implies that the most recent overturn event happened in the last 250-750 Myr, and the CR hypothesis attributes the mostly unmodified crater population to low levels of tectonic or volcanic activity during the following quiescent period [40, 49]. Convection models from previous studies support the CR hypothesis by producing cyclic global overturn events under certain conditions [21, 22, 23, 24, 25, 26, 50].

Despite being compatible with first-order cratering constraints, the CR model is not unequivocally supported by all models and observations. The offset between the center of mass and center of figure (CM-CF) of Venus is a measurable quantity that can signal large-scale density anomalies in a planet's surface (topography) and interior (thermal anomalies). King (2018) analyzed the immediate and long-term effects of one or more global overturns on the calculated CM-CF offset in models of Venus. The calculated offsets were significantly larger than the the observed CM-CF offset, indicating the observed offset is incompatible with a global resurfacing event [51]. Furthermore, the CR hypothesis can be rejected because a uniform surface age contradicts observations that different stages of impact crater degradation are associated with different geological regions on Venus [52, 53, 54]. Combined with the association between crater density and geology, the three average model surface age (AMSA) provinces dividing the surface of Venus into relative ages (old, intermediate, and young) [55, 56], point toward a more complex resurfacing history.

The competing idea to explain Venus's unique style of resurfacing is the regional equilibrium resurfacing (RER) hypothesis. It suggests Venus' crater population is a balance between steady-state crater formation and the removal of craters by tectonic or volcanic processes occurring at different rates regionally [42, 57]. Although some early

statistical analyses could not reconcile the observed crater population with frequent, smaller resurfacing events [44, 58], more recent Monte Carlo experiments found that the uniform crater distribution and number of modified craters can be explained by regional equilibrium resurfacing [59, 60]. The RER model may also be compatible with both the observed CM-CF offset for Venus [51] as well as the association with crater population and geology [56]. The RER hypothesis is further supported by evidence of regional-scale volcanic activity from thermal emissivity anomalies observed at volcanoes [61] and chasma rift zones [62]. Surface emissivity data indicating a lack of chemical weathering at coronae and volcanoes over plume-associated topographic rises also signify geologically-recent volcanism on Venus [63].

In addition to volcanic processes, there is evidence that tectonic processes may also drive regional-scale resurfacing events. Sandwell and Schubert (1992) observed that trench-outer rise topography and lithospheric flexure across several of Venus' largest coronae are comparable to various arcuate subduction zones on Earth [2]. This is interpreted as evidence for retrograde subduction which may have initiated due to interactions between the lithosphere and a rising mantle plume. The viability of plume-induced subduction at Venusian coronae has since been studied in both numerical [18] and laboratory experiments [64] and is the favored model for regional-scale subduction on Venus - in part because the plume provides a mechanism to weaken and break the lithosphere. Melt weakening [18] and loading due to surface volcanism [2] may cause the lithosphere to break and its edges to sink and migrate radially outward. Plume-induced subduction may be ongoing at present, as evidenced by anomalously-high thermal emissivity at Quetzalpetlatl corona indicating geologically-recent volcanism [64].

Plume-lithosphere interactions are a mechanism to induce weakness in the lithosphere and facilitate subduction initiation, but subduction itself is primarily driven by the negative buoyancy of the plate. For Venus, subduction and lithospheric recycling may be complicated by the presence of positively-buoyant plates. Large regional variations (and

uncertainties) in crust and lithosphere thickness [11, 65] and potentially warmer mantle temperatures with higher degrees of melting and crust formation affect the net buoyancy of the lithosphere and its ability to subduct. In order to better understand the viability of regional-scale tectonic resurfacing, it is important to constrain a range of conditions for which lithospheric recycling may occur on Venus without the added complexities of plume-lithosphere interactions. In addition to coronae, thousands of kilometers of chasmata (Dali and Diana chasmata, Hecate Chasma, Parga Chasma, etc.), or rift zones, are proposed to be possible sites of subduction on Venus [2, 3]. Here, we present 2D numerical models of a simplified Venusian chasma rift zone over a range of crust and mantle conditions to identify if and how regional-scale lithospheric recycling can occur without assistance from mantle plume interactions.

2.2 Methods

2.1 Model Setup

We performed a series of numerical experiments using StagYY, a finite-volume code which models solid-state mantle convection by solving the conservation of mass, momentum, and energy equations on a staggered grid [19, 66]. We consider viscous flow of an infinite Prandtl number fluid and assume an incompressible mantle using the Boussinesq approximation. Composition is tracked using over 13.6 million (13694800) tracer particles in a 2048x512 resolution grid space. All visualization was performed using StagLab [67].

2.2 Initial Condition

A complete list of model parameters is given in Table 2.1. The model geometry is a two-dimensional 180° spherical annulus [33]. The initial condition consists of a lithosphere with a single discontinuity where a 250 km-wide gap separates two edges of the lithospheric mantle (Fig. 2.1). The gap is filled with relatively warm asthenospheric material. The gap is a simplified representation of a rift zone or an area where a previous thermal upwelling

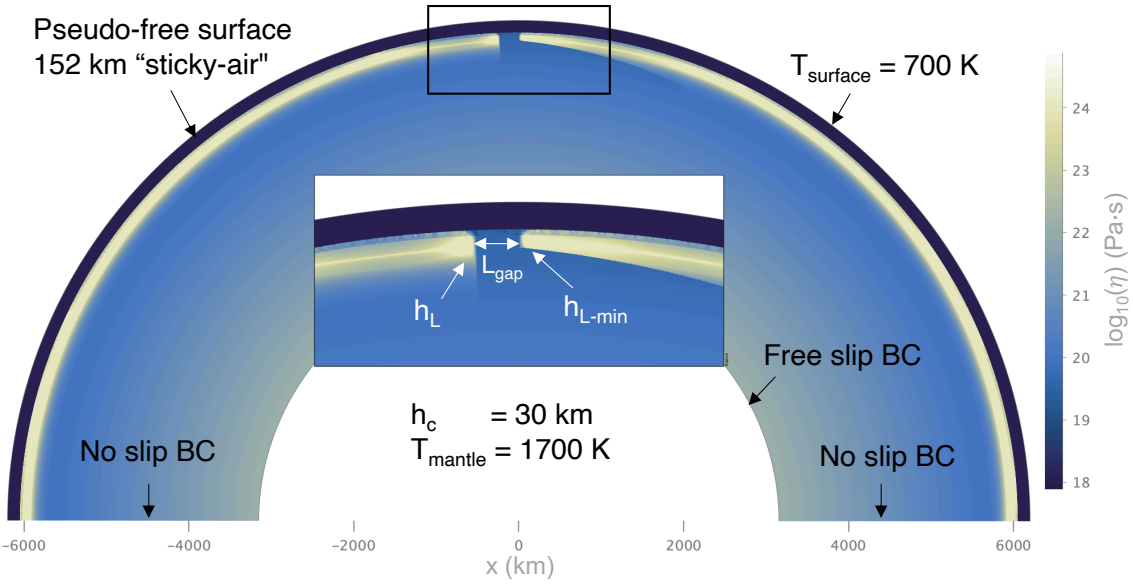

Figure 2.1. Viscosity field of initial model setup. A gap (L_{gap} = 250 km) separates two plate edges with thicknesses h_L = [200, 250, or 300] km (left) and h_{L-min} = 100 km (right). The lithosphere with thickness h_{L-min} gradually thickens to be thickness h_L. The gap represents a simplified rift zone or an area having undergone previous magmatic weakening. The model setup is designed to study buoyancy-driven lithospheric recycling events in the absence of an imposed velocity field or slab perturbation as to be more representative of Venus.

left behind an area of magmatically-weakened lithosphere. Rift widths are locally similar to the model gap between plates. For example, the 10,000 km-long fracture zone of Parga Chasma varies from 90-590 km; the trough is 60-230 km wide and 0.5-2 km deep [68]. A 30 km-thick layer of basaltic crust (h_c) covers the entire domain including the gap. The plate to the left of the gap is uniformly thick (h_L = [200, 250, 300] km) and covers an upper range of lithosphere thicknesses that may be present on Venus [65]. The plate to the right of the gap is thinned at its edge (constant h_{L-min} = 100 km) and gradually thickens to h_L. The asymmetry in lithospheric thickness across the gap may reflect cases of observed asymmetry across Venusian chasmata [3]. We use a mantle potential temperature of 1700 K [5, 69] and define lithosphere thickness by the 1600 K isotherm. There is no initial velocity-field perturbation or pre-existing plate bending to assist the initiation of plate motion.

2.3 Boundary Conditions

All models employ a pseudo-free-surface upper boundary condition with 152 km of "sticky-air" which allows for the development of realistic topography and is known to influence lithosphere dynamics [20]. The surface temperature is defined by a 700 K isothermal boundary. We use a free-slip lower boundary and no-slip sidewall boundary conditions. The no-slip sidewall boundaries simulate the resistance of the surface to slab pull during potential lithospheric recycling events, which may best represent an effectively single-plate planet such as Venus. The sidewall boundaries are sufficiently far from the gap so there is no interference with local mantle flow.

2.4 Viscosity

Diffusion creep and plastic failure are assumed to be the only deformation mechanisms. Temperature and pressure-dependent viscosity is defined by the Arrhenius law used in StagYY [19]:

$$\eta(T,p) = \eta_0 \cdot exp\left[\frac{E_a + (1-z)V_a}{T} - \frac{E_a}{T_0}\right] \tag{2.1}$$

where E_a and V_a are the activation energy and volume, respectively, and the reference viscosity, η_0, is 10^{20} Pa·s at zero pressure and 1600 K. An activation energy of 240 kJ/mol was chosen corresponding to a wet olivine rheology. We use an activation volume of 10^{-7} m^3/mol to approximate a pressure- and temperature-dependent viscosity increase of three orders of magnitude over the depth of the mantle. Viscosity variations in the mantle were restricted to six orders of magnitude with a maximum viscosity of 10^{25} Pa·s and a minimum viscosity of 10^{19} Pa·s. The viscosity of the sticky-air was 10^{18} Pa·s. The maximum viscosity of the lithosphere was controlled separately and varied between three values spanning two orders of magnitude, $\eta_{max} = [10^{23}, 10^{24}, 10^{25}]$ Pa·s (Appendix A: Fig. 6.1).

2.5 Yield Strength

Plasticity is implemented using the Drucker-Prager criterion based on Byerlee's law to calculate the pressure-dependent brittle yield stress

$$\tau_{y,brittle} = C + p\mu \tag{2.2}$$

with cohesion, C, confining pressure, p, and friction coefficient, μ. The models described here all use a surface cohesion of 10 MPa and a friction coefficient of 0.25. The effective yield stress τ_y is then calculated as the minimum between $\tau_{y,brittle}$ and a constant maximum yield stress

$$\tau_y = min[\tau_{y,brittle}, \tau_{max}] \tag{2.3}$$

which effectively limits the yield stress to a maximum value of τ_{max} at higher pressure and depth. When stress levels exceed the yield stress, the material strength is reduced by converting the viscosity into an effective viscosity

$$\eta = \frac{\tau_y}{2\dot{\epsilon}_\Pi} \tag{2.4}$$

For the conditions where $\tau_y >= \tau_\Pi$ where τ_Π is the second invariant of the stress tensor and $\dot{\epsilon}_\Pi$ is the second invariant of the strain rate tensor. When the yield stress is exceeded, stresses in the lithosphere are redistributed to accommodate the decrease in material strength. While previous models of global overturns on Venus use maximum yield stresses (τ_{max}) near 100 MPa [21], we chose to employ a maximum yield stress of 500 MPa. This will give a yield stress (τ_y) with depth that is stronger throughout the depth of the lithosphere (Fig. 2.2). The crust on Venus is suspected to be relatively weak and decoupled from the underlying mantle [70, 34, 71, 72] and in our models is represented by a material with uniform strength (cohesion of 10 MPa and friction coefficient approximately zero) which readily yields to tectonic forces [22].

2.6 Phase Transitions

Tracer particles are used to track compositions within the olivine and basalt/garnet systems. Compositional phase transitions were implemented as depth-dependent density contrasts within the two systems relative to the reference density (ρ_0 = 3300 kg/m^3). Several Earth-like phase changes were included with depths adjusted to Venus's lower gravity (Fig. 2.3) [73].

At cooler temperatures inside the subducting slab, the postspinel phase boundary in the olivine system is deflected to deeper depths. Estimates of the value of the postspinel Clapyeron slope, γ_{psp}, range from -0.2 to -3.0 MPa/K [74, 75, 76, 77], where more recent estimates fall closer to zero [78] (see references therein). It is also reported that the effect of the negative Clapyeron slope is stronger in 2D models than in 3D [73]. A larger Clapyeron slope will deflect the phase boundary to deeper depths and result in a larger region of positive buoyancy within the slab; conversely, a smaller Clapeyron slope may only weakly deflect the postspinel phase boundary. Our models use a value of γ_{psp} = -1.0 MPa/K in

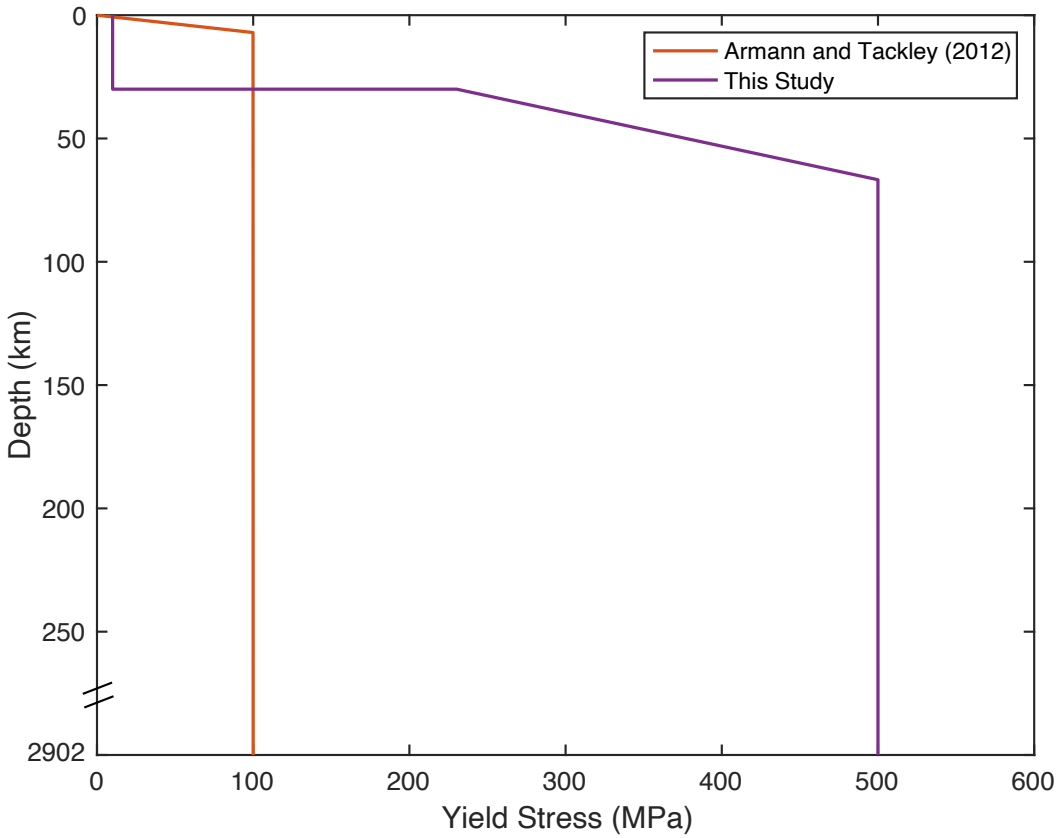

Figure 2.2. Depth vs yield stress (τ_y) throughout the depth of the mantle. Armann and Tackley (2012) observed vigorous episodic lid overturns when the maximum yield stress (τ_{max}) was 100 MPa. Our models employ weak crust at the surface and a higher maximum yield stress of 500 MPa through the majority of the lithosphere.

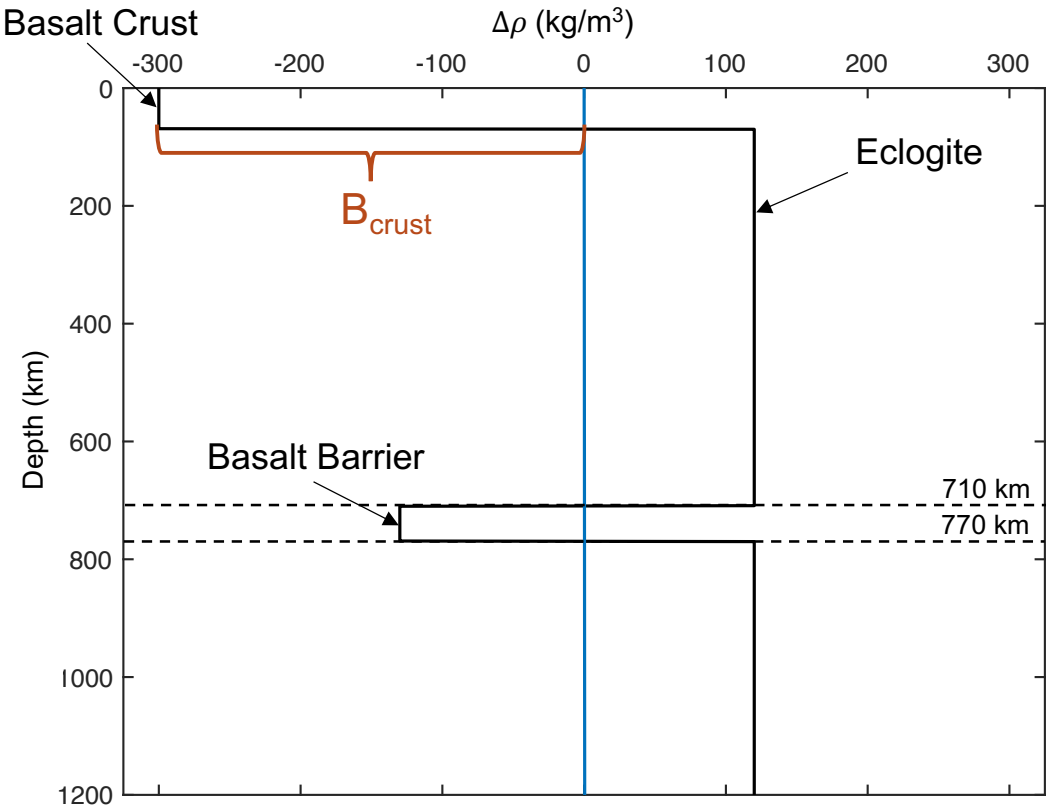

Figure 2.3. Relative compositional density contrast between basalt-garnet system and olivine system through the depth of the mantle. At the surface, basaltic crust is positively buoyant compared to the reference density (blue line) with $\Delta\rho_c = B_{crust}$ kg/m^3 (variable). Eclogite forms and becomes denser than the reference mantle ($\Delta\rho_{ec}$ = 120 kg/m^3) at 70 km depth. The "basalt barrier" results in a region of positive buoyancy ($\Delta\rho_{bb}$ = -130 kg/m^3) in the basalt-garnet system between 710 and 770 km depth. Adapted from Ogawa and Yanagisawa (2014).

order to understand, but not overstate its effect.

At 70 km depth, the positively buoyant crust ($\Delta\rho = B_{crust}$ kg/m^3) transforms into denser eclogite ($\Delta\rho_{ec}$ = 120 kg/m^3). Between 710 and 770 km, the garnet-bridgmanite transition occurs gradually, which results in a region of positive buoyancy ($\Delta\rho_{bb}$ = -130 kg/m^3) in the basalt/garnet system relative to bridgmanite. This is referred to as the garnet trap, or basalt barrier [79], and it coincides with the positively buoyant region within the slab that arises due to deflection of the postspinel boundary. Thus, there are two separate sources of positive buoyancy within the down-going plate beginning at 710 km depth, which combined have the potential to inhibit slab sinking. Below the garnet trap, the density contrast of the basalt-garnet system returns to $\Delta\rho$ = 120 kg/m^3.

2.7 Crust Density

The positive compositional buoyancy of the crust counteracts some of the negative buoyancy of the lithosphere, both of which determine the net buoyancy of the entire plate. In order to explore the effect of crustal buoyancy, we specified the compositional density contrast, B_{crust} = $\rho_{0,crust}$ - ρ_0, which was prescribed to all crust particles. An average crust thickness of 30 km [11] was held constant in order to isolate the effects of net crust buoyancy from the effects of variable crust thickness. We vary B_{crust} = [-175, -265, -300, -350, -400] kg/m^3 (Fig. 2.3). The lowest density contrast, B_{crust} = -175 kg/m^3, represents the compositional density contrast between olivine and pyroxene-garnet used by Armann and Tackley (2012) in models of global overturns; the highest density contrast, B_{crust} = -400 kg/m^3, represents the expected density contrast for an Earth-like basaltic crust with ρ_{crust}=2900 kg/m^3. Ogawa and Yanagisawa (2014) predict B_{crust} to be -300 kg/m^3 for crust and mantle compositions of $A_{0.1}B_{0.9}$ and $A_{0.64}B_{0.36}$, respectively, where A is harzburgite and B is garnet and pyroxene [73]. In addition to compositional density, we consider thermal effects on density. The crust covering the gap is warmer, and therefore less dense than the crust covering the plate. A minimum crust thickness of 15 km has been enforced over the entire domain to prevent entrapment of sticky-air particles due to

Table 2.1. Parameters common to all models

Parameter	Description	Value
R	Planetary radius	6052 km
R_{cmb}	Core radius	3150 km
nx	Horizontal cells	2048
nz	Vertical cells	512
g	Gravitational acceleration	8.9 ms^{-2}
ρ_0	Reference density	3300 kgm^{-3}
Cp	Heat capacity at constant pressure	1200.0 J K^{-1}
k	Thermal conductivity	3 $\mathrm{Wm}^{-1}\mathrm{K}^{-1}$
α	Coefficient of thermal expansion	$3 \times 10^{-5}\mathrm{K}^{-1}$
T_s	Surface temperature	700 K
T_m	Mantle potential temperature	1700 K
η_0	Reference viscosity at $T = 1600$ K	$1 \times 10^{20}\mathrm{Pa} \cdot \mathrm{s}$
E_a	Activation energy for wet olivine diffusion	240 kJ/mol
V_a	Activation volume	10^{-7} m^3/mol
η_{air}	Air layer viscosity	$1 \times 10^{18}\mathrm{Pa} \cdot \mathrm{s}$
h_{air}	Air layer thickness	152 km
h_c	Crustal thickness	30 km
C_{mantle}	Mantle cohesion	10 MPa
μ_{mantle}	Mantle coefficient of friction	0.25
$C_{weak\ crust}$	Weak crust cohesion	10 MPa
$\mu_{weak\ crust}$	Weak crust coefficient of friction	0.001
γ_{710}	Clapeyron slope of postspinel transition	-1.0 MPaK^{-1}

the low viscosity contrast between air and mantle material inside the gap.

2.3 Results

We investigated lithospheric recycling at a Venusian rift zone for a suite of 42 numerical models with variable crust density, lithosphere thickness, and maximum viscosity (see Table 2.2). Each model within the suite was identified as in either (I) a peel-back delamination regime or (II) a stagnant-lid regime. In this section, we discuss the characteristics of the two regimes and the factors affecting their development. Model 23 is referred to as the reference model due to having intermediate values of crustal buoyancy, plate thickness, and maximum viscosity (B_{crust} = -300 kg/m^3, h_L = 250 km, $\eta_{max} = 10^{24}$ Pa·s).

Table 2.2. Summary of model parameters and outcomes

Model	Crust Density (kg/m^3)	Lithosphere Thickness (km)	Max. Viscosity (Pa·s)	Outcome
1	-175	200	10^{23}	Delamination
2	-175	200	10^{24}	Delamination
3	-175	200	10^{25}	Delamination
4	-175	250	10^{23}	Delamination
5	-175	250	10^{24}	Delamination
6	-175	250	10^{25}	Delamination
7	-175	300	10^{23}	Delamination
8	-175	300	10^{24}	Delamination
9	-175	300	10^{25}	Delamination
10	-265	200	10^{23}	Stagnant-Lid
11	-265	200	10^{24}	Stagnant-Lid
12	-265	200	10^{25}	Stagnant-Lid
13	-265	250	10^{23}	Delamination
14	-265	250	10^{24}	Delamination
15	-265	250	10^{25}	Delamination
16	-265	300	10^{23}	Delamination
17	-265	300	10^{24}	Delamination
18	-265	300	10^{25}	Delamination
19	-300	200	10^{23}	Stagnant-Lid
20	-300	200	10^{24}	Stagnant-Lid
21	-300	200	10^{25}	Stagnant-Lid
22	-300	250	10^{23}	Delamination
23	-300	250	10^{24}	Delamination
24	-300	250	10^{25}	Delamination
25	-300	300	10^{23}	Delamination
26	-300	300	10^{24}	Delamination
27	-300	300	10^{25}	Delamination
28	-350	200	10^{23}	Stagnant-Lid
29	-350	200	10^{24}	Stagnant-Lid
30	-350	200	10^{25}	Stagnant-Lid
31	-350	250	10^{23}	Delamination
32	-350	250	10^{24}	Delamination
33	-350	250	10^{25}	Stagnant-Lid
34	-350	300	10^{23}	Delamination
35	-350	300	10^{24}	Delamination
36	-350	300	10^{25}	Delamination
37	-400	250	10^{23}	Stagnant-Lid
38	-400	250	10^{24}	Stagnant-Lid
39	-400	250	10^{25}	Stagnant-Lid
40	-400	300	10^{23}	Delamination
41	-400	300	10^{24}	Delamination
42	-400	300	10^{25}	Delamination

3.1 Tectonic Regimes

3.1.1 Regime I: Peel-Back Delamination

Peel-back delamination is a type of lithospheric recycling where the lithospheric mantle detaches and peels away from the lower crust along the Moho, similar to what is described in Bird (1979). It differs from rollback subduction because the majority of the basaltic crust remains at the surface as the denser lithospheric mantle is recycled. It also differs from the Rayleigh-Taylor lithospheric dripping style of delamination [80, 81, 82, 83] because the full depth of the lithospheric mantle is recycled coherently in each event. The following descriptions apply to all observed cases of peel-back delamination.

Delamination initiation is characterized by several distinct stages (Fig. 2.4). First, the relatively dense sub-crustal lithospheric mantle (SCLM) begins to bend, which induces yielding in the overlying weak crust. As the stress in the crust exceeds its yield strength, the viscosity of the crust is limited to the effective viscosity (Eqn. 4), forming a weak layer near the plate edge which facilitates decoupling of the crust and SCLM (Fig. 2.4A). As the SCLM continues to bend, buoyant asthenosphere from the gap is wedged between the surface and top of the SCLM. A small amount of buoyant crust (approximately 5 km thick) remains attached to the down-going SCLM, while the majority of crust remains at the surface or as part of a crustal root forming at the hinge of the delaminating plate (Fig. 2.4D). Once the thin layer of crust on the SCLM reaches the eclogite transition at 70 km depth, it becomes dense relative to the underlying mantle. Simultaneously, the weak zone of yielded crust propagates along the Moho accompanying trench retreat (Fig. 2.4E-F). As more SCLM progressively detaches from the crust, the crustal root at the trench thickens. When the base of the crustal root reaches 70 km depth, thicker layers of crust undergo the eclogite density inversion (Fig. 2.4H). The thick layers of eclogite add negative buoyancy to the delaminating plate that help sustain sinking. The thinner lithosphere to the right of the gap never undergoes delamination.

After delamination is initiated (Fig. 2.5A-B), the slab continues to sink until it

approaches the postspinel phase transition at 710 km depth (Fig. 2.5C). Due to the negative Clapeyron slope of the postspinel phase change, the cooler SCLM becomes positively buoyant relative to the surrounding mantle until it reaches sufficient pressure to undergo the phase transition. The tip of the delaminating slab is deflected in response to encountering both the postspinel density inversion and resistance from the radial viscosity increase with depth in the mantle (Fig. 2.5C). As the negatively buoyant eclogite layer reaches the basalt barrier between 710-770 km depth, it undergoes a separate density inversion making the basaltic material positively buoyant in relation to the surrounding mantle. As a result, slab sinking is inhibited by two distinct sources of positive buoyancy in the down-going plate beginning at 710 km depth (Fig. 2.6). As the radial viscosity increases with depth and the slab reaches both density inversions, the plate bends and the slab tip is deflected to shallower mantle depths (Fig. 2.5D). When the SCLM and crust material eventually sink past the density inversions due to the weight of the slab, they once again become dense relative to the surrounding mantle. Sinking of the bent plate continues until thinning and viscous necking at the slab hinge cause the plate to break off at the surface (Fig. 2.5E). All delamination models were run until slab break-off occurred (between 5.32 and 30.6 Myr).

3.1.2 Regime II: Stagnant-Lid

A total of thirteen models were categorized as stagnant-lid (see Table 2.2). A stagnant-lid regime is characterized by the absence of delamination or any other significant form of lithospheric recycling. The warm mantle inside the gap is cooled due to being surrounded by the colder surface and lithosphere. Over time, the plate edges are smoothed by the growth of the thermal boundary layer. Model runs were ended when the gap was cooled enough to effectively fuse the plate edges together across the gap. In some cases when the maximum viscosity was relatively low ($\eta_{max} = 10^{23}$ Pa·s), the lithospheric mantle that did not undergo recycling contracted and widened the gap. Ultimately, these plates were unable to bend and initiate crustal yielding on timescales that would weaken the

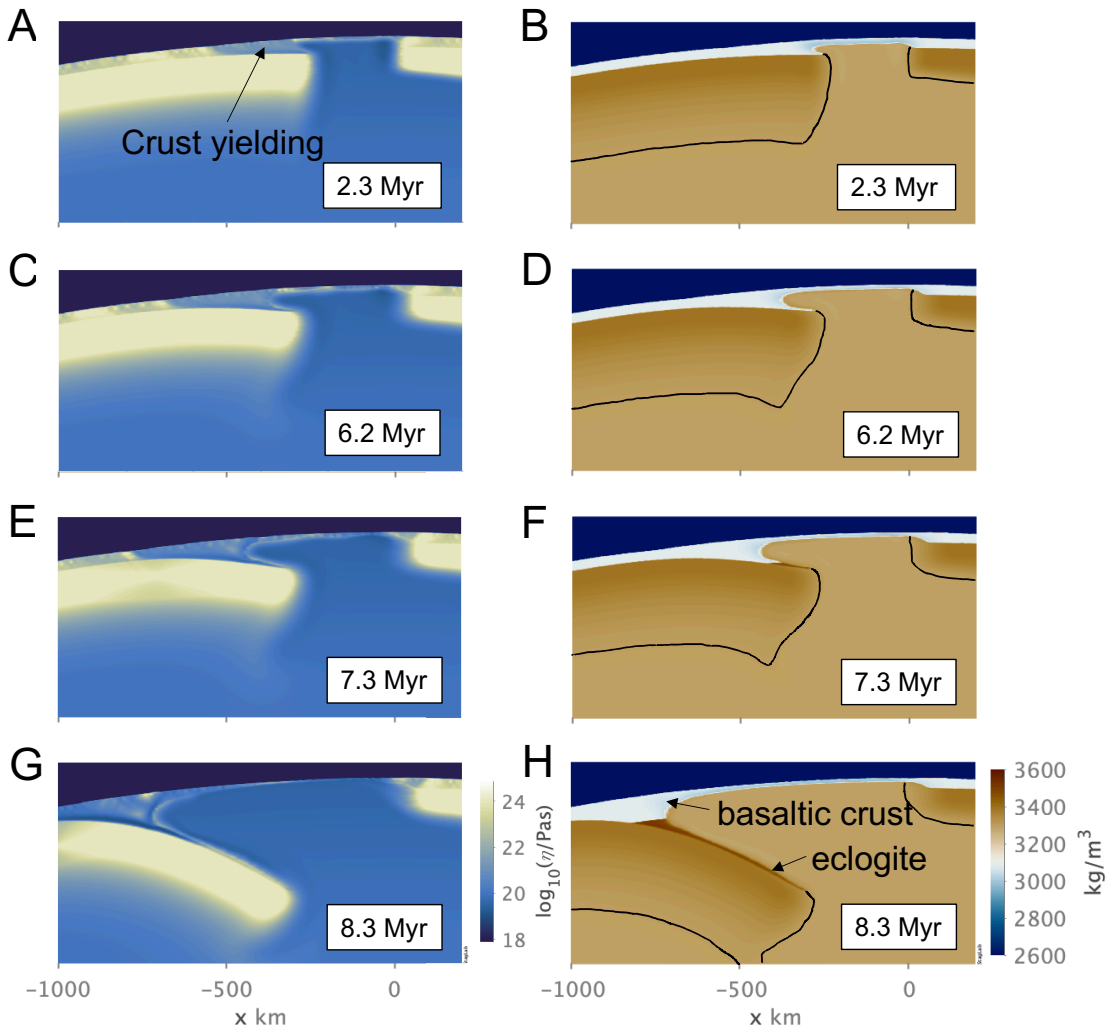

Figure 2.4. Progression of peel-back delamination initiation shown in the viscosity (left) and density (right) fields of reference model 23 (B_{crust} = -300 kg/m^3, h_L = 250 km, η_{max} = 10^{24} Pa·s). A black line is added to the density field to show the boundary of the lithospheric mantle and asthenosphere defined by the 1600 K isotherm. (A-B) Initial bending of the negatively buoyant lithospheric mantle causes weak crust over plate edge to yield and a small weak zone to form. Crustal yielding appears as a local reduction in viscosity. (C-D) The weak zone propagates as the crust is further yielded and buoyant asthenosphere spreads over the delaminating plate edge. Only a thin layer of crust (5 km) is attached to the delaminating plate. (E-F) Asthenospheric mantle material is wedged deeper into the space between the crust at the surface and the top of the delaminating plate. The crustal root over the delaminating plate hinge thickens and reaches the eclogite transition at 70 km depth, resulting in a density inversion which makes the crust more negatively buoyant than the underlying mantle. (G-H) The delaminating plate continues to detach and peel back from the overlying weak crust layer. Sinking is enhanced by the added negative buoyancy of the eclogitized crust. The thickness of crust attached to the delaminating plate increases as the crustal root deepens and more eclogite is formed. Dark blue layer = sticky-air.

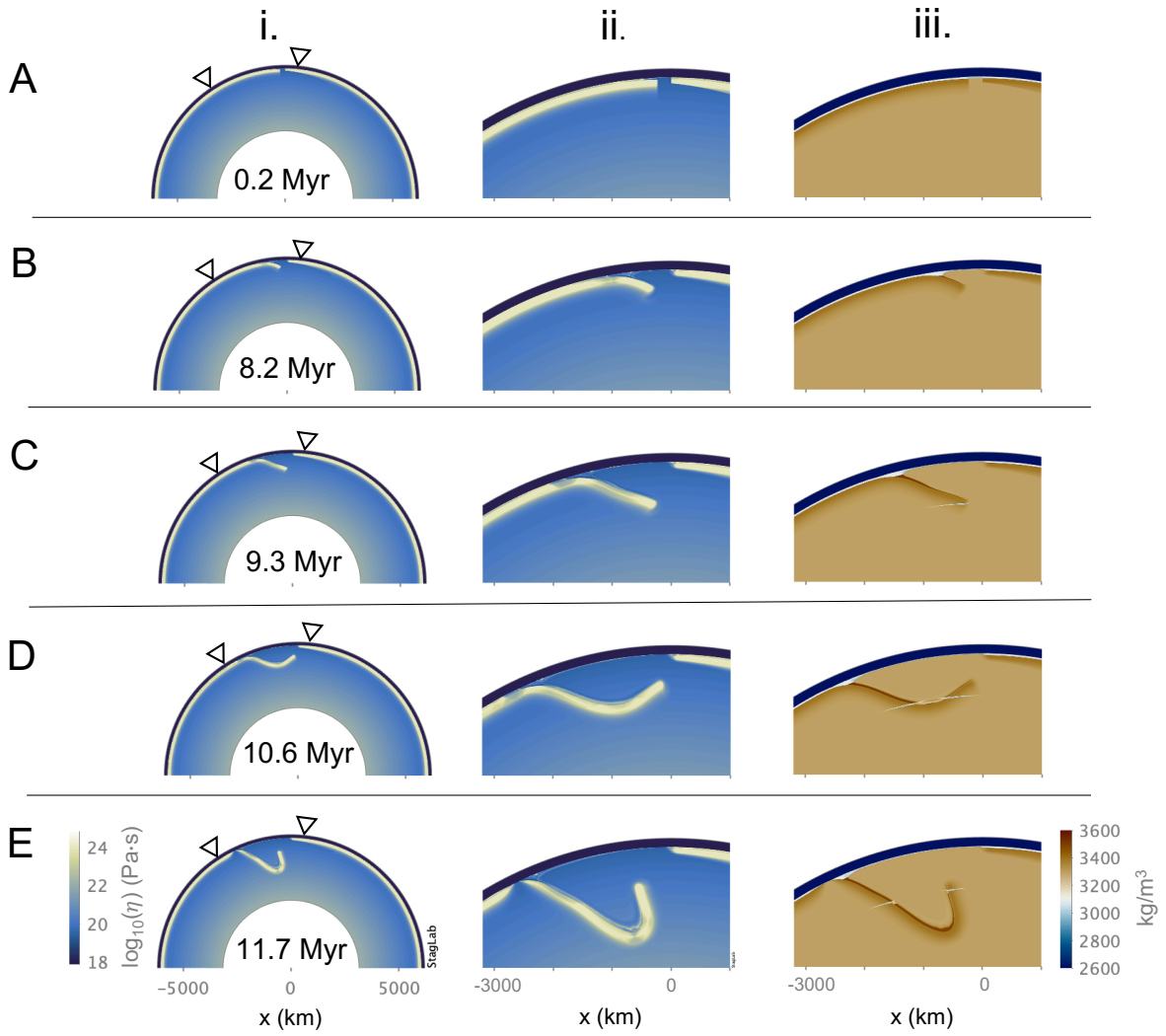

Figure 2.5. Typical evolution of a peel-back delamination event shown in the (i) full-scale viscosity field, (ii) local viscosity field, and (iii) local density field of reference model 23 (B_{crust} = -300 kg/m^3, h_L = 250 km, $\eta_{max} = 10^{24}$ Pa·s). (A) A 250 km-wide gap separates the thicker plate edge on the left (h_L) from the 100 km plate edge to the right of the gap. (B) The edge of the thicker plate is bent downward due to the negative buoyancy of the lithospheric mantle. A layer of eclogite is formed in the thin layer of crust still attached to the down-going plate. (C) The lithospheric mantle continues to peel-back from the surface and thicker layers of crust are recycled due to eclogitization of the growing crustal root over the delamination hinge. The slab tip encounters the phase transitions near 710 km depth and (D) is deflected upward. (E) The plate necks and thins at the delamination hinge prior to slab break-off at the surface.

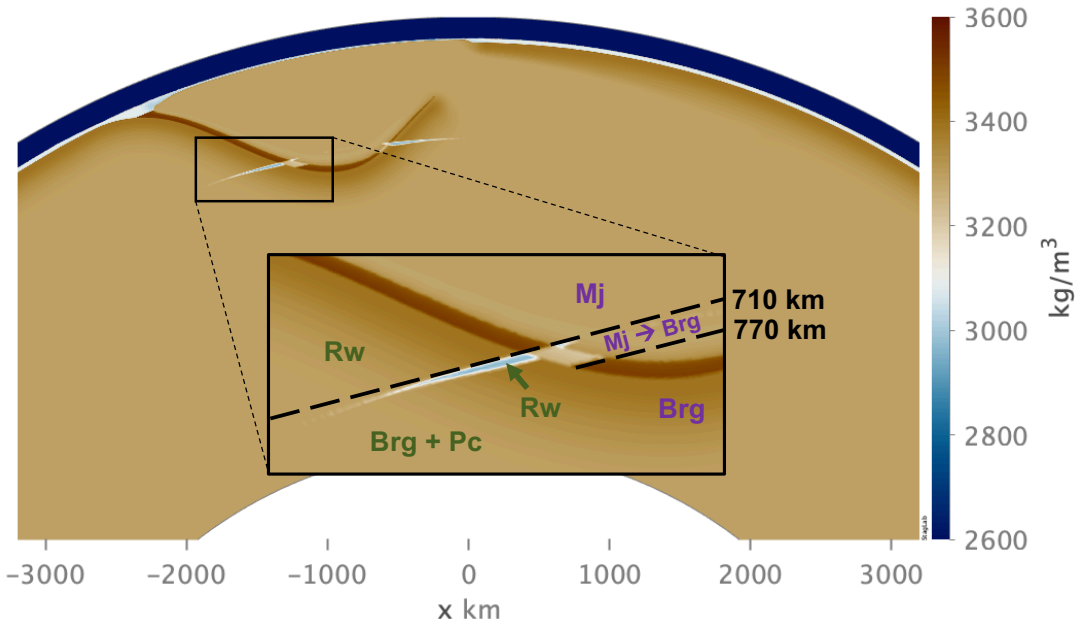

Figure 2.6. Two separate sources of mid-mantle positive buoyancy within the delaminating slab shown in the density field of the reference model 23. The first is in the olivine system (green text) where the negative Clapeyron slope (-1.0 MPa/K) of the postspinel phase transition deflects the phase boundary to deeper depths within the cold regions of the slab. The transition of ringwoodite (Rw) to bridgmanite (Brg) and periclase (Pc) is delayed, resulting in a thin layer of positive buoyancy within the slab (light blue). The second source of positive buoyancy occurs within the basalt-garnet system (purple text). The basalt barrier is the result of the gradual transition of majorite garnet (Mj) to bridgmanite over 710-770 km depths (light beige).

crust sufficiently for a delamination interface to form. Despite some initial bending of the lithospheric mantle, the absence of a weak zone prevented it from delaminating.

3.2 Analysis of Regimes

3.2.1 Radius of Curvature

The radius of curvature of a down-going slab is a useful metric to describe delamination because it is dependent on both the negative buoyancy of the slab and the viscosity ratio between the slab and upper mantle [84, 85]. The radius of curvature (R_c) was calculated for each delamination model every 50 model time steps. The radius of curvature calculation was adapted from the version provided in StagLab [67]. A least squares approximation of a circle was fit to the 1100 K isotherm, which defines the core of the slab from a distance of 400 km behind the trench to a depth of 900 km. This range was chosen to include the effect of slab tip deflection resulting from the phase transitions in the mid-mantle to be used as a diagnostic tool.

Different stages of delamination evolution were apparent in the calculated R_c plotted over time (Fig. 2.7). The radius of curvature was largest before delamination is initiated and oscillated as the plate edge began to founder. Delamination initiation is defined as the point when the plate edge began to bend and sink continuously, which corresponded to the time when the radius of curvature began decreasing steadily at 2.2 Myr. The largest decrease in R_c occurred in the early stages of slab sinking as the plate began bending and delaminating from the surface. The R_c in all delamination models increased slightly when the slab tip was deflected by postspinel density inversion at 3.8 Myr. A steady-state peel-back delamination stage was defined as the period of time from 4.0-5.9 Myr with a steadily or weakly decreasing R_c after the slab encountered the 710 km density inversions. The radius of curvature was calculated until the slab began necking prior to slab break-off at 6.5 Myr.

All models with the densest crust (B_{crust} = -175 kg/m^3) delaminated. In order to analyze the effects of variable lithosphere thickness and maximum viscosity, R_c curves

were plotted against each other (Fig. 2.8). Within this subset of models, all R_c evolutions contained the same major characteristic changes as model 5 described in Figure 2.7. The bending radius during steady-state peel-back delamination was largest for the thickest lithosphere (h_L = 300 km) and decreased with decreasing plate thickness. Delamination occurred on shorter timescales for the thickest plates and initiation timescales increased with decreasing plate thickness. When lithosphere thickness was the same, the weaker plates (i.e. those with lower maximum viscosity) underwent delamination on shorter timescales than stronger plates with higher maximum viscosity.

3.2.2 Topography

Surface topography was calculated every 50 time steps for all delamination models. As the plate began to delaminate, a topographic low developed at the trench near the delamination hinge, and a local topographic high was associated with the flexural bulge behind the trench of the bending plate. The height and location of the forebulge and the depth and location of the trench were tracked over time and used to estimate the timing of the end of steady-state peel-back delamination. Specific changes in trench depth, forebulge height, and their locations were identified as a precursor to slab break-off (Appendix A: Fig. 6.2). Viscous necking at the plate hinge during slab break-off indicated the end of steady-state delamination.

3.2.3 Delamination Timescale Analysis

The timing of delamination initiation and slab break-off constrain the beginning and end of a delamination event, respectively. Initiation timing was determined using the radius of curvature and slab break-off timing was determined using the topography analyses. When all other parameters were constant, increasing positive crustal buoyancy (decreasing B_{crust}) prolonged delamination initiation and slab break-off (Fig. 2.9). Increasing plate thickness, h_L, generally caused delamination to occur on faster timescales. Weaker plates with a lower maximum viscosity delaminated on faster timescales than plates with a higher maximum viscosity. The effect of maximum viscosity on delamination initiation

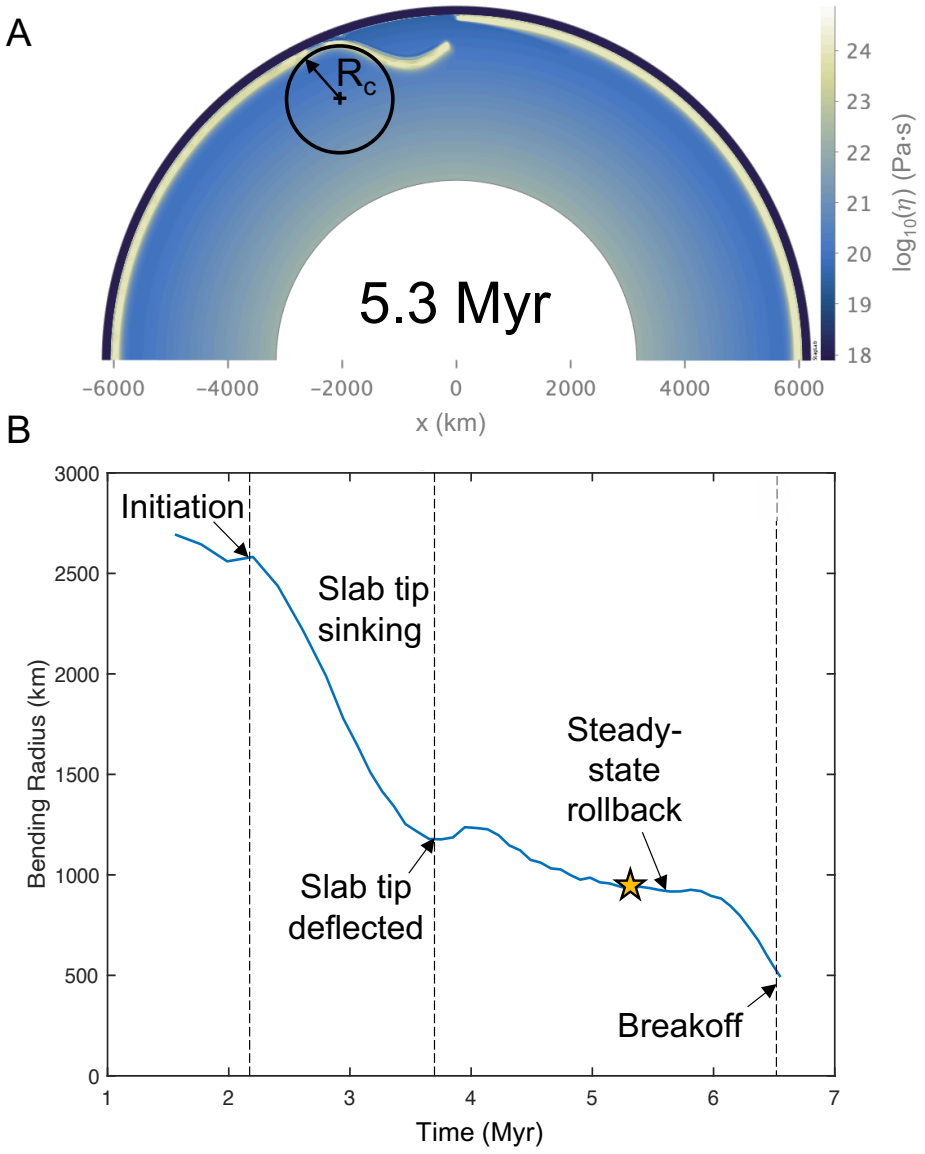

Figure 2.7. A least squares approximation of a circle to the 1100 K isotherm was used to estimate the radius of curvature, (R_c), during delamination. (A) The R_c for model 5 with B_{crust} = -175 kg/m^3, 250 km-thick lithosphere, and $\eta_{max} = 10^{24}$ Pa·s at t = 5.3 Myr is 930.74 km (indicated by star symbol). (B) The evolution of the R_c over time for the same model. All delamination models exhibit the following features in their respective R_c evolutions: At the onset of delamination, the radius of curvature decreases sharply as the slab tip begins bending and sinking. The R_c increases briefly as the slab encounters the postspinel phase transition and then decreases slightly until reaching a relatively constant value throughout a period of steady-state peel-back delamination. The R_c decreases sharply during slab break-off.

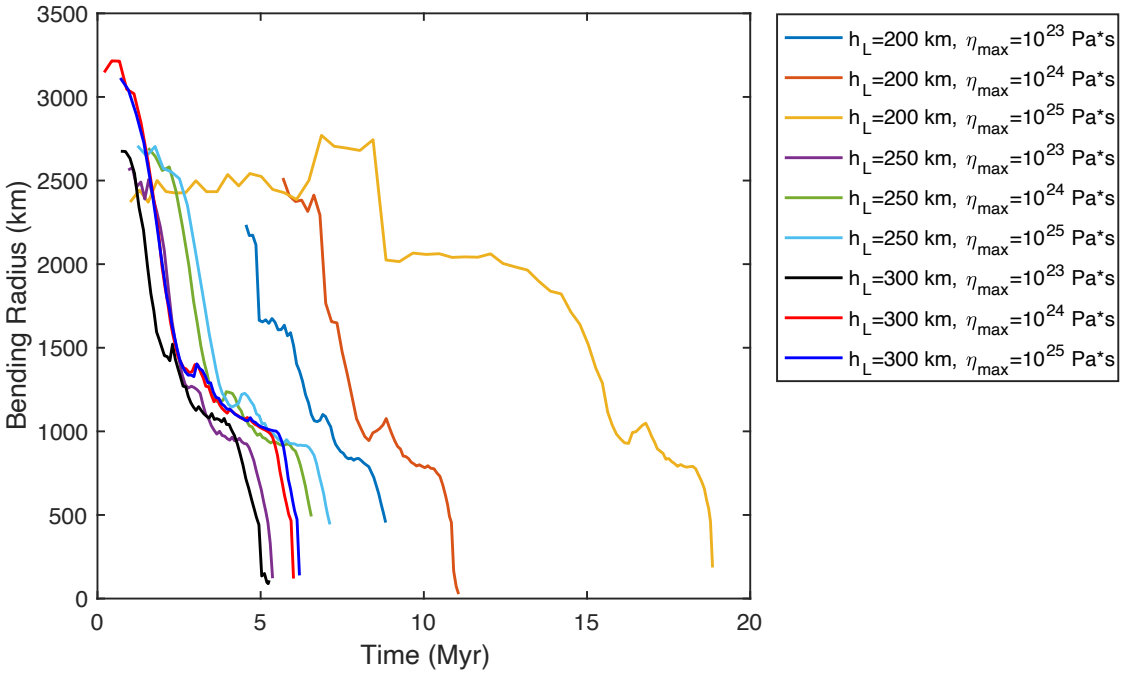

Figure 2.8. Radius of curvature evolution for all models with B_{crust} = -175 kg/m^3, which represents the least buoyant crust. This subset of models was selected because all cases resulted in delamination. All models began at time t=0, but the R_c data begin when initial plate bending was detected and end prior slab break-off. Delamination occurs on faster timescales with increasing plate thickness and decreasing maximum viscosity. Maximum viscosity plays a larger role in delamination timescales when the plate is thinner and closer to neutral buoyancy.

became increasingly significant for increasingly positive plate buoyancy (decreasing h_L and/or decreasing B_{crust}). The total duration of a delamination event also increased with increasing maximum plate viscosity. For example, a complete delamination event took 1.34 Myr in model 40 ($\eta_{max} = 10^{23}$ Pa·s), took 3.93 Myr in model 41 ($\eta_{max} = 10^{24}$ Pa·s), and took 6.77 Myr in model 42 ($\eta_{max} = 10^{25}$ Pa·s). This effect became stronger with increasing crustal buoyancy.

3.2.4 Net Plate Buoyancy

On Earth, subduction is driven by the negative buoyancy of oceanic plates with respect to the underlying mantle. The net buoyancy of the lithosphere can be used to determine if a plate has a propensity to sink or remain at the surface. Net plate buoyancy was controlled by two of the three variables in our parameter space: lithosphere thickness and crust density. Increasing both crust density and lithosphere thickness increases the net-negative buoyancy of the plate. The total density of each plate was calculated as a function of depth, including both thermal and compositional components (Fig. 2.10). A density profile was calculated for each combination of lithosphere thickness and crustal buoyancy in the model suite. The density profiles were integrated over depth to obtain a single value, $\Delta\rho_{plate}$, describing the net density contrast of the plate with respect to the underlying mantle:

$$\Delta\rho_{plate} = \int_0^{h_L} (\rho(z) - \rho_0)\, dz \tag{2.5}$$

The outcomes of all models are plotted in a regime diagram as a function of the net plate buoyancy and maximum viscosity (Fig. 2.11). All plates that were negatively buoyant with respect to the underlying mantle delaminated; however, a subset of positively buoyant plates delaminated as well. This highlights a key difference between the mechanisms driving subduction and delamination: negative net plate buoyancy is not required for lithospheric recycling via peel-back delamination.

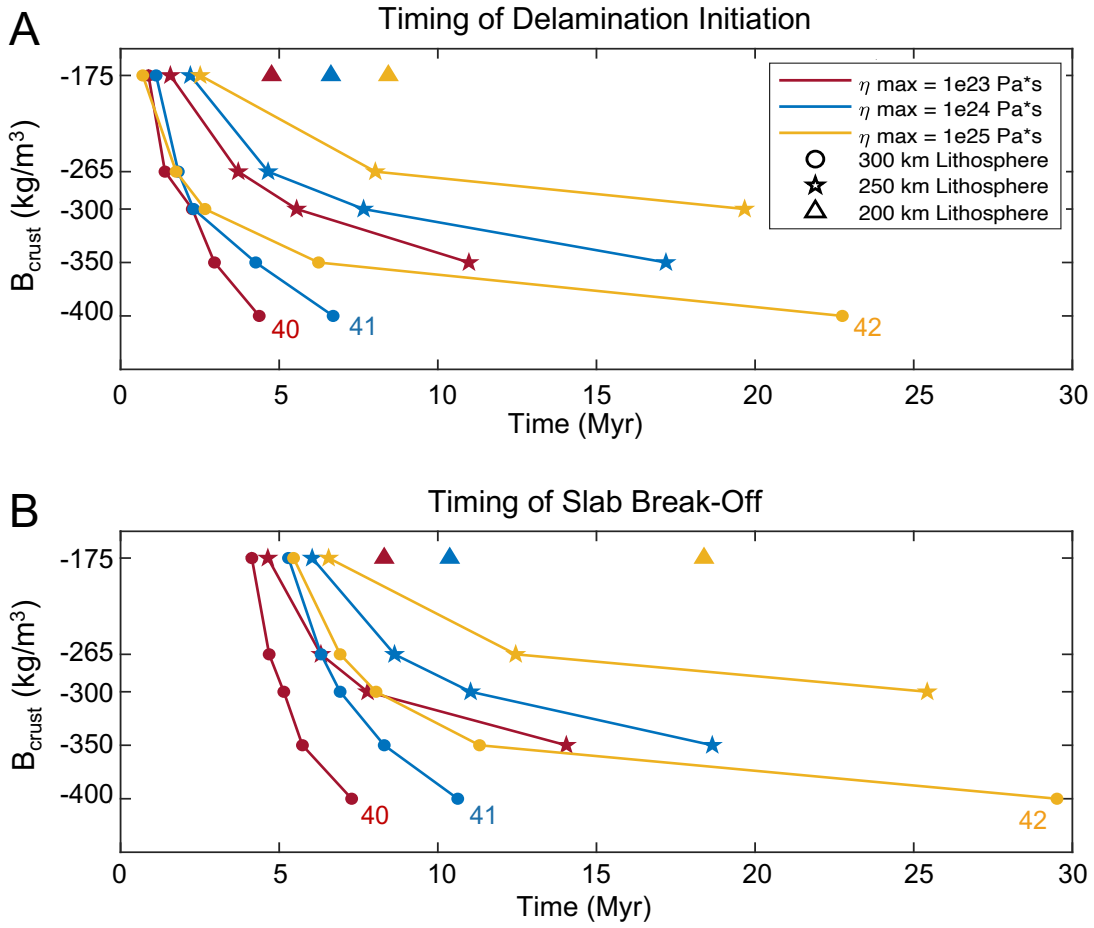

Figure 2.9. The timing of delamination initiation (A) and the timing of slab break-off (B) are plotted for each model that underwent peel-back delamination. Solid lines connect models with identical maximum viscosity and lithosphere thickness to highlight the effect of crustal buoyancy on delamination progression. Increasing crustal buoyancy (decreasing B_{crust}) increases the time it takes for delamination to be initiated and completed. When B_{crust} is constant, delamination occurs on faster timescales for thick, weak plates. Model numbers (see Table 2.2) are included for models that are discussed in this section.

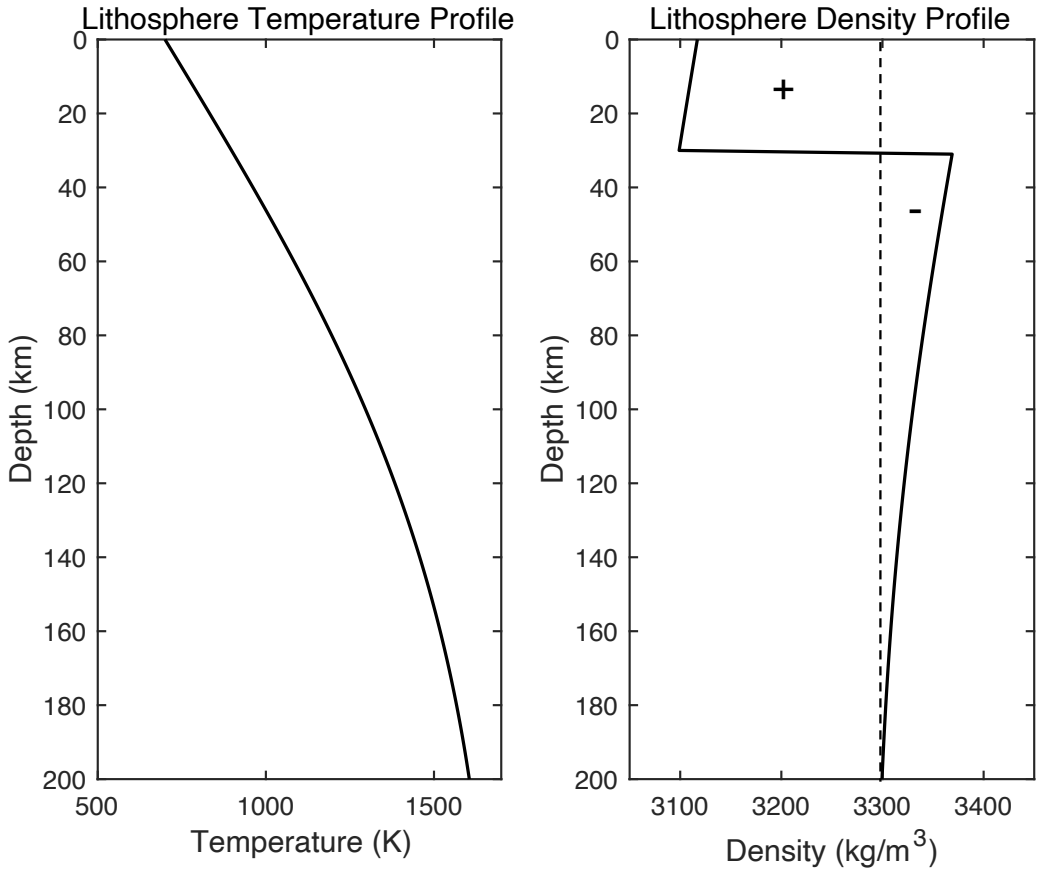

Figure 2.10. The temperature profile through the depth of the lithosphere (left) is used to calculate the density profile through depth (right) for each combination of lithosphere thickness and crustal buoyancy. Shown here is a 200 km-thick plate with B_{crust} = -265 kg/m^3 corresponding to models 10-12. The density profile includes both compositional and thermal density contributions. The reference density of the underlying mantle, ρ_0 = 3300 kg/m^3, (dotted line) differentiates positively and negatively buoyant regions within the lithosphere.

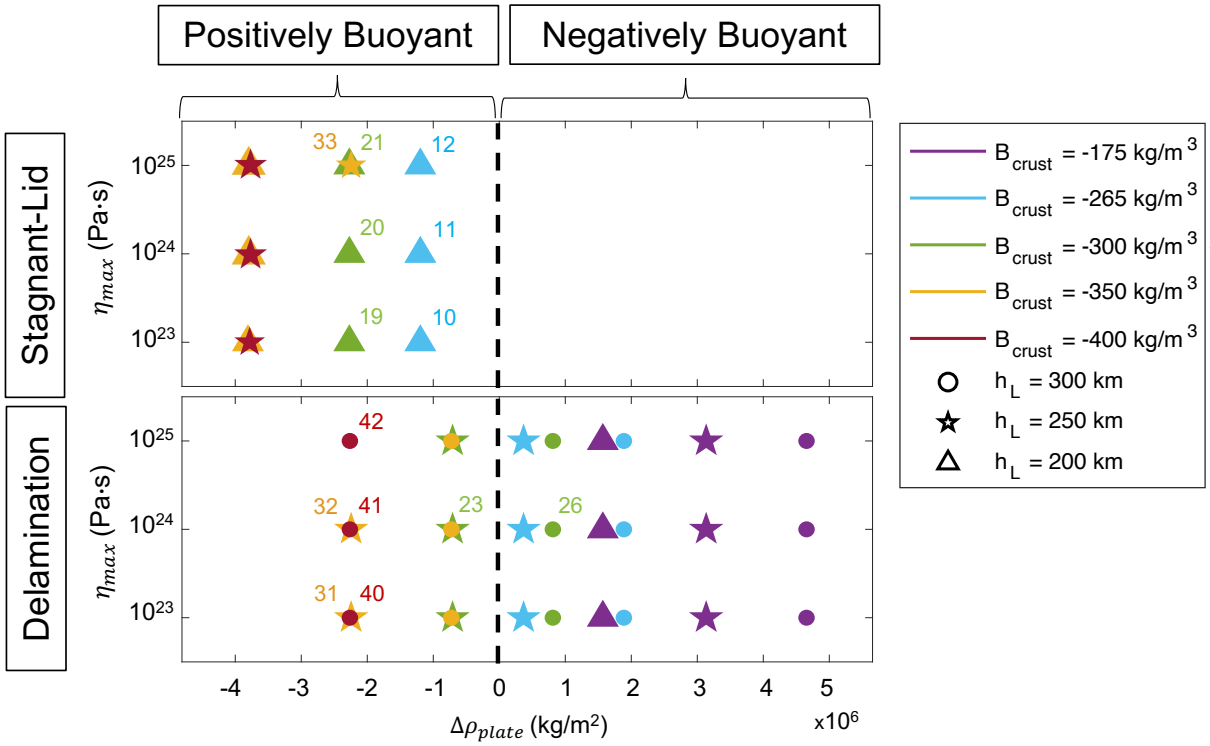

Figure 2.11. Tectonic regime outcomes are plotted for maximum viscosity vs integrated plate density. Stagnant-lid models (top) are separated from delamination models (bottom). Model numbers (see Table 2.2) are included for those mentioned in the discussion. Plates with a positive integrated density contrast ($\Delta\rho_{plate}$) are denser than the underlying mantle and therefore have a net-negative plate buoyancy, while a negative $\Delta\rho_{plate}$ means a density deficiency and therefore a net-positive plate buoyancy. All negatively buoyant plates delaminated. A subset of positively buoyant plates also delaminated (lower left quadrant), even though other models with nearly identical net plate buoyancy were stagnant-lid.

2.4 Discussion

4.1 Peel-Back Delamination Initiation

To understand why certain positively buoyant plates delaminate but others with the same net buoyancy do not, we must understand the mechanisms driving peel-back delamination. Delamination is a form of lithospheric recycling in which the sub-crustal lithospheric mantle (SCLM) detaches and peels away from a layer of overlying crust remaining at the surface. Peel-back delamination propagates along the Moho (the largest strength discontinuity over the depth of the plate) where weak, buoyant crust is juxtaposed with stronger, more negatively buoyant lithospheric mantle. Like subduction, the delamination mechanism is primarily driven by the excess density of the lithospheric mantle with respect to the underlying asthenosphere [86]. Thus, delamination is facilitated by plates having a thick, negatively buoyant mantle lithosphere.

We model a compositionally-homogeneous upper mantle, so the colder lithospheric mantle is always negatively buoyant with respect to the sub-lithospheric mantle. However, delamination is resisted by (1) the coupling of the plate across the lower crust-upper mantle boundary and (2) the viscous strength of the mantle. A low-viscosity lower crust layer allows mechanical decoupling along the crust-mantle boundary which is crucial for delamination to occur [87, 88, 89, 90, 91]. Early in our delamination model evolutions, the yield strength of the crust is exceeded near the plate edge due to extensional stresses resulting from the initial displacement of the gravitationally unstable lithospheric mantle. Consequently, the yielded crust forms a low-viscosity layer which facilitates decoupling of the crust from the lithospheric mantle. The amount of crustal yielding increases by increasing the thickness of the lithosphere and therefore increasing its negative buoyancy (Fig. 2.12). Within the subset of net-positively buoyant plates, the thickest plates (h_L = 300 km) always delaminated while the thinnest plates (h_L = 200 km) always remained stagnant-lid. This dichotomy was even observed when the 200 and 300 km-thick plates

had nearly identical net plate buoyancy (Fig. 2.11: see models 19-21 vs. models 38-40). Even when the 200 km plate was more net-negatively buoyant than the 300 km plate, it still remained stable in the stagnant lid regime (Fig. 2.11: see models 10-12 vs models 38-40). The thinner lithosphere to the right of the gap (h_{L-min} = 100 km) never delaminated because there is less negative buoyancy to overcome the coupling of the crust and lithosphere. When the lithospheric mantle portion of the plate is sufficiently dense, the forces driving delamination prevail; however when the lithospheric mantle has insufficient negative buoyancy, plate coupling inhibits delamination.

It is worth reiterating that delamination is driven by the negative buoyancy of the lithospheric mantle with respect to the underlying mantle, and not the density contrast across the Moho. While it may be seem reasonable to assume that increasing the density contrast between the crust and lithosphere would always promote decoupling, varying crustal buoyancy has a more complicated effect. This can be observed in the subset of positively buoyant plates with a 250 km-thick lithosphere: those closer to neutral buoyancy delaminated (B_{crust} = [-300, -350] kg/m^3), while increasing crustal buoyancy favored a stagnant-lid outcome (B_{crust} = [-350, -400] kg/m^3) (Fig. 2.11). Although the lithospheric mantle portion of the plate maintained the same integrated negative buoyancy, increasing the positive buoyancy of the crust (and therefore the entire plate) inhibits delamination. The positive buoyancy of the crust resists plate bending, thereby preventing crustal yielding and the development of the weak zone required for delamination. Compared to thicker plates with excess negative buoyancy, thinner plates require less positively buoyant crust in order to undergo bending and delamination.

4.2 Plate Strength

In addition to plate coupling across the crust-mantle boundary, the viscous strength of the lithospheric mantle is another resisting force to delamination. By varying the maximum viscosity of our models over two orders of magnitude [10^{23}, 10^{24}, 10^{25} Pa·s], we systematically varied the strength of the cold upper portion of the lithosphere. The

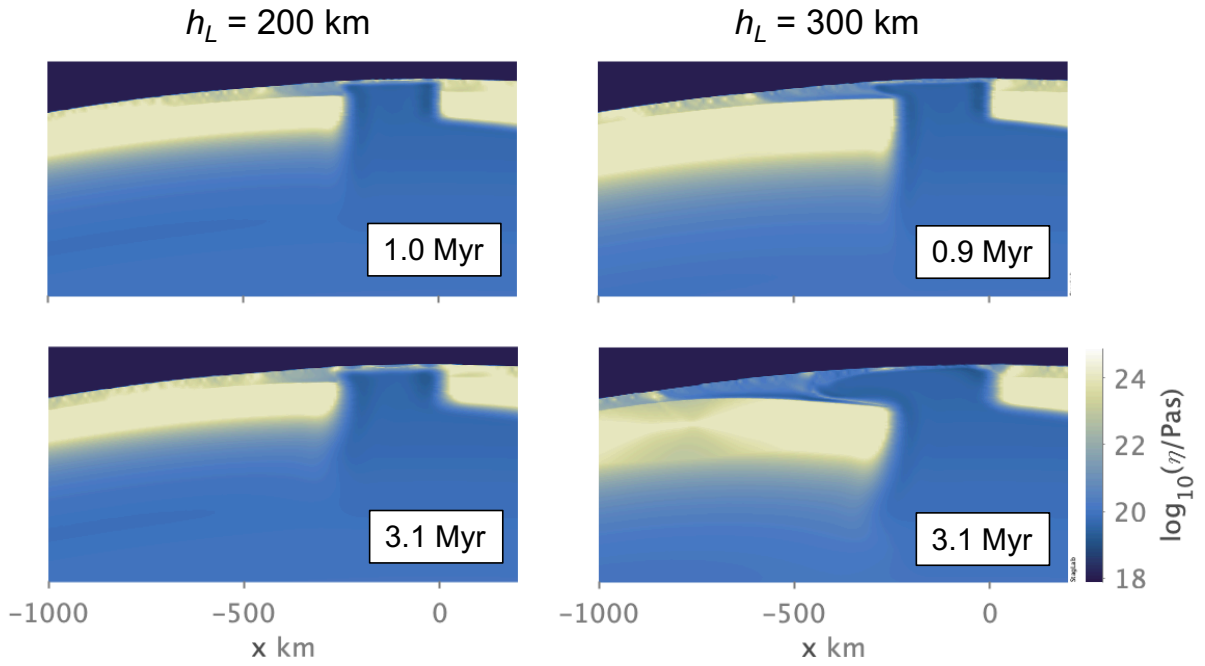

Figure 2.12. Viscosity field comparison of crust yielding and weak zone formation for stagnant-lid model 20 (left) vs. delamination model 26 (right). Models were identical (B_{crust} = -300 kg/m^3, η_{max} = 10^{24} Pa·s) except for plate thickness. The 300 km-thick plate in model 26 has a thicker and denser lithospheric mantle, causing it to bend further and induce more crustal yielding over the plate edge. The yielded crust is weak and facilitates decoupling and delamination of the lithospheric mantle. Although some crust weakening is observed over the plate edge of model 20, its thinner lithospheric mantle has less negative buoyancy to form a sufficient delamination weak zone. If the crust is yielded but delamination is not initiated (left), the strength (i.e. viscosity) of the weakened crust increases over time.

energy required for plate bending is proportional to its viscosity; therefore plate bending, which is required for the formation of the delamination weak zone, becomes more difficult with increasing maximum viscosity. For example, models 32 and 33 were identical except for a one order-of-magnitude difference in maximum viscosity ($\eta_{max,32}$ = 10^{24} Pa·s and $\eta_{max,33}$ = 10^{25} Pa·s). The weaker plate in model 32 delaminated while the stronger plate in model 33 remained a stagnant lid (Fig. 2.13). The effect of increasing maximum viscosity can further be observed in the timescales of delamination (Fig. 2.9). In models with identical lithosphere thickness and crustal buoyancy, increasing maximum viscosity increases the timescales of the delamination process. The effect of maximum viscosity on

delamination timing becomes increasingly important with increasing crustal buoyancy, because increasing crustal buoyancy also prolongs delamination. When the crust is more positively buoyant, it takes significantly longer for the strongest plate (e.g. model 42) to go unstable than the weakest plate (e.g. model 40) due to the combination of effects which discourage plate bending.

The viscous strength of the mantle as a resisting force to delamination not only refers to the strength of the plate itself, but also the resistance of the sublithospheric mantle to deformation from a sinking plate. Although we did not vary the radial viscosity over the depth of the mantle, a higher viscosity asthenosphere would inhibit delamination and prolong timescales of delamination, while a weak asthenosphere may promote delamination on shorter timescales. We used a single value for mantle potential temperature (1700 K), but we expect that higher temperatures would favor delamination on shorter timescales. A warmer interior would decrease the viscosity of the sublithospheric mantle, which would facilitate delamination. Warmer mantle temperatures and higher temperature gradients across the lithosphere would reduce plate strength, which would also facilitate plate bending and delamination. Conversely, a colder mantle temperature would likely inhibit delamination and slab sinking. Such details can be pursued by future investigations.

4.3 Crustal Thickness and Buoyancy

Gravity and topography predict large regional variations in Venus' crustal thickness (0-110 km) [65] and estimates for the average crustal thickness typically fall between 8-50 km [11]. Although in our models we assume a constant 30 km basaltic crust consistent with the global average, variations in crustal thickness could complicate delamination initiation. On one hand, thicker layers of buoyant crust will increase the positive buoyancy of the plate and inhibit plate bending and delamination. However, increasing crustal thickness in our models would result in less cold, strong lithospheric mantle to resist plate bending. The basalt-eclogite transition occurs at deeper depths in Venus' mantle than on Earth, requiring crust to subduct to deeper depths before the added negative buoyancy

from eclogite can help sustain delamination. Yet if crust on Venus is thicker than on Earth, less crust displacement is necessary for eclogitization depths to be reached. If we consider a multi-stage basalt-eclogite transition beginning at shallower depths than 70 km [92], a thick layer of crust may reduce the compositional buoyancy of the crust and stimulate recycling of the lower crust and lithosphere on faster timescales.

Not all models of global episodic overturns consider the chemical buoyancy of the crust and its effect on subduction [25], and others may underestimate its effect [21, 22, 23, 24]. To isolate the effect of crustal buoyancy on lithospheric recycling, we varied the density contrast of the crust, B_{crust}, over 5 values (-175 to -400 kg/m^3) for a uniformly-thick crust (h_{crust} = 30 km). Our results indicate that the chemical buoyancy of the crust is an important factor understanding delamination initiation because it (1) affects the net buoyancy of the plate and (2) resists the bending of the lithospheric mantle that is a precursor to delamination. More work will need to be done to understand the role that crustal thickness and buoyancy play on the different styles of resurfacing proposed for Venus.

4.4 Yield Stress

For Earth, there is a discrepancy between the maximum yield stress predicted by laboratory experiments [7] and those used in numerical models to study subduction [19]. A mobile-lid is generally favored when the yield strength parameterization is limited by a low maximum yield stress with depth, and increasing the maximum yield stress promotes a stagnant-lid [50]. Armann and Tackley (2012) found that 5-8 global overturns can occur when the yield stress is limited to 100 MPa [21] and other studies have modeled global overturns on Venus by employing similarly low yield stresses [22, 23, 25, 24]. Higher yield stresses (up to 300 MPa) also produced global overturns, though the duration of the mobile-lid period was shorter and less vigorous [21].

Since the yield strength profile with depth is even less constrained for Venus, we tested a higher limiting yield stress (500 MPa) than in previous global overturn models. We

were able to model regional-scale lithospheric resurfacing with a relatively high yield stress in part because the the crust strength is limited by a relatively low yield stress (surface cohesion = 10 MPa). Venus' lower crust is predicted by some to be weak relative to the upper crust and underlying lithospheric mantle and deformable on relatively short geologic timescales [34, 35, 70, 71, 72, 93]. Previous experimental studies may have overestimated the strength of Venus' crust [8] by using diabase instead of plagioclase at the brittle-ductile transition where Peierls creep is the primary deformation mechanism [34, 35]. We also consider that crustal yielding and weak zone formation is driven by extensional forces in the crust owing to the gravitational instability of the lithospheric mantle. In this context, a weak crust parameterization may be appropriate since the yield strength of the crust is expected to be lower under extension than compression. A higher crustal yield strength would inhibit weak zone formation; delamination would likely require thicker lithospheres in order to generate sufficient stresses in the crust.

Still, the weak zone could come from a variety of tectonic processes, including melting and thermal weakening near the Moho [94, 95] and intrusive magmatism in the lithosphere [32]. If there was a pre-existing weak zone in the plate that did not require crustal yielding, it is possible that thinner plates may also undergo delamination. Higher strength crust may still yield and form a weak zone in the presence higher lithospheric stresses due to ongoing tectonic deformation. The origin of the weak zone is not considered to be within the scope of this study but is important in understanding how delamination could operate on Venus.

4.5 Uncertainties

In our simplified rift zone setup, we model a sharp temperature gradient across a vertical boundary separating the plate edge and the gap containing relatively warm mantle material. The lithospheric gap itself is only a first order representation for the thermal structure at rift zones on Venus and lacks finer details. However, it is an appropriate starting point as we acquire a better understanding of the relationship between the strength

and buoyancy of a plate and its tendency to delaminate.

In the early stages of delamination, only a thin layer of crust is attached to the down-going plate. Once the crustal root reaches the eclogite transition depth, thicker layers of crust remain attached to the delaminating plate due to the eclogite density inversion (see Fig. 2.6). The thickness of the crustal root over the delamination hinge is important in determining how much crust is eclogitized, which has implications for slab sinking dynamics. We imposed a minimum crust thickness of 15 km to prevent sticky-air particles from becoming embedded in the mantle material exposed at the surface of the gap due to its low viscosity contrast. Though this feature may potentially overestimate the amount of crust at the surface, we expect that new crust would be generated in the delamination zone. Since our models currently do not include melting processes, the volume of crust at the surface is an approximation.

4.5 Implications for Resurfacing

A peel-back delamination event on Venus would undoubtedly have a unique surface expression. During the initial stages of delamination, it is clear that the majority of the crust remains at the surface or within the crustal root formed at the slab hinge (Fig. 2.4D). As the lithospheric mantle peels away, it is replaced by warm asthenosphere flowing beneath a thinned layer of crust at the surface. Delamination of the lithospheric mantle in Earth-like conditions is predicted to lead to enhanced surface magmatism, local tectonic uplift, and horizontal surface deformation in the region overlying the delamination zone [86, 96, 97]. Yet, due to uncertainties in the exact volume of remaining surface crust, the style and extent of resurfacing that may follow a delamination event still remains unclear. Perhaps the delamination zone would be fully resurfaced due to a high degree of induced surface volcanism - or perhaps delamination may only be a source of surface deformation and crater modification via localized, thin lava flows consistent with the regional equilibrium resurfacing model [60].

Without modeling melt processes, the extent of resurfacing will remain unclear.

However, we can compare our results to delamination models in an Archean Earth environment [98, 99, 100] when the mantle was thought to be hotter [101] and more comparable to Venus than at present. Our initial condition resembles the starting point for the initiation of "peel back convergence" in a numerical modeling study of delamination in the Archean Earth by Chowdhury et al. (2020) (see their Fig. 2.1c). Peel back convergence is described as a form of rollback delamination initiated at a sharp lateral lithospheric discontinuity at a convergent margin [99]. While the weak zone delamination surface in our models originated from yielding of a weak lower crust, the weak zone in Chowdhury et al. (2020) was generated by melting and weakening of a protocontinental crust. Following a delamination event, they observed a region of thinned, hot crust at the surface characterized by localized volcanism, including underplating melt and rising melt domes. A more modern analogue on Earth may be found in East Anatolia over the Arabia-Eurasia collision zone. The lithosphere beneath the East Anatolian plateau is thought to have been recycled in an event comparable to peel-back delamination and was accompanied by surface uplift, distinct zones of extension and compression, high heat flow, and volcanism [102, 103, 104]. Evidence for similar delamination processes may also be present in the Southeast Carpathians [105, 106], the Northern Tibetan plateau [107], and other locations on Earth (see Memiş et al., (2020) and references therein).

In addition to the surface expression of a delamination event, is also important to constrain the total delamination area in order to understand the extent of resurfacing that is possible. The timing of slab break-off appears to be strongly influenced by the slab's interaction with the two sources of positive buoyancy near 710-770 km depth. During the steady-state delamination stage, the zone of positive buoyancy effectively helps support the weight of the slab as peel-back delamination progresses at the surface. Eventually the slab sinks through this barrier, and the slab pull force (and therefore stresses at the delaminating plate hinge) sharply increases, which results in yielding and necking of the plate at the surface in a process that is consistent between all delamination models. If there

was less positive buoyancy in the slab at 710 km-depth (e.g. if the Clapeyron slope of the postspinel transition was closer to zero), the location and timing of slab-breakoff may vary more significantly between different delamination models. Slab break-off is also influenced by the yield strength parameterization throughout the slab; if the limiting yield stress was lower, break-off may occur earlier in the delamination process as stresses accumulate in the slab hinge. We estimate the total length of a single peel-back delamination event to be between 2500-3000 km (approximately 1/7 of the surface). Since our models are two dimensional, we possibly over- or underestimate the scale of the delamination zone. Future directions may include modeling peel-back delamination in 3D, since three-dimensional models are important for understanding the mantle dynamics and tectonics associated with the toroidal component of flow induced by a sinking slab [108, 109]. This may have implications for slab sinking geometry, predicted melt volumes, and total amount of resurfacing that may occur during a delamination event.

2.5 Conclusions

Despite the thousands of kilometers of chasma rift zones that have been identified as potential subduction sites on Venus [2, 3], there have been no studies to date which have investigated the dynamics of lithospheric recycling initiated at Venusian rift zones. Here, we presented the first 2D numerical models to indicate that peel-back delamination initiated at a lateral lithospheric discontinuity may be a viable mechanism for lithospheric recycling and heat loss on Venus. Delamination has been proposed to occur on Venus, however it is typically studied within the context of plume-lithosphere interactions and coronae formation [18, 64, 110, 111]. We showed that in the absence of plume-lithosphere interactions, the full depth of the sub-crustal lithospheric mantle can detach and peel away from the crust remaining at the surface.

Delamination is primarily driven by the excess density of the lithospheric mantle.

It requires a weak lower crust for decoupling to propagate and a connection between the Moho and asthenosphere for buoyant material to rise and fill the space between the crust and down-going plate. When these criteria are satisfied we observe that, unlike subduction, both net-positively and net-negatively buoyant plates may undergo delamination. Our results indicate that positive crustal buoyancy inhibits delamination by impeding plate bending which drives crust yielding and weak zone formation. However once the crust reaches the basalt-eclogite transition depth, the eclogite density inversion helps sustain delamination. Delamination may only occur when the mantle lithosphere is sufficiently negatively buoyant to bend and counteract the initial positive buoyancy of the crust. In cases with insufficient mantle lithosphere thickness, excess crustal buoyancy, or the absence of a conduit connecting crust and asthenosphere, a stagnant-lid regime may persist.

Peel-back delamination may have important implications as a source of regional-scale resurfacing within the framework of the regional equilibrium resurfacing (RER) hypothesis. Following a delamination event, the emplacement of hot asthenosphere beneath a layer of thinned crust may enhance surface deformation and volcanism. Perhaps the evidence for the highly deformed [112] and globally fragmented lithosphere [113] can be viewed as forms of surface tectonics associated with delamination events. Not only is delamination compatible with Venus' style of surface deformation, but it may be responsible for some of the observed heterogeneity in crust and lithosphere thickness [65]. Though more work will need to be done to determine if it can satisfy cratering and CM-CF offset constraints, the regional-scale peel-back delamination regime may be able to explain some aspects of Venus' unique resurfacing history.

2.6 Acknowledgments

Authors are grateful for support from NASA Award 80NSSC22K0100. Computational resources were provided by Extreme Science and Engineering Discovery Environment

(XSEDE), which is supported by National Science Foundation grant number ACI-1053575. The authors are grateful for technical assistance from Fabio Crameri with StagLab, acknowledge helpful reviews from Oğuz Göğüş and one anonymous reviewer, and thank David Sandwell for helpful discussions. A. Adams also thanks CIG for travel support to 2019 Ada Lovelace Workshop on Modelling Mantle and Lithosphere Dynamics.

Chapter 2, in full, is a reprint of the material as it appears in Journal of Geophysical Research: Planets: Adams, A. C., Stegman, D. R., Smrekar, S. E., Tackley, P. J. (2022). Regional-scale lithospheric recycling on Venus via peel-back delamination. Journal of Geophysical Research: Planets, 127, e2022JE007460. https://doi.org/10.1029/2022JE007460. The dissertation author was the primary investigator and author of this paper. See ref [114] for available data.

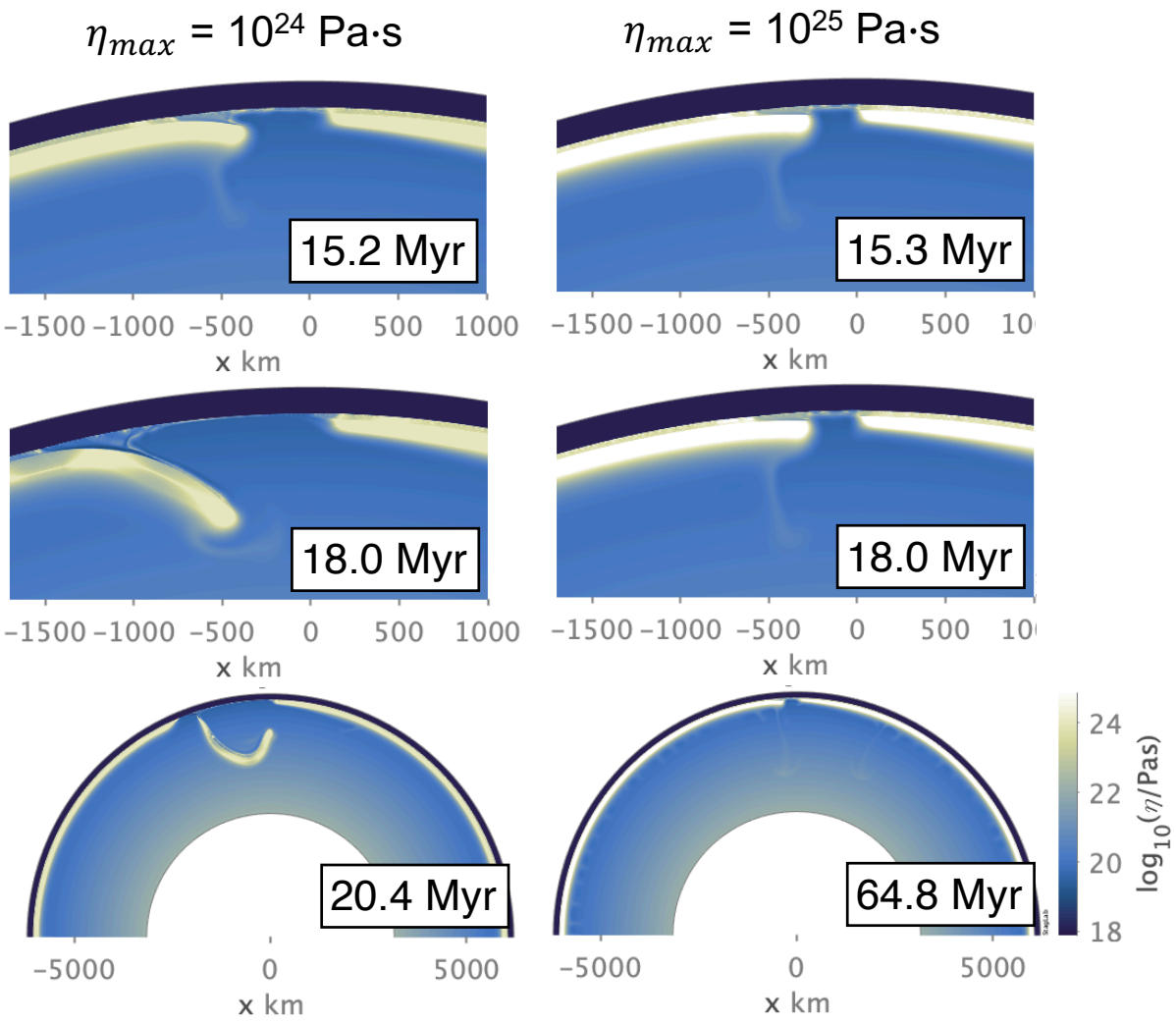

Figure 2.13. Viscosity field comparison of model 31 with a maximum viscosity of 10^{24} Pa·s (left) vs. model 32 with a maximum viscosity of 10^{25} Pa·s (right). Both plates are positively buoyant with identical net buoyancy, plate thickness (h_L = 250 km) and crust buoyancy (B_{crust} = -350 kg/m^3). The weaker plate is able to undergo bending and delamination, yet only a one order-of-magnitude increase in viscosity causes the stronger plate to resist bending and remain immobile.

Chapter 3

Plume-Induced Delamination Initiated at Rift Zones on Venus

3.1 Introduction

It is generally agreed that Venus does not have Earth-like plate tectonics. Unlike Earth, Venus lacks a global, continuous system of crust formation at mid-ocean ridges and lithospheric recycling at subduction zones [1]. Despite having a diverse surface of volcanic plains, highly-deformed tesserae, highland regions, chasma rift zones, and quasi-circular structures called coronae, Venus is typically categorized as a stagnant-lid planet [27], where the mantle is actively convecting beneath an effectively single-plate lithosphere with no clear system of plate boundaries. This raises the question of how Venus has evolved over time, given that the surface is estimated to be relatively young (240-800 Myr) on geologic timescales [38, 39, 57]. Following NASA's Magellan mission, two competing theories emerged to describe the potential resurfacing styles of Venus: (1) the catastrophic resurfacing (CR) hypothesis predicts nearly all of the lithosphere was recycled into the mantle during one or more discrete tectonic events [21, 40, 44, 41, 45, 58, 115], whereas (2) the regional equilibrium resurfacing (RER) hypothesis predicts resurfacing is a combination of regional-scale processes occurring throughout time that may result from a variety of tectonic and volcanic mechanisms [42, 59, 57, 60].

Across Venus, the tendency of the lithospheric mantle to sink is in constant

competition with a layer of crust that is compositionally less dense than mantle and adds significant positive buoyancy to the plate. Admittance spectra calculated from gravity and topography data reveal regional variations in crust and lithosphere thickness, with lithosphere thickness estimates ranging from 7-284 km [116] and crustal thicknesses between 0-100 km [65]. Estimates of the global average crustal thickness on Venus fall between 20-30 km [11, 12, 117], which adds substantially more positive buoyancy to the lithosphere than oceanic crust of subducting plates on Earth. Calculations of the density defect thickness [118] versus cooling age indicate that lithosphere with 8 km of oceanic crust on Earth will become negatively buoyant after 40 Myr; yet lithosphere on Venus with 24 km of crust is predicted to remain gravitationally stable up to 550 Myr [3] with other estimates as low as 300 Myr [45]. While the potential agreement between this threshold age for gravitational instability and the estimated surface age of Venus may be used to argue in favor of a global overturn resurfacing event, evidence for strong lithospheric heterogeneity [116] and globally inconsistent net plate buoyancy on Venus may be indicative of a more complex resurfacing model. A major question in Venusian tectonics is whether, similar to subduction on Earth, negative plate buoyancy is a requirement for lithospheric recycling; if not, how can positively buoyant plates on Venus be recycled?

A popular conceptual model for coronae formation is plume-induced subduction, which is thought to occur when a rising mantle plume penetrates the lithosphere and pushes the plate edges downward into the mantle from above, creating an annular retreating trench [2, 10]. In theory, subduction can occur despite the plate initially being positive buoyant because crustal density increases at the basalt-eclogite transition during the magma loading stage, and a higher-density eclogite layer may help sustain subduction [2, 18]. Plume-induced subduction via surface loading has been validated in laboratory tank experiments [64], though the thickness and density of the crust were unable to be controlled independently. While lithosphere that is too thick may hinder plume penetration, lithosphere that is too thin may be unable to support viscous plate bending

and subduction. Lithospheric flexure near coronae is generally associated with relatively small elastic thicknesses (<20 km) and high heat flow, indicating that most coronae may preferentially form on thin lithosphere [116, 119], yet the smaller subset of coronae showing evidence of plume-induced subduction typically occur in relatively older, thicker lithosphere aged between 25-140 Myr [2]. The plume-induced subduction mechanism has only been modeled for a spherical plume embedded at shallow depths beneath a thin lithosphere (30 km crust + 15 km lithospheric mantle) [18], and it is unclear how a rising plume would interact with, and potentially recycle, older and thicker lithosphere.

Delamination may be an alternative mechanism of recycling thick, yet positively buoyant lithosphere on Venus, particularly near chasmata which have pre-existing lithospheric fractures and abundant coronae, many of which likely form above small-scale plumes. Subduction and delamination are sometimes used in the literature interchangeably, but here we differentiate between the two terms: subduction involves significant crustal recycling, whereas delamination refers to only partial lithospheric recycling, either by lithospheric dripping [81, 82, 120] or by decoupling of the lithospheric mantle along the Moho [86, 88, 89, 91, 90, 99]. Delamination of the lower lithosphere has been suggested as a mechanism for heat loss resulting from plume-lithosphere interactions on Venus [110, 111]. However, the idea of regional-scale delamination has mostly been applied to Earth, including in the northwest US [121] and the Rwenzori mountains in Africa [122].

Adams et al. (2022) modeled a specific delamination mechanism called "peel-back delamination" (PBD) at a chasma-like rift margin on Venus which resulted in the full sub-crustal lithospheric mantle being recycled on a regional-scale. PBD occurs when the negatively buoyant lithospheric mantle decouples and peels away from the positively-buoyant, overlying crust along the Moho. Following a PBD event, a hot, thinned layer of deformed crust remains at the surface. Peel-back delamination driven solely by lateral density contrasts across a pre-existing lithospheric fracture, or buoyancy-driven PBD, was observed for both positively and negatively buoyant lithosphere [123]. It is primarily

dependent on the thickness of the lithospheric mantle, which defines the extent of its negative thermal buoyancy. Buoyancy-driven PBD consistently occurred in models with 300-km-thick lithosphere, despite having a net-positive buoyancy from 30 km of positively buoyant crust. Conversely, all cases with a positively buoyant 200-km-thick lithosphere resulted in a stagnant-lid due to having insufficient negative buoyancy in the lithosphere mantle; this was true even when crustal density was adjusted to yield the same net plate buoyancy as the 300 km lithosphere delamination models. Between these two endmember scenarios, delamination in 250-km-thick lithosphere was dependent on crustal density, with PBD requiring reduced crustal buoyancy to go unstable.

To isolate the effects of plate buoyancy on the peel-back delamination mechanism, Adams et al. (2022) did not consider the role of plume-rift interactions; however, rift zones on Venus may require this additional complexity. Small compensation depths [124] and a geoid gradient and stress field orientation consistent with a swell-push model [125] do not support the existence of a large broad-scale active upwelling below any of the large chasma; instead, chasmata may be strongly associated with localized plume activity, as evidenced by high heat flows [116] and a relatively high density of coronae at certain chasmata [124, 126]. While the mechanisms for corona formation are not well understood and may include non-plume origins [120, 127, 128], the majority of models attribute corona formation either directly or indirectly to interactions between the lithosphere and a mantle upwelling [18, 64, 111, 129, 130, 131, 132, 133, 134, 135, 136]. The next step in understanding delamination initiated at rift zones on Venus is to consider whether adding a rising mantle plume could destabilize the lithospheric mantle and trigger PBD in even younger, more positively buoyant plates than was possible for purely buoyancy-driven subduction. It is unclear how a plume would affect the mechanism of delamination initiation, and whether the outcome would be some form of delamination, subduction, or obstruction of lithospheric recycling due to the uplifting force of a rising plume.

In this study, we use 2D numerical models to investigate the dynamics of plume-rift

interactions and the consequences for delamination initiation. We systematically vary lithosphere thickness, crustal density, plume radius, and width of the rift zone to identify the conditions where peel-back delamination may be a viable mechanism for regional-scale lithospheric recycling within the context of the regional equilibrium resurfacing (RER) hypothesis. We propose a new framework for plume-assisted lithospheric recycling at rift zones on Venus which is primarily dependent on lithospheric thickness and plume radius. We then identify specific rift zones on Venus where our models indicate delamination may be most likely to occur.

3.2 Model Setup

We performed a series of 2D numerical simulations using StagYY, a finite volume code used to model planetary-scale convection problems [19, 66]. All post-processing and visualization was performed using StagLab 6.0 [67, 137]. Additional details of the code and model setup are described in Adams et al. (2022). Like Adams et al. (2022), the initial condition is a 180 degree half-spherical annulus geometry with a simplified rift zone, which is modeled as a horizontal lithospheric gap separating two plate edges with a maximum viscosity of 10^{24} Pa*s (Fig. 3.1). The lithospheric thickness to the left of the gap is varied between h_L = [150, 200, 250] km. To the right of the gap, the lithosphere is 100 km thick and gradually thickens to a value of h_L at a distance of 2100 km from the rift zone. We use a constant crust thickness (h_c = 30 km), but vary the compositional buoyancy of the crust with respect to the reference mantle density ($B_{crust} = \rho_{0,crust}$ - ρ_0 = [-265, -300, -350, -400] kg/m^3) to control crustal buoyancy. For example, 30 km of crust with B_{crust} = -265 kg/m^3 represents the same amount of crustal buoyancy as a 20 km crust with a density anomaly of B_{crust} = -400 kg/m^3. Previously in Adams et al. (2022), the gap was kept a constant width of L_{gap} = 250 km in order to minimize the stabilizing effect a smaller gap size could have on spontaneous, buoyancy-driven lithospheric recycling events. To further

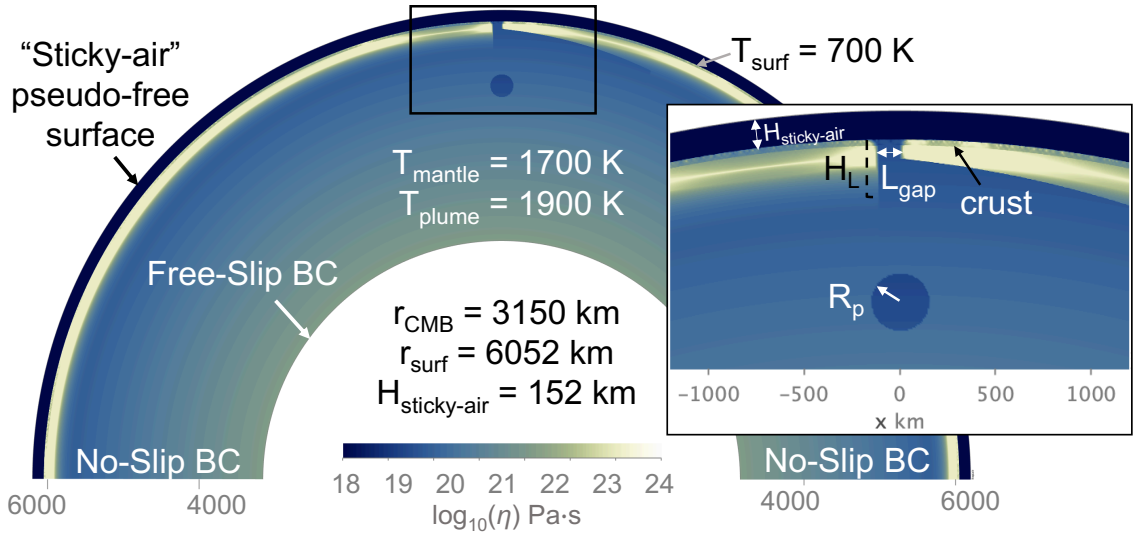

Figure 3.1. Initial model setup in the viscosity field. Rift width (L_{gap}) is varied between 60, 125, and 250 km, but shown here is a 125 km-wide rift gap (see Appendix B: Fig. 6.3 for further details). Plume radius (R_p = 150 km shown here) and lithospheric thickness of the left plate edge (H_L = 250 km here, defined by 1600 K isotherm) are also varied between models. The thickness of the plate edge to the right of the rift gap is fixed at 100 km and gradually increases to H_L over a distance of 2100 km from the rift. The distance from the surface to the top of the plume head is 700 km regardless of plume size. At the surface, a continuous layer of buoyant crust (H_c = 30 km) with variable density (B_{crust}) covers the lithosphere and the rift gap. Above the surface, 152 km of low-viscosity sticky-air is used as a pseudo-free surface boundary condition to allow the development of realistic topography.

investigate the role that rift zone geometry may play in delamination initiation, we now vary the width of the rift zone, L_{gap}, between 250, 125, and 60 km (Appendix B: Fig. 6.3), which is compatible with observations of chasma trench width on Venus [3, 68]. We ignore the effects of plume cooling as it rises through the warm mantle prior to reaching the surface, since the timescales of cooling are on the order of 100s of millions of years [132].

In order to better understand rift zone destabilization, we incorporated a purely thermal mantle plume below the gap. The radius of the plume, R_p, was varied in order to investigate a range of plume buoyancy forces. The buoyancy force, F_B, of a circular plume

is given as:

$$F_B = \pi R_p^2 \Delta\rho g \tag{3.1}$$

where g is gravitational acceleration and the density anomaly of a thermal plume, $\Delta\rho$, is defined by:

$$\Delta\rho = \rho_{p,0}\alpha\Delta T \tag{3.2}$$

where $\rho_{p,0}$ is the density of the plume at the ambient mantle temperature, T_m, α is the coefficient of thermal expansion, and ΔT is the temperature anomaly of the plume with respect to T_m. We hypothesize the buoyancy force of the plume will play an important role in destabilizing the lithosphere adjacent to the rift gap; however, it is important to keep in mind that a limitation of the 2D spherical annulus geometry (x,z) is that both the lithosphere and plume represent infinitely long features in the in the y-direction. As a result, our calculated plume buoyancy force is only an approximation. We adopt a modest temperature contrast of only 200 K, which may represent the small temperature drops that occur across the core-mantle boundary in stagnant-lid planets [138]. Although plume temperature could also be used to vary the plume buoyancy force, we used a constant mantle and plume temperature in order to maintain a constant viscosity contrast (T_m = 1700 K, ΔT = 200 K). The plume is always centered below the edge of the plate to the right of the gap, and the top of the plume head is initially positioned at a depth of 700 km to ensure a realistic plume shape and rise velocity as it encounters the lithosphere and rift zone.

3.3 Results

Of the 49 total models that were run, 32 models resulted in a plume-induced peel-back delamination event. These 32 delamination models described in the following sections are divided into 3 subgroups based on the ratio of plume radius to rift gap width,

R_p/L_{gap}. The remaining 16 models were classified in the stagnant-lid tectonic regime, which is characterized by a lack of significant horizontal or vertical surface displacement of the lithosphere throughout the model evolution. No other model outcomes were observed. A summary of the parameter space and model outcomes is given in Appendix B: Tables 6.1-6.2.

3.3.1 Plume-Induced Peel-Back Delamination

Type I: Plume Radius ≈ Gap Width

A representative plume-induced peel-back delamination event is shown in Fig. 3.2 for a reference model with a 250-km-radius plume rising into a 200-km-thick lithosphere with a 250-km-wide gap and a crustal density anomaly of B_{crust} = -300 kg/m^3. The following description of the model evolution applies to all plume-induced PBD models where plume radius is similar in magnitude to the rift zone width. The top of the plume head is initially located 700 km below the surface and is centered directly beneath the edge of the right plate edge (Fig. 3.2A-C). As the plume rises, it develops a distinct plume head-tail structure, which flattens as it encounters higher viscosity mantle material at the base of the lithosphere. When the plume reaches the base of the gap, a small separation between crust and lithospheric mantle can be observed at the top edge of the left plate. The induced mantle flow from the rising plume pushes the gap material into the weak crustal layer, which initiates decoupling (Fig. 3.2D-F). Like in buoyancy-driven PBD, yielding in the crust forms a weak zone delamination surface allowing decoupling to propagate along the Moho (Fig. 3.5). The plume head deforms as a portion of the plume rises directly into the gap, while part of the plume underplates the base of the right plate edge (Fig. 3.2G-I). The plume pushes into the left plate edge, but does not produce significant underplating of the lithospheric mantle as slab sinking progresses. Decoupling between the crust and lithospheric mantle continues, but it is still the ambient mantle from inside the gap rather than plume material that is wedged between them. The lithospheric mantle begins to peel

away, and the plume head spreads into the space between the remaining layer of crust at the surface and the upper boundary of the delaminating slab (Fig. 3.2J-L). The slab tip is deflected upward by the sources of positive buoyancy from phase changes beginning at 710 km depth (Fig. 3.2M-O) (see Adams et al. (2022) for details). The plate edge to the right of the gap (100 km thick) remained stable throughout all model evolutions.

In the early stages of decoupling, only a thin layer of crust approximately 5 km thick is attached to the down-going slab, while the majority of crust remains at the surface (Fig. 3.2I). As the edge of the plate bends downward into the mantle, a crustal root is formed at the slab hinge (Fig. 3.2L). The base of the crustal root undergoes the basalt-eclogite phase transition at 70 km depth, resulting in higher density crustal material and an increase in crustal recycling. Nevertheless, the majority of crust remains at the surface and is deformed near the rift zone to accommodate the formation of the crustal root and the migration of the trench. There were no observed cases where eclogite formation occurred and peel-back delamination did not continue. Slab sinking is moderated by Earth-like phase transitions in the mid-mantle, which consistently results in stress focusing and break-off of a moderate-sized slab ($\approx$ 2500 km in length). Slab break-off is the final stage of a peel-back delamination event, and related details are discussed in Adams et al. (2022).

Type II: Plume Radius < Gap Width

When the ratio R_p/L_{gap} is approximately less than or equal to 0.5, the stages of plume-induced PBD progression are slightly different than described above. Smaller plumes take longer to reach the gap than larger plumes with a higher buoyancy force. Once the small plume encounters the edge of the right plate, it is deflected almost entirely into the gap, rather than underplating the right plate (Fig. 3.3A). In some cases, the forces from the small plume entering the gap are able to induce crustal yielding and decoupling at the crust-mantle interface, which results in a similar evolution of peel-back delamination. The smaller plume diffuses into a very thin layer along the base of the crust, with the

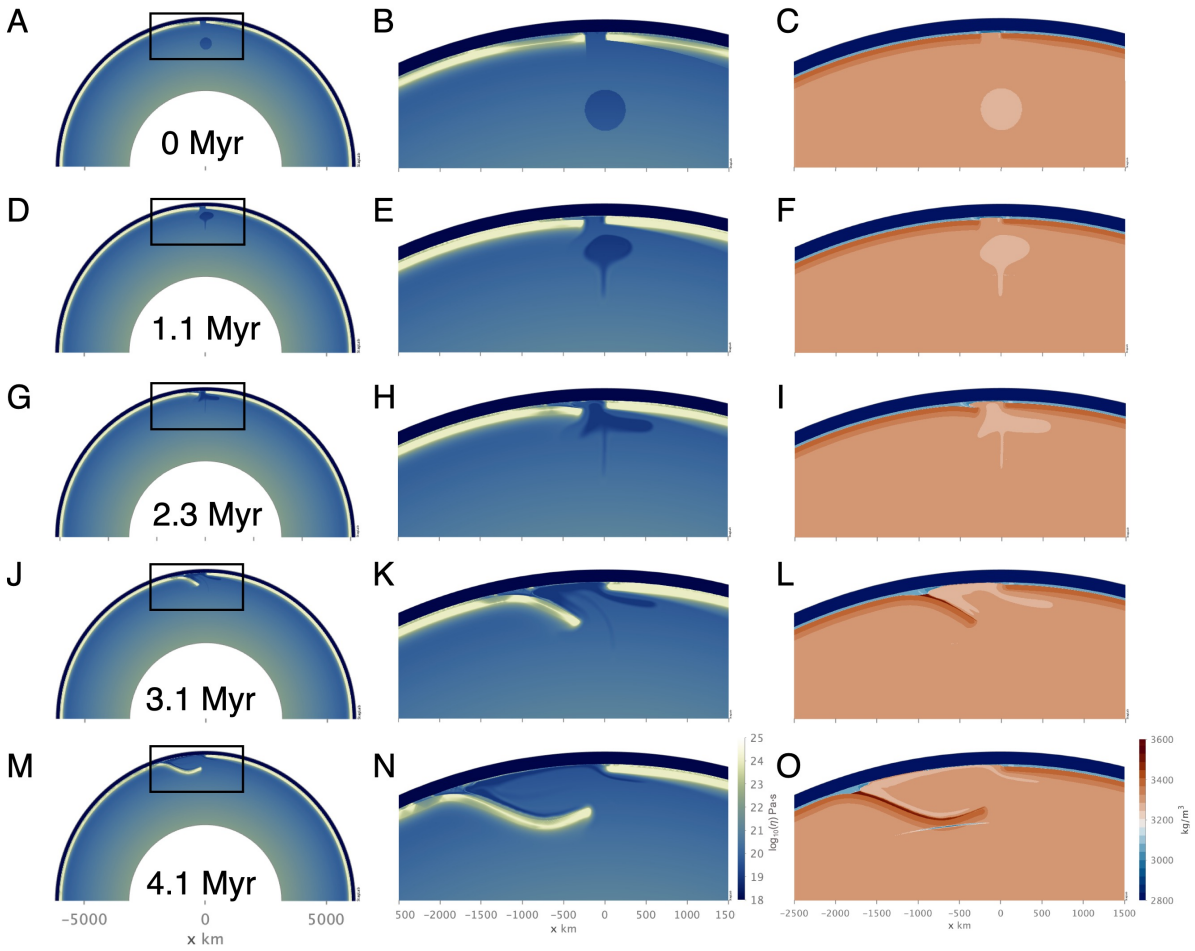

Figure 3.2. A typical plume-induced peel-back delamination event shown in the global viscosity field, local viscosity field, and local density field (h_L = 200 km, L_{gap} = 250 km, R_p = 250 km, and B_{crust} = -300 kg/m^3). (A-C) The initial condition shows the location of plume and lithospheric gap. (D-F) The plume rises and flattens as it encounters the lithosphere. (G-I) The lithospheric mantle continues decoupling from the crust as the plume head rises into the gap and spreads beneath the right plate edge. (J-L) The lithospheric mantle peels away from the surface and (L) eclogite formation (dark red) in the base of the crustal root (light blue) helps sustain slab sinking. (M-O) The slab tip is deflected upward by regions of positive buoyancy in the slab due to Earth-like phase transitions beginning at 710 km depth.

thickest layer of plume material being located above the plate hinge (Fig. 3.3D). Although some cases of small plumes initiating delamination have been observed, many result in a stagnant-lid.

Type III: Plume Radius > Gap Width

When the ratio R_p/L_{gap} is greater than or equal to 2, only a small portion of the plume can rise into the empty gap space (Fig. 3.3C). Whereas a small plume/large rift-gap combination only results in uplift of the right plate edge, a large plume also exerts an upward force beneath the delaminating plate edge when the gap is small. The positively buoyant excess plume material is spread beneath the lithosphere on both sides of the rift zone, further inhibiting plate bending and crustal yielding which is necessary for plate decoupling to occur; however, increasing plume size results in higher pressures in the gap which can facilitate decoupling at the base of the crust. Once decoupling begins, the excess negative buoyancy of the lithospheric mantle and eclogitized crust can drive the slab to sink despite the upward force on the plate edge from the plume. As the lithospheric mantle peels away, the large plume is spread into a relatively thick layer along the base of the right plate, the base of the crust in the gap, along the top of the delaminating slab, and around the slab tip.

3.3.2 Effects of Plume Radius, Gap Width, and Crustal Buoyancy on Delamination Initiation

In Adams et al. (2022), all positively buoyant plates with 200-km-thick lithosphere were stagnant-lid, unable to undergo buoyancy-driven peel-back delamination. In Figure 3.4, we present the tectonic regime outcomes of either plume-induced PBD (closed circles) or stagnant-lid (open circles) for various 200 km lithosphere models following interactions with a rising mantle plume. Using the same gap width as in Adams et al. (2022), L_{gap} = 250 km, relatively small plumes (R_p = 50 km) are unable to destabilize the rift zone, regardless of the crustal buoyancy of the plate (Fig. 3.4A). Plume-induced PBD is observed after increasing plume radius to 100 km, but only in plates with the least positively buoyant crust (B_{crust} = [-265, -300] kg/m^3). A stagnant-lid persists in models with lower density crust (B_{crust} = [-350, -400] kg/m^3), indicating positive crustal buoyancy has a stabilizing

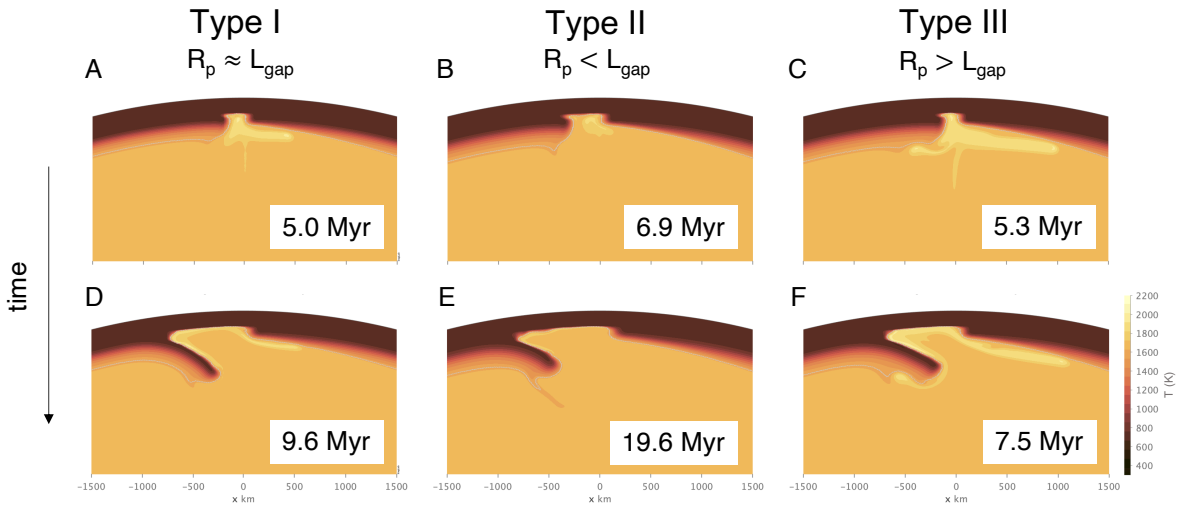

Figure 3.3. Temperature field progression of plume-induced peel-back delamination is given for the three types of plume-rift interactions. The 152 km-thick sticky-air layer covering the top of the lithosphere is the same temperature as the surface, and the top of the rift gap indicates the depth of the surface-air boundary. (A,D) Type I: plume radius is approximately equal to the gap width (R_p = 150 km, L_{gap} = 125 km) and there is only underplating of the right plate, (B,E) Type II: plume radius is much smaller than gap width (R_p = 75 km, L_{gap} = 250 km) and there is no underplating, and (C,F) Type III: plume radius is much larger than gap width (R_p = 250 km, L_{gap} = 60 km), and there is underplating of both plate edges. Note: Timing of delamination is also dependent on lithosphere thickness and crustal buoyancy, which is not constant between these three models.

effect on the rift zone. When the gap was large (L_{gap} = 250 km), plume-induced PBD was initiated for all plume radii greater than or equal to 150 km regardless of crustal buoyancy.

Gap width was held constant in previous models of buoyancy-driven delamination, but here we tested smaller gap sizes to determine its effect on rift zone stabilization. When gap width is decreased from 250 km to 125 km, a 150-km-radius plume which previously always initiated delamination now results in a stagnant-lid at the highest crustal buoyancies (B_{crust} = [-350, -400] kg/m^3) (Fig. 3.4B). Increasing the plume radius to 250 km can destabilize more positively buoyant plates than the 150 km plume (B_{crust} = -350 kg/m^3), but a stagnant-lid persists for the most positively buoyant crust (B_{crust} = -400 kg/m^3). For an even smaller gap width of 60 km, all plumes smaller than 250 km resulted

in a stagnant-lid outcome; only one model underwent plume-induced PBD, and it only occurred for a combination of the largest plume size (R_p = 250 km) and the least buoyant crust (B_{crust} = -265 kg/m^3). Collectively, these data show a trend between decreasing gap width and increasing rift zone stability, particularly in cases with more positive crustal buoyancy.

Notably, both stagnant-lid and plume-induced PBD outcomes were observed for all three types of plume-rift interactions (see sections 3.1.1-3.1.3). For an on-rift-axis plume, the style of plume-lithosphere interaction depends on the ratio of plume radius to gap width. A small plume rising directly into the gap (Type II) occurs when the R_p/L_{gap} ratio is small (<0.5) (Fig. 3.4A). A plume that underplates the right plate edge and only slightly encounters the left plate edge (Type I) occurs when the R_p/L_{gap} ratio is approximately 0.5-1.5 (Fig. 3.4A-B). When the R_p/L_{gap} ratio is greater than 1.5, the plume is large enough to underplate both sides of the rift while the upper part of the plume enters the gap (Fig. 3.4B-C). Although the R_p/L_{gap} ratio may characterize the style of plume-rift interaction, the actual tectonic outcome is depending on plume radius, gap size, and crustal buoyancy. For each of the three types of plume-rift interactions, increasing plume size, increasing gap width, and decreasing crustal buoyancy all facilitate plume-induced PBD. Although the relationship between R_p/L_{gap} and the different types of plume-rift interactions applies to a plume centered below the right plate edge, these results provide a general idea of how plume-rift dynamics depend on plume size and subsurface lithospheric structure (see also Appendix B: Fig. 6.4).

3.4 Discussion

3.4.1 Stagnant-Lid Scenarios

There are three scenarios that can result in a stagnant-lid outcome. The first is when the lithosphere is thin and lacks sufficient negative buoyancy in the sub-crustal

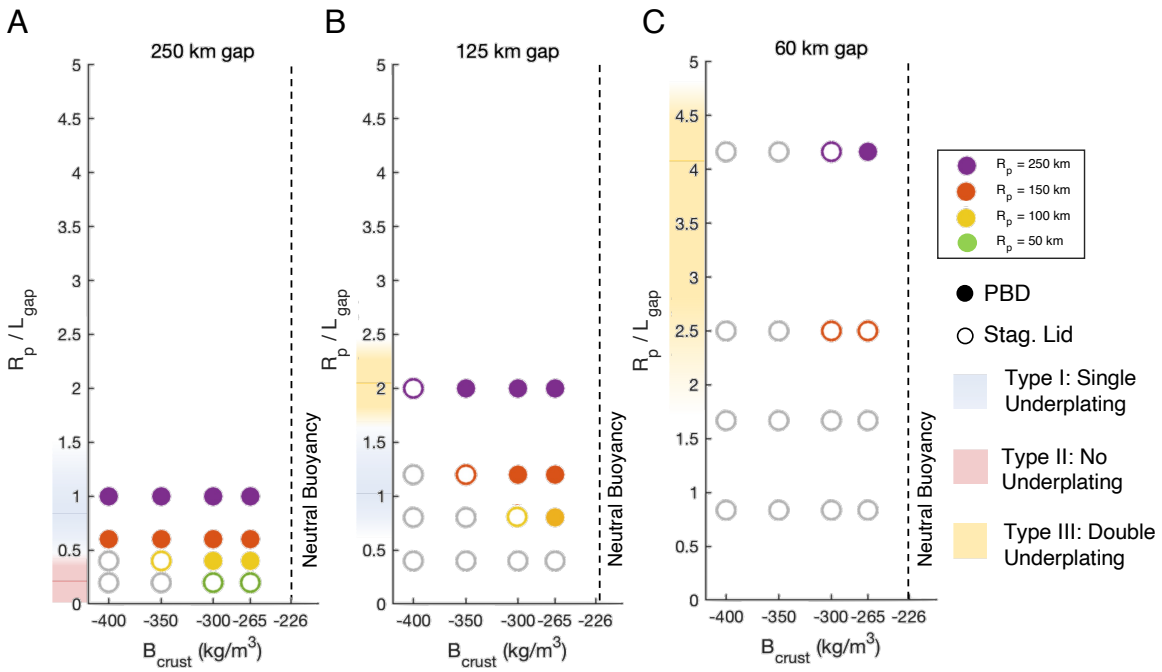

Figure 3.4. Model outcomes for 200-km-thick lithosphere with a (A) 250 km gap, (B) 125 km gap, and (C) 60 km gap plotted for the ratio of plume radius to gap width (R_p/L_{gap}) vs. crustal density anomaly (B_{crust}). Unfilled gray circles are models inferred to be stagnant-lid based on the stabilizing effect of decreasing gap size and increasing positive crustal buoyancy (i.e. if a model is stagnant-lid, increasing positive crustal buoyancy and/or decreasing plume size can also be expected to remain stagnant-lid. We can also assume that if a model did not delaminate with a 50 km-radius plume with a 250 km-wide gap, it will also not delaminate with a 125 or 60 km-wide gap.). Colors on the y-axis indicate the style of plume-lithosphere interaction; (blue) Type I: the plume and gap are similar in size and underplating occurs below the right plate edge only, (red) Type II: The plume is small and enters gap without underplating, and (yellow) Type III: the plume is larger than gap and underplates both plate edges. All plates are positively buoyant, and increasing distance from the line of neutral buoyancy represents increasingly positive net plate buoyancy.

lithospheric mantle to induce delamination, regardless of any added plume buoyancy forces. The majority of 150 km lithosphere models were stagnant-lid, with the exception of one model with an anomalously large plume (R_{plume} = 500 km) (see Appendix B: Fig. 6.5). This is also why the 100 km-thick lithospheric mantle to the right of the rift gap remains stable in all models. The second is a type II plume-rift scenario when the plume is small ($R_p \approx< 100$ km) and has an insufficient buoyancy force which is unable to drive

decoupling between the crust and mantle lithosphere. These models were typically run for several millions of years after the plume reached the surface and had been weakened by additional thermal diffusion. The third stagnant-lid scenario occurred in cases with type III plume-rift scenario, where PBD was inhibited by a combination of high positive plate buoyancy (thinner lithosphere and/or more positively buoyant crust) and extensive plume underplating. The plumes remained in the gap and beneath the plate edges for millions of years after reaching the surface while continuously eroding the base of the lithosphere. These models were run until it was clear that thermal erosion had removed substantial negative buoyancy from the mantle lithosphere, which is a requirement for delamination to occur.

3.4.2 Viability of Plume-Induced Delamination on Venus

The thickness of the lithosphere is arguably the most important factor in determining whether peel-back delamination can occur or if the rift will remain in a stagnant-lid regime. Both buoyancy-driven and plume-induced PBD are primarily driven by the excess negative buoyancy of the lithospheric mantle, which becomes more negatively buoyant with increasing plate thickness and age. Adams et al. (2022) found that in buoyancy-driven PBD, bending of the dense lithospheric mantle induces extensional stresses in the overlying crust near the plate edge. When the stresses exceed the yield strength of the crust, the viscosity of the crust is reduced to an effective viscosity, forming a weak delamination surface which allows decoupling to propagate. Due to enhanced bending stresses, the thickest plates (300 km) were always able to undergo buoyancy-driven PBD without plume-assisted destabilization despite having a net positive plate buoyancy [123]. Plume-induced PBD is initiated via the same mechanism of crustal yielding as buoyancy-driven PBD, and plume-rift interactions can increase crustal stresses and facilitate decoupling compared to models without a plume (Fig. 3.5). Here, we found that 150-km-thick lithosphere did not delaminate for plumes (+200 K) up to 400 km in radius. The 150- and 300-km-thick

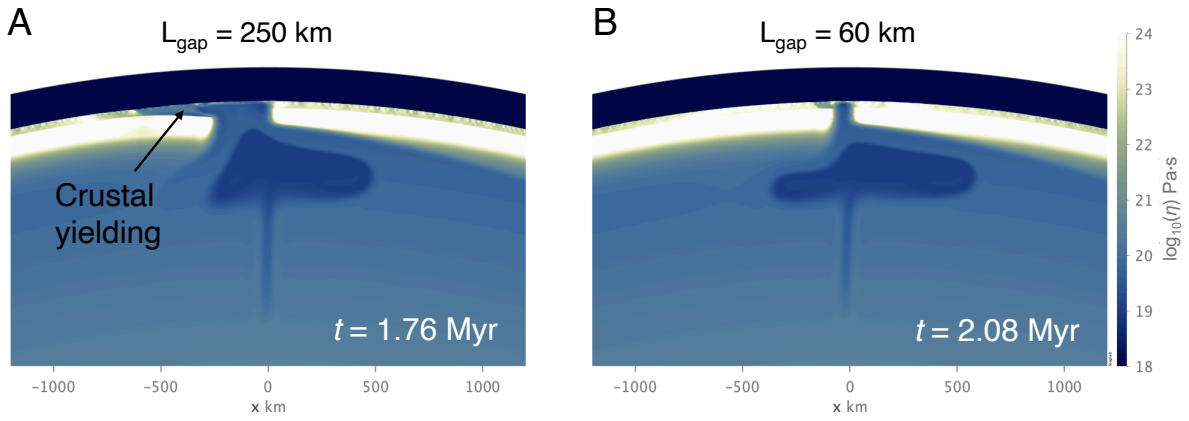

Figure 3.5. Delamination initiation requires crustal yielding and weakening above the delaminating plate edge to allow decoupling to propagate along the Moho (see Adams et al. (2022) for details). (A) For a 250 km-wide rift gap, there is minimal spreading of the plume beneath the delaminating plate. The plate edge is able to bend and induce stresses in the overlying crust which exceed the yield stress, and this allows delamination to progress, despite being stagnant-lid in the absence of plume interactions [123]. (B) For a smaller gap width (60 km) and an increasing R_p/L_{gap} ratio, enhanced underplating of the buoyant plume exerts an upward force on the plate edge from below. This inhibits plate bending and crustal yielding, which ultimately results in a stagnant lid. The two models are identical (R_{plume} = 250 km, h_L = 200 km, B_{crust} = -265 kg/m^3) with the exception of gap width.

lithosphere may represent minimum and maximum threshold values, respectively, which constrain the conditions where plume-induced PBD may operate for these rift geometries. The threshold thicknesses may shift to higher values depending on the structure of the rift zone, since narrowing gap widths has a stabilizing effect on the rift margin.

In this study, we focused on the range of lithosphere thicknesses where plume-induced PBD is most likely to operate. The model outcomes for 200- and 250-km-thick plates are shown in the parameter space of plume buoyancy force (F_B), a destabilizing force, vs. the integrated density contrast between the plate and underlying mantle ($\Delta\rho_{plate} = \int_0^{h_L}$ ($\rho(z)$ - ρ_0) dz), which represents net plate buoyancy (Fig. 3.6). Multiple regime boundaries are plotted as solid black lines based on gap width, where models above and to the right of the regime boundary are PBD. The dotted lines in Figure 3.6A are representative of an extrapolated regime boundary, based on evidence that positively buoyant plates can

remain stagnant-lid for gap widths less than 250 km (Fig. 3.6B), although the exact shape of the regime boundary there is still unknown. Figure 3.6A shows that for the same gap width and crustal buoyancy, 200-km-thick plates require higher plume buoyancy forces for destabilization than the 250-km-thick plates in Figure 3.6B. Decreasing the gap width to 60 km has a stabilizing effect, particularly when combined with smaller plumes and more positively buoyant crust. Plume-induced PBD becomes less likely to occur with decreasing gap size, both due to the stabilizing nature of a more narrow weak zone and the increased probability that plume-rift interactions will result in underplating and uplift. As predicted, the 250 km lithosphere models undergo delamination more readily due to having a more negatively buoyant lithospheric mantle. The majority of 250 km lithosphere models (B_{crust} = [-265, -300, -350] kg/m^3) with a 250 km-wide gap did not require a plume for delamination to occur. Only a relatively small plume (R_p = 75 km) was necessary to destabilize the remaining stagnant-lid model (B_{crust} = -400 kg/m^3).

The relationship between positive plate buoyancy and the required plume buoyancy force to destabilize the rift is quasi-linear, indicating a force balance when the gap is large (L_{gap} = 250 km, Fig. 3.6A) and there are minimal direct interactions between the plume and the left plate edge (Fig. 3.4A). However as the gap width is decreased to 125 km, the required plume buoyancy force for delamination increases exponentially with increasing positive crustal buoyancy (decreasing $\Delta\rho_{plate}$). The change in the slope of the required buoyancy force may be a reflection of the shift from Type II to Type I and Type III plume-lithosphere interaction scenarios. When the plumes are relatively small (F_B <10), there is no underplating or uplift below the delaminating plate edge (Type II). As the radius of the plume increases (F_B=12.5, R_p=150 km), the plume exerts a small upward force on the delaminating plate edge (Type I, Fig. 3.3B). Although underplating alone is not sufficient to prevent delamination initiation, the combination of positive crustal buoyancy and plume uplift effectively work together to inhibit plate bending. When the plume is even larger (F_B=34.6, R_p=250 km), there is extensive uplift beneath the

delaminating plate edge (Type III, Fig. 3.3C). At this point, the slope of the regime boundary is much steeper, showing that positive crustal buoyancy has a more significant stabilizing effect when there is more underplating.

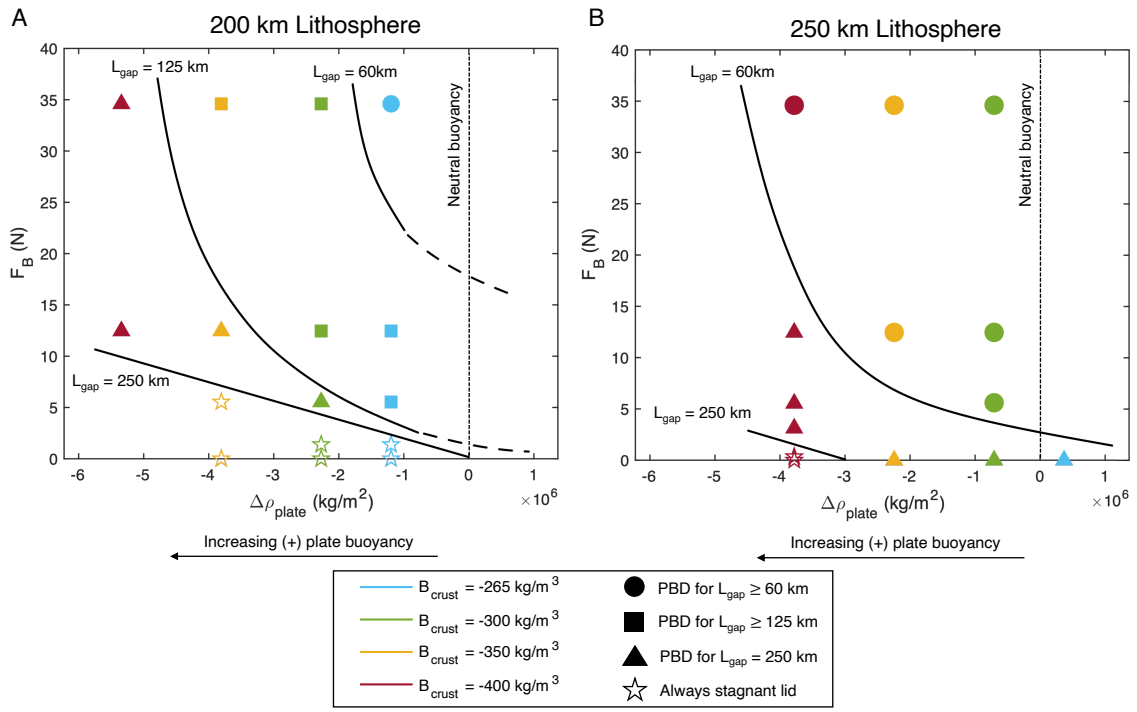

Figure 3.6. Tectonic regime diagrams for (A) 200-km-thick lithosphere and (B) 250-km-thick lithosphere. Solid lines indicate estimated location of regime boundaries. Dotted lines indicate extrapolated estimation of regime boundary behavior, based on evidence that negatively buoyant plates can also remain stagnant-lid when gap width is small and crustal buoyancy is weak. For reference, the outcomes of the non-plume models from Adams et al. (2022) are plotted along $F_B = 0$. The vertical dotted line at $\Delta\rho_{plate}$ is the line of neutral plate buoyancy - a negative $\Delta\rho_{plate}$ corresponds to a plate with a net positive integrated buoyancy. Without a plume, the most positively buoyant plate to undergo buoyancy-driven PBD had a $\Delta\rho_{plate}$ of -2.24 kg/m^2 [123], but plume-induced PBD was observed for significantly more buoyant plates up to $\Delta\rho_{plate}$ = -5.34 kg/m^2.

3.4.3 The Progression of PBD Mechanisms with Plate Age

In the absence of significant lithospheric extension or compression, the thickness of the lithospheric thermal boundary layer is primarily dependent on the age of the plate. We find that plume-induced peel-back delamination is less likely to occur when the lithosphere

is less than 150 km thick, which corresponds to a plate age of 130 Myr as defined by an error function describing the lithospheric temperature profile. Buoyancy-driven PBD may be the dominant lithospheric recycling mechanism when the lithosphere is 300 km thick, or 625 Myr old, due to the significant negative buoyancy in the lithospheric mantle. Plume-induced PBD may be most applicable to zones of lithosphere on Venus that are between 130-625 Myr old and near a pre-existing weak zone, though plume destabilization may also be relevant for older lithosphere with more narrow, stable rift structures. Here, we modeled plume-induced PBD in lithospheres that were 300 and 450 Myr old (200 and 250 km thick, respectively). We observed that a larger plume was required to initiate PBD in younger, thinner lithosphere than in thicker lithosphere with more negative thermal buoyancy (Fig. 3.6).

A large fraction of coronae on Venus may be preferentially associated with thin, rifted lithosphere [119, 116, 139]. However, our results suggest that the peel-back delamination mechanism may not operate on Venus until the plate is moderately thick, corresponding to a minimum age between 130-300 Myr old depending on the radius of the plume. In Figure 3.7, we provide an interpretive summary of our results. If the lithosphere is younger than the minimum age and/or thinned via rifting, we expect no or minimal lithospheric recycling. As the lithosphere ages and thickens, or if a thick plate is weakened due to uplift-related lateral fracture propagation [3], we expect plume-lithosphere interactions to preferentially result in peel-back delamination. However, if the plate is near the minimum threshold age for PBD, a larger plume buoyancy force (i.e. larger plume radius) is required to initiate delamination (Fig. 3.7A-C). As the lithosphere continues to age and thicken, smaller plumes with less buoyancy force can destabilize the lithosphere and initiate PBD because the driving force of PBD is greatly enhanced by increasing lithosphere thickness (Fig. 3.7D-I). Eventually when the lithosphere reaches the maximum threshold age between 450-625 Myr old, a plume will no longer be required, and buoyancy-driven PBD will be the dominate recycling mechanism provided the weak zone in the lithosphere persists (Fig.

3.7J-L).

3.4.4 Potential Delamination Sites on Venus

A global map of coronae locations show a relatively high concentration near the Beta-Atla-Themis (BAT) region where these three large volcanic rises are connected by three major rift zones: Parga, Hecate, and Devana Chasma (Fig. 3.8A). Of the >500 coronae on Venus' surface, 131 are found in the Parga Chasma region [68]. In theory, a high density of coronae may facilitate PBD initiation due to enhanced lithospheric perturbation; however the results of this study and Adams et al. (2022) demonstrate that sufficient negative buoyancy from a thick lithospheric mantle is the primary requirement for PBD. Low elastic thicknesses and higher than average heat flow estimates in the Parga rift zone and nearby coronae indicate that the lithosphere is thin with respect to a global average thickness of 70 km +/- 47.3 km [116]. The trench geometry in the Parga Chasma system is highly variable, with trough widths measured between 80-200 km in the easternmost main branch and 50-250 km in the overlapping branches in its western end [68]. Given that the minimum threshold lithosphere thickness to undergo PBD in our models is approximately 150-200 km (for R_{plume}<=250-500 km, L_{gap}<=250 km), Parga Chasma is unlikely to undergo regional-scale PBD in the near future despite its high density of coronae.

Of the possible subduction sites proposed by Schubert and Sandwell (1995), the Dali-Diana Chasmata system has the highest estimated plate bending moments (12.9e16 N, 12.4e16 N) and relatively high elastic thicknesses (34.3 km, 22.5 km) [3]. Within the Dali-Diana system, Artemis Corona and Atahensik (Latona) Corona also have relatively high plate bending moments (4.7e16 N, 6.4e16 N) and elastic thicknesses (34.6 km, 34.3 km) indicative of thicker lithosphere, thus making Dali and Diana Chasmata good candidates for PBD. Although there are fewer coronae in this region overall when compared to Parga Chasma (Fig. 3.8A), this may be due to a filtering effect of the thicker lithosphere rather than an absence of mantle upwellings. Topography and lithospheric flexure surrounding

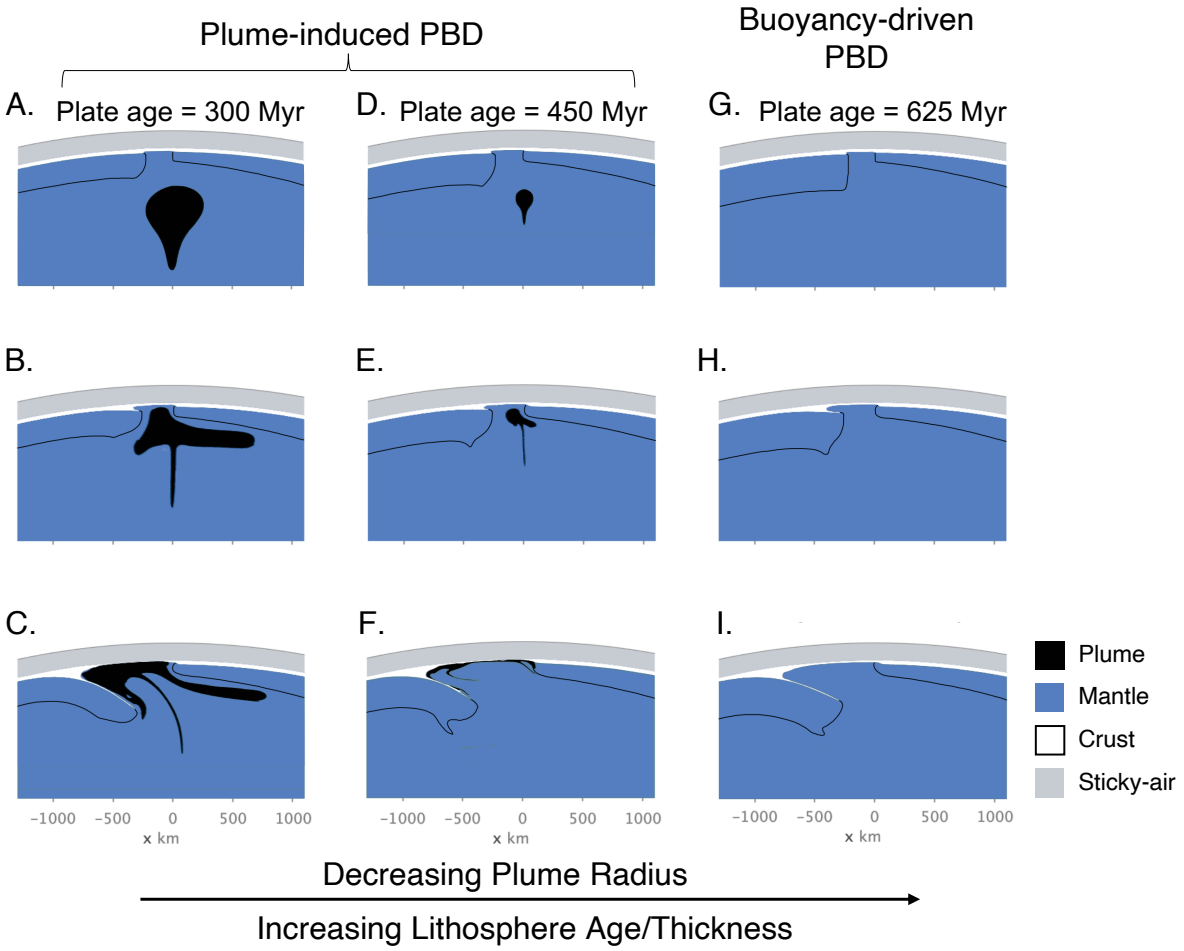

Figure 3.7. The dominant peel-back delamination mechanism on Venus progresses from plume-induced to buoyancy-driven with increasing plate age. (A-C) Plume-induced delamination may occur once the minimum plate thickness has been reached (between 150-200 km thick, 130-300 Myr old) so that there is sufficient negative buoyancy in the lithospheric mantle. A larger plume buoyancy force is required to destabilize younger, less negatively buoyant plates (Fig. 3.6). (D-F) As the plate ages and the lithospheric mantle becomes more negatively buoyant, comparatively smaller plumes can initiate PBD. (G-I) As the plate reaches 300 km thick (approximately 625 Myr old) a plume is no longer necessary to initiate delamination, since the lithospheric mantle is sufficiently dense to be gravitationally unstable in the absence of a plume perturbation. Plates thicker than 300 km can be expected to undergo buoyancy-driven delamination in the presence of a lithospheric weak zone.

Artemis Corona, the largest corona on Venus, indicates that it is a site of rollback lithospheric recycling where the trench is migrating radially outward to the south of Diana Chasma (Fig. 3.8B) [2, 10], similar to the rollback delamination process shown by our models of PBD. A major feature of the highly deformed interior of Artemis is a band of lineated fractures inferred to be extensional rifting [140, 141], and similar features have been generated in analogue experiments of plume-induced subduction via magmatic loading [64]. Interestingly, we also observe crustal thinning and extensional rifting in the interior of the delaminated zone due to slab rollback and trench migration (Fig. 3.8C). More work will be needed to model PBD in three dimensions to fully analyze surface topography and compare to Artemis Corona.

In our models, we implemented an asymmetrical lithospheric thickness across the rift zone so that the positive buoyancy of the thinner lithosphere would prevent a second concurrent delamination event from complicating our understanding of the delamination process. The results of this study and Adams et al. (2022) show that increasing the net positive buoyancy of the lithosphere inhibits delamination initiation, so by thinning the lithospheric mantle across the rift zone, we effectively removed negative buoyancy from the system. Opposite the rift zone from Artemis Corona, a large crustal plateau called Thetis Regio likely has a similar effect. Thetis Regio comprises a large portion of Aphrodite Terra, which is the largest highland terrain on Venus and is inferred to pre-date the formation of the Dali-Diana rift system [142, 143]. The thickened crust on this side of the rift contributes significant positive buoyancy to the lithosphere which would likely inhibit delamination initiation - similar to the effect of thinning the lithospheric mantle. As a result, delamination initiated at this section of Diana Chasma would likely only progress into its southern adjacent lithosphere rather than north into Aphrodite Terra.

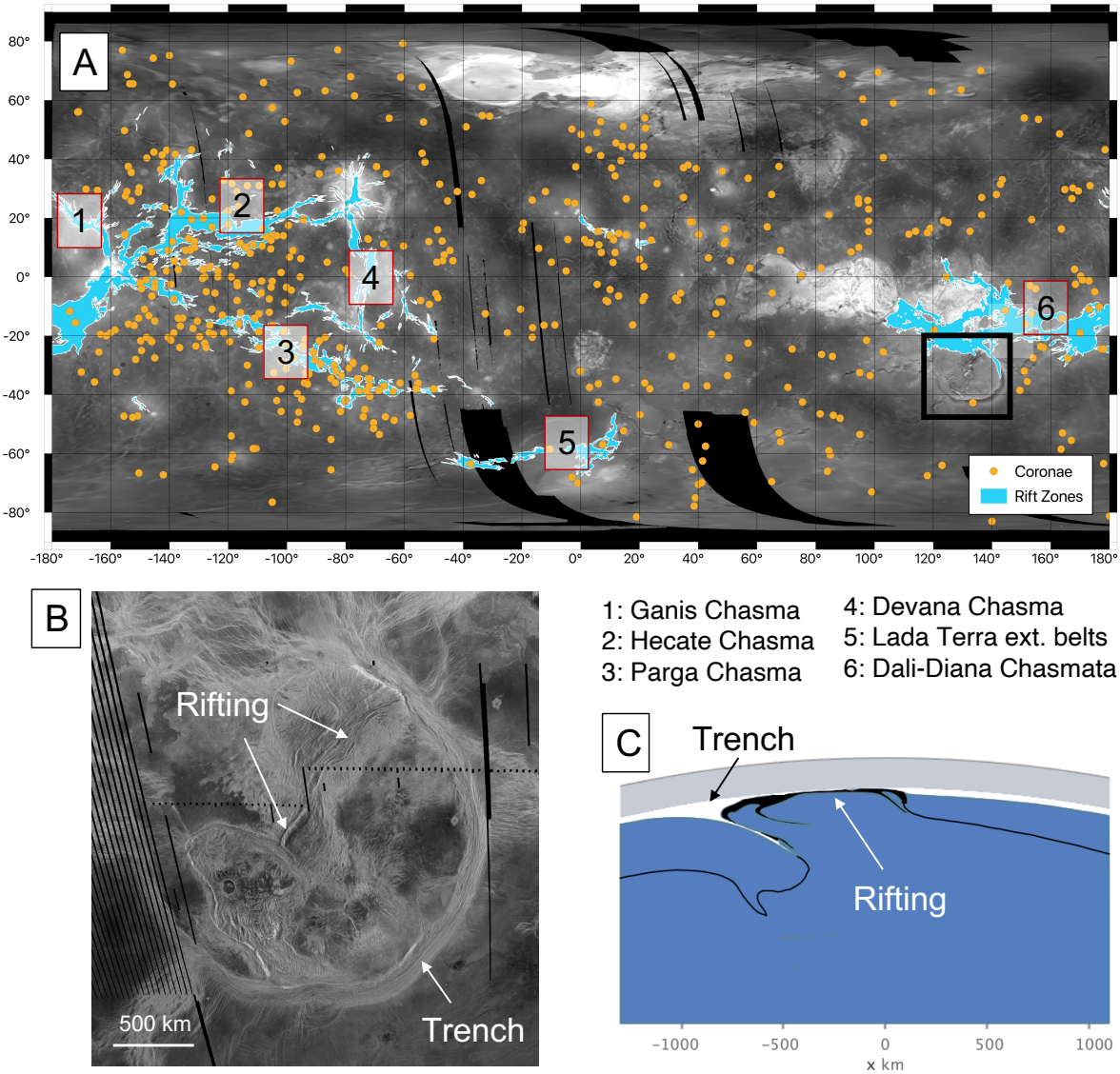

Figure 3.8. (A) Magellan global topography showing rift zones [144] and approximately 500 coronae locations [135]. Six of the largest rift zones are labeled, 5 of which contain chasma trenches. The black box denotes Artemis Corona shown in (B). Artemis is characterized by a large arcuate trench thought to have migrated radially outward; it surrounds a highly deformed interior divided by linear bands of rifting. (C) In comparison, modeled plume-induced PBD events also display trench retreat causing rifting of thinned lithosphere in the center of the newly delaminated area (Fig. 3.7F).

3.4.5 Significance of Crustal Assumptions and Uncertainties

Constraining the thickness, density, and composition of Venus' crust is crucial to determining the viability of potential mechanisms of lithospheric recycling. Negative

buoyancy in the lithospheric mantle is a driving force for all proposed forms of lithospheric overturn, whether it occurs regionally (buoyancy-driven PBD, plume-induced PBD, plume-induced subduction) or globally (catastrophic overturn). Similarly, a relatively thick layer of low-density crust on Venus may inhibit all proposed mechanisms of lithospheric recycling by increasing the positive buoyancy of the plate. To account for heterogeneity in crustal thickness [11, 12, 65], we varied crustal density over a range, B_{crust}, which gives a net positive buoyancy representative of various combinations of compositional density and crustal thickness.

Still, an incomplete understanding of Venus' crustal composition may lead to further uncertainties - in particular the depth of the basalt-eclogite transition. The formation of eclogite not only adds negative chemical buoyancy to the already negatively buoyant lithospheric mantle, but also removes positive buoyancy from the remaining layer of basaltic crust, thereby making it an important feature of lithospheric recycling on a potentially thick-crust planet such as Venus [145]. The few measurements of Venusian crust taken from the Venera 13, Venera 14, and Vega 2 missions indicate that the bulk composition of the crust at the landing sites resembles terrestrial basalt [146, 147, 148]. However, uncertainties in both the composition as well as unknown parameters such as water content and oxygen fugacity can produce large variations in calculations of the Venusian basalt stability field, and subsequently, the depth of the basalt-eclogite transition. Variations in thermal gradient near rift zones [116] may also support a complex basalt-eclogite transition. Several recent studies of resurfacing on Venus have approximated the eclogite transition using experimental data of a tholeiitic Earth basalt stability field with a positive Clapeyron slope of ≈ 1.76 MPa/K [92], which yields a gradual eclogite transition depth beginning as shallow as 20-40 km [18, 36]. Conversely, Venus' high surface temperature combined with a shallow thermal gradient may cause eclogite formation to occur deeper in Venus' mantle than within Earth [11]; it has been estimated to occur between 50-70 km depth and is often approximated an instantaneous density jump ($\gamma = 0$ MPa/K) near these depths

[21, 23, 24, 73]. More recently, P-T density maps calculated from the Vega 2 composition which assume full water saturation show a gradual transition to eclogite beginning at approximately 70 km depth and continuing at deeper depths [149]. Here, we chose to model the eclogite transition as an instantaneous density jump ($\Delta\rho = 420$ kg/m^3, $\gamma = 0$ MPa/K) at 70 km depth, which helps sustain delamination but does not play a role in the early stages of its initiation. Going forward, it will be important to consider variations in the depth of the basalt-eclogite transition in order to understand the style and scale of lithospheric recycling possible for Venus. Depending on the local thermal gradient, the depth of the crust may overlap with the eclogite transition depth and result in shallower eclogite than previously expected. This would strongly affect the net lithospheric buoyancy which would have significant implications for the proposed modes of lithospheric recycling.

Lastly, the yield strength of the crust is another parameter which is heavily debated, though not well constrained. We assume a weak crustal rheology [36, 70, 71, 72, 93] consistent with the effects of Peierls creep of a plagioclase rheology at the brittle-ductile transition [34, 35]. Yet in addition to experimental data supporting a relatively strong (yet weak compared to olivine) crustal rheology [8], numerical models of rift formation on Venus may also require a strong crust [150]. Though the peel-back delamination mechanism as we have modeled is reliant on the existence of a weak crustal layer ($C_0 = 10$ MPa), delamination events on Earth are thought to result from a variety of mechanisms other than crustal yielding, including melting and thermal weakening near the crust-mantle boundary [94, 95]. Intrusive magmatism in Venus' lithosphere [32] may also facilitate full or partial lithospheric decoupling. The magmatic effects of plume-lithosphere interactions on Venus will also play a role [151], however this is not within the scope of this study.

3.5 Conclusions

Compared to buoyancy-driven peel-back delamination [123], delamination initiated by plume-rift interactions was found to be viable for thinner, more positively buoyant lithosphere on Venus. Though both mechanisms can result in recycling of positively buoyant lithosphere, the upward force from a rising plume increases stresses in the crust adjacent to the rift gap, which facilitates decoupling of the lithospheric mantle from the overlying crust. Like buoyancy-driven PBD, plume-induced PBD is driven by the negative buoyancy of the lithospheric mantle and inhibited by positive crustal buoyancy. Increasing the plume buoyancy force by increasing plume radius is shown to have a destabilizing effect on the rift margin, particularly when the width of the rift is large. However, increasing plume size with a smaller rift width can cause a range of underplating scenarios which can hinder delamination initiation. Though the positive buoyancy of the crust alone may not be sufficient to prevent destabilization of the lithospheric mantle, an underplating plume may contribute to stabilization by uplifting the plate edge from below. The combination of underplating and high positive crustal buoyancy results in a stronger resisting force to delamination, and a stagnant-lid may persist.

Systems of fractures in rifted lithosphere on Venus are an ideal environment for peel-back delamination to occur, because there is a pre-existing lithospheric weakness. We propose a new age-dependent framework for regional-scale lithospheric recycling at rift zones on Venus which includes both plume-induced and buoyancy-driven peel-back delamination. A young or recently thinned lithosphere may not be sufficiently negatively buoyant to undergo spontaneous PBD, but may be destabilized by a plume with a large buoyancy force. Yet as the plate ages and thickens, little or no plume interaction is needed to destabilize the rift margin. This indicates a certain inevitability of recycling rift-adjacent lithosphere via delamination processes, provided a weakness in the lithosphere persists. Although the rift margin may heal as the lithosphere ages and thickens, increasing plume buoyancy

force is shown to drive destabilization in narrower, more stable margins. Plume-induced fracturing of off-axis lithosphere may be another mechanism of introducing weakness in thicker lithosphere [3], which can provide a starting point for future delamination events. Our models provide a rough estimate of the amount of time a lithospheric weakness could exist before being destabilized by a direct encounter by a rising mantle plume. Due to potentially large variability in crust and lithosphere thickness, rift structure, and expected plume buoyancy force, different forms of peel-back delamination may operate independently at different times and in different locations on Venus. Currently, the Dali-Diana Chasmata system may be an ideal environment for delamination to occur due to its thick adjacent lithosphere. Rollback lithospheric recycling and internal rifting at Artemis Corona south of Diana Chasma may be evidence of a modern peel-back delamination event on Venus.

3.6 Acknowledgments

The authors are thankful for support from NASA Award 80NSSC22K0100. Computational resources were provided by Extreme Science and Engineering Discovery Environment (XSEDE), which is supported by National Science Foundation grant number ACI-1053575. H.M. was supported by Computational Infrastructure for Geodynamics (CIG) which is supported through National Science Foundation award NSF-21491256. The authors would like to thank A. Davaille, J. Schools, and A. Gülcher for helpful discussions, and F. Crameri and H. Harper for technical support. We would also like to thank C. Thieulot and O. Göğüş for helpful reviews.

Chapter 3, in full, is a reprint of the material as it appears in Journal of Geophysical Research: Planets: Adams, A. C., Stegman, D. R., Mohammadzadeh, H., Smrekar, S. E., Tackley, P. J. (2023). Plume-induced delamination initiated at rift zones on Venus. Journal of Geophysical Research: Planets, 128, e2023JE007879.
https://doi.org/10.1029/2023JE007879. The dissertation author was the primary investi-

gator and author of this paper. See ref [152] for available data.

Chapter 4

Modeling Peel-Back Delamination on Venus in Three Dimensions

4.1 Introduction

Nearly ten thousand kilometers of subduction sites on Venus have been proposed at certain annular-rim features called corona and at rift zone trenches called chasmata [3]. Although there are approximately 500 coronae of variable size and potentially differing origin [10], those with the most similarities to subduction on Earth are often found in lithosphere with large bending moments and elastic thicknesses [2, 10]. When compared to subduction zones on Earth (e.g. Aleutian trench, Chile trench, South Sandwich trench), several coronae on Venus (e.g. Artemis, Quetzlpetlatl, Latona, Eithinoha etc.) exhibit similarities in topographic flexural response [2]. At subduction zones on Earth, higher bending moments are the result of increased negative buoyancy and therefore relatively thick lithosphere.

Given the correlation between corona proposed to be subduction sites and the lithospheric fractures at chasmata trenches, it is possible that thicker lithosphere may be destabilized at these pre-existing weaknesses. Adams et al. (2022) first tested the viability of lithospheric recycling initiated at Venusian chasmata and found that instead of subduction, delamination may be the favored tectonic regime to recycle 250-300 km net positively buoyant lithosphere [123]. "Peel-back delamination" (PBD) is a form

of lithospheric recycling where negatively buoyant lithospheric mantle decouples from overlying positively buoyant crust and is recycled into the mantle. Using 2D numerical models, Adams et al. (2022) identified that PBD is driven by negative plate buoyancy (i.e. lithospheric mantle thickness) and inhibited by positive crustal buoyancy and increasing plate strength. In Adams et al. (2023), interactions between fractured lithosphere and a rising mantle plume were shown to destabilize even thinner, more positively buoyant plates. These 2D models showed that decreasing crustal buoyancy, increasing plume size and increasing chasma trench width facilitated PBD initiation in lithosphere as thin as 150-200 km [153].

Yet since all current delamination models are two-dimensional, it is still unclear if and how PBD will operate in three dimensional models and over what spatial and temporal scales. Lateral variations slab morphology in 3D may affect the buoyancy of the slab (e.g. how much crust is eclogitized and where), and it is unknown how this will affect slab sinking dynamics. Extending mantle flow associated with delamination to three dimensions also has implications for slab sinking rates and slab break off dynamics. Laboratory models of retrograde subduction in 3D show poloidal and toroidal components to mantle flow, which result from viscous coupling between the slab and the mantle and lateral slab migration, respectively (Fig. 4.1) [154]. The lateral toroidal component of mantle flow was unable to be studied using 2D models, but is thought to be 3-4 times larger than the poloidal component which dominates mantle flow in 2D [108, 155]. The toroidal component has been shown to strongly affect slab morphology during rollback lithospheric recycling [156, 157]. In addition to the buoyancy and viscosity contrasts between the slab and mantle, slab width in 3D may also affect trench retreat rate and mantle flow velocities [108, 154].

Adams et al. (2023) identified that based on rift zone locations and inferred relative lithospheric thicknesses, delamination is most likely to initiate near the Dali-Diana chasmata region. Artemis Corona in particular was identified as the surface expression of a

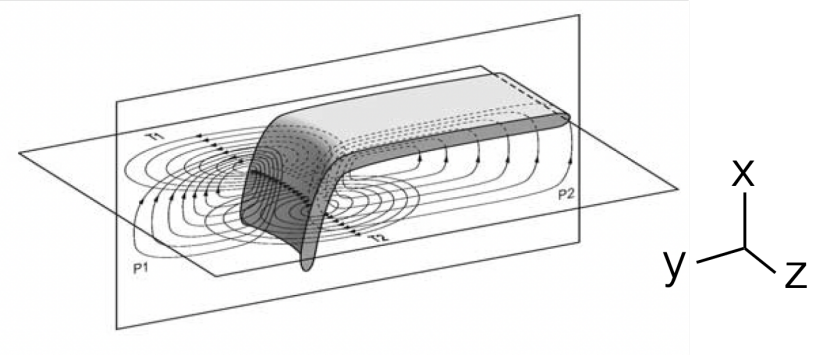

Figure 4.1. A schematic sketch of the poloidal and toroidal components of mantle flow expected during 3D retrograde subduction. Two poloidal flow cells dominate in the x-y plane and two toroidal flow cells surround the lateral slab edges in the y-z plane. Poloidal and toroidal components interact in front of and behind the slab during rollback. Adapted from Fig. 10 in Schellart et al. (2004).

possible peel-back delamination event. If delamination occurs in 3D, how much lithosphere can be recycled in one delamination event? Is PBD is a mechanism of corona formation or if the resulting surface expression is something else entirely? The following chapter seeks to answer these questions by building and analyzing three dimensional models of lithospheric recycling at chasma rift zones on Venus. The results expand on the 2D parameter studies which have helped guide intuition for which conditions are most likely to result in delamination.

4.2 Methods

A series of 3D numerical models were created using the finite volume code, StagYY [19] and visualized with VisIt. StagYY solves the Stokes equations for highly viscous flow over a three dimensional grid space. The reference model presented here has a grid resolution of 256x512x256 in a spherical geometry and contains a minimum of 20 tracer particles per grid cell. The lateral model domain is (π,π/4) in the (y-z) plane, and covers a radial domain of 2902 km from the surface of the crust to the core mantle boundary. Whereas the 2D sidewall boundary conditions were no-slip in order to mimic three dimensional resistance to plate motion, we now utilize reflecting sidewall boundary

conditions to extend the model domain and limit boundary effects. A 152 km "sticky-air" upper boundary condition allows topography to develop at the surface.

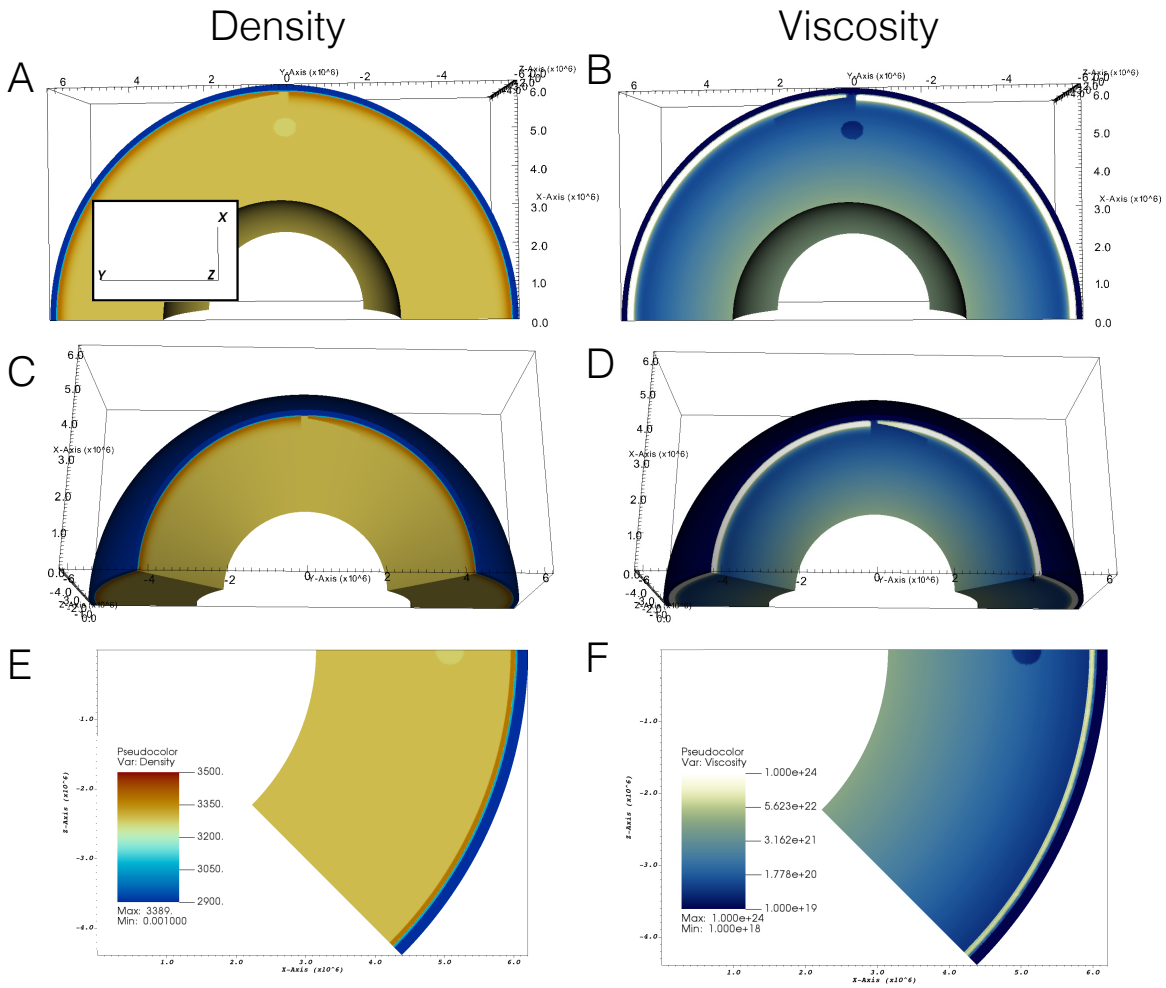

Figure 4.2. Density (A,C,E) and viscosity (B,D,F) of initial model setup of 3D rift-plume geometry at $t = 0$. (A,B) A view of the equatorial plane identical to the model setup of Chapter 3 (see Fig. 3.1 for additional details about model setup). The maximum lithosphere thickness is 300 km and all other variables can be found in Table 4.1. The model uses reflecting boundary conditions across this (x,y) plane because the plume and rift geometry is fully symmetric. (C,D) A view of the back of the model domain showing the extent of the rift gap. (E,F). A slice through the (x,z) plane at y = 0 through the center of the gap to show the full plume geometry. The edge of the thinned 100 km lithosphere is visible below 30 km of crust. A layer of low viscosity "sticky-air" covers the crust across the entire model domain.

The model was run using the San Diego Supercomputing Center (Expanse) cluster over a minimum of two nodes with 128 cores per node. The version of StagYY described in

Chapters 2-3 is effective for computing 2D numerical models, but was subject to memory leaks when running across multiple nodes. For 3D models of this resolution, it is necessary to compute in parallel across multiple nodes. All features written into the code in Chapters 2-3 (crustal buoyancy, eclogite transition, mid-mantle phase transitions, etc.) were first migrated to the latest StagYY 2023 branch and then validated in 2D. Refer to Ch. 2-3 for additional information about phase transitions and plasticity.

An initial condition was constructed to reflect a similar starting point as the previous 2D models. An identical chasma rift geometry was written in the (x,y) plane and extended into three dimensions (Fig. 4.2). As previously, a simplified rift zone trench separates two edges of lithosphere. One side has variable lithospheric thickness controlled by the parameter, h_L. The other side has a constant lithospheric thickness of 100 km which gradually thickens to h_L moving away from the rift zone. Whereas the thick lithosphere was previously to the left of the rift gap, it is now to the right. The rift maintains a uniform geometry across the entire surface. 30 km of positively buoyant crust covers the entire lithosphere including the rift gap. The compositional density contrast between crust and average mantle is again defined by the parameter, B_{crust}. A purely thermal plume ($\Delta T_{plume} = +200$ K) begins centered below the thicker plate edge (h_L) with the top of the plume head at 700 km depth. The front model sidewall resembles the 2D cross section of a plume and rift gap from Chapter 3, though the boundary conditions reflect the model domain across this boundary. Effectively, the nearly spherical plume is centered at the equator with a uni-axial continuous rift overhead.

4.3 Results

In addition to sharing the same parameters as the 2D models described in Table 2.1 (except grid resolution), the reference model presented here uses the variables described in Table 4.1. Based on the results of Ch. 2-3, these parameters are most likely to initiate

a delamination event on relatively short timescales. Since the results of Ch. 2-3 show that lithospheric thickness is the most important factor in predicting delamination, the reference model was chosen to have relatively thick 300 km lithosphere. Plume size was shown to only affect timescales and not spatial scales of delamination, so a relatively large 250 km-radius plume was chosen to minimize computation time. Similarly, peel-back delamination has been shown for thinner rift widths (60 km, 125 km) in Chapter 3, but had no significant effect on delamination dynamics. A relatively wide 250 km rift is used here to speed up timescales of delamination initiation.

The overall progression of delamination initiation is similar to what was observed in the 2D plume-induced delamination models of Chapter 3 (Fig. 3.2). At the start of the model, the positively buoyant plume is located 700 km below the thinned edge of the rift gap (Fig. 4.3A). The plume rises directly into the gap (Fig. 4.3B) and the associated increase in crustal stress results in yielding and the development of a low-viscosity crustal layer above the delaminating plate edge (Fig. 4.4). The weakness of the yielded crust allows the lithospheric mantle to decouple from the majority of the overlying positively buoyant crust. Initially, only a thin layer of crust is still attached to the downgoing plate which then transitions into denser eclogite at 70 km depth (Fig. 4.3C). The thickness of the recycled crustal layer increases as the base of the crustal root at the trench reaches 70 km depth. Two separate phase transitions produce positive buoyancy in the slab beginning at 710 km depth: the garnet trap and the postspinel phase boundary deflection (see section 2.2.6 for details) (Fig. 4.3D). The slab is sinking in a convex shape when the slab tip first encounters the 710 km phase transitions, but then inverts to a concave shape as the slab continues to roll back (Fig. 4.3E). The thinned plate edge to the left of the rift gap never goes unstable throughout the model evolution.

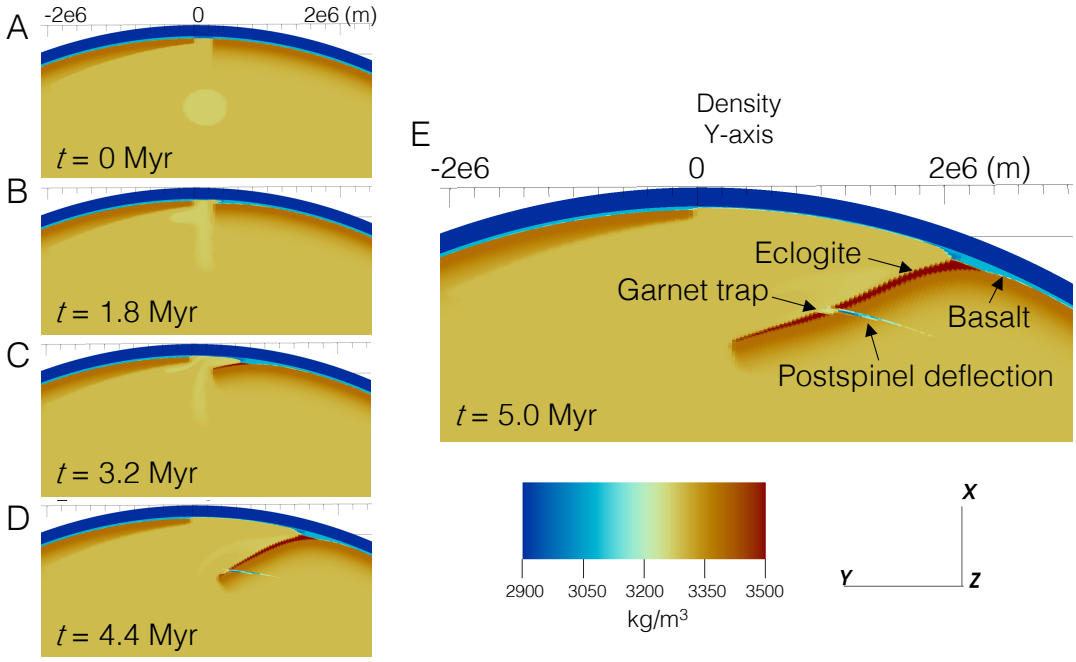

Figure 4.3. 3D plume-induced peel-back delamination progression shown in the density field. (A) The initial condition is a warm 250 km-radius mantle plume centered below a uni-axial rift zone with 250 km width. The maximum lithosphere thickness is 300 km defined by the 1600 K isotherm. (B) The positively buoyant plume rises into the rift gap. (C) The edge of the lithospheric mantle decouples from the majority of crust remaining at the surface. The positively buoyant basaltic crust (light blue) converts to denser eclogite (dark red) 70 km depth. (D) The slab continues to roll back accompanied by trench retreat. The slab tip encounters two mid-mantle phase transitions: the garnet trap and the postspinel phase boundary deflection. (E) The sinking slab inverts from a convex to a concave shape. More crust is recycled as the base of the crustal root at the trench reaches the eclogite transition depth.

4.4 Discussion

The 3D model reproduces the overall style of delamination observed in the 2D studies, however there are some notable differences between the 2D and 3D model geometries. In 2D, the model with 300 km lithosphere was predicted to go unstable both with and without plume-rift interactions due to its strong negative buoyancy. In Chapter 3, the 300 km lithosphere was destabilized as an immediate consequence of interactions with a 250 km-radius plume. The 3D model shows that delamination and slab sinking is highly

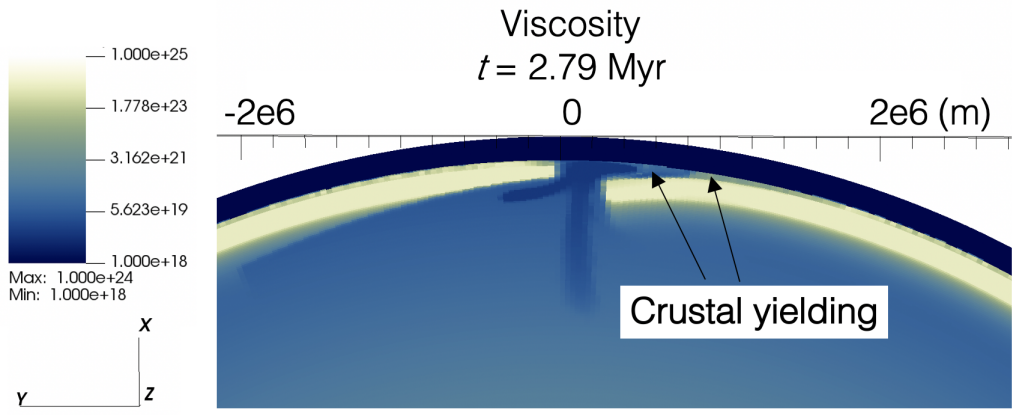

Figure 4.4. Crustal yielding can be observed above the delaminating slab edge as a reduction in viscosity in the weak crustal layer. The yielded crust forms a weak zone which has been shown to facilitate decoupling of the lithospheric mantle (see Ch. 2-3 for details). Although it was necessary to lower the grid resolution in 3D models, it is important to validate that the resolution is sufficient to model crustal yielding; otherwise, delamination may never occur.

variable along the rift axis, with the plume side delaminating on a similar timescale as its 2D analogue. Based on timing information from Fig. 2.9, the equivalent 2D lithosphere with no plume interactions is expected to initiate purely buoyancy-driven delamination approximately 2.5 Myr after the start of the model. However, by 5 Myr the lithosphere furthest from the plume has still not been destabilized (Fig. 4.5A). This change in model behavior between 2D and 3D versions may be attributed to the effects of 3D mantle flow influencing the far field rift area. As the plume-destabilized area of slab begins to sink, the toroidal mantle flow accompanying slab sinking may act to stabilize the down-axis lithosphere. Alternatively, the discrepancy could indicate that lithospheric instability is resisted more strongly by a three dimensional slab geometry and requires additional negative buoyancy or some plume buoyancy force to initiate delamination.

Another difference between the 2D and 3D models is the absence of slab tip deflection in 3D. In 2D, the mid-mantle phase transitions deflected the slab tip back towards the surface before the crustal layer ever reached 710 km depth. The breakthrough

Table 4.1. 3D reference model variables

Parameter	Description	Value
nx	Horizontal (x) cells	256
ny	Horizontal (y) cells	512
nz	Vertical cells	256
h_L	Maximum lithosphere thickness	300 km
B_{crust}	Crustal density contrast	-300 kg/m^3
η_{max}	Maximum lithosphere viscosity	10^{24} Pa·s
L_{gap}	Chasma rift width	250 km
R_{plume}	Plume radius	250 km
T_{plume}	Plume temperature contrast	+200 K
σ_{max}	Maximum yield strength	500 MPa

of the slab tip through this region of positive buoyancy induced an increase in stresses at the slab hinge which facilitated slab breakoff. So far in the 3D model, the slab has experienced less effects from the garnet trap and postspinel phase transition at 710 km, though the slab does undergo a shift from convex to concave slab morphology (Fig. 4.6). This may affect slab breakoff dynamics, though the decrease in viscosity associated with yielding at the slab hinge is currently visible in the viscosity field. One possible cause of this discrepancy is the 3D toroidal return flow expected to push mantle material around from behind the slab and into the area in front of the slab [108, 154, 157], which may be inhibiting slab tip deflection. Another possibility is that the 3D model is lower resolution compared to the 2D models and the stress field is being "smoothed" over coarser grid cells. Consequently, this would result in lower maximum stresses in both the slab tip and slab hinge and inhibit yielding and deformation.

A major question left at the end of Chapter 3 was whether 3D models of delamination could reproduce any surface features of Venus. Specifically, Artemis Corona at Dali-Diana chasmata was identified as a potential peel-back delamination zone based on its proximity to what is likely relatively thick lithosphere. Similar to Artemis, the 3D delamination models show a radially retreating trench accompanied by a flexural bulge near the slab hinge. The diameter of Artemis is approximately 2500 km. The newly recycled area in

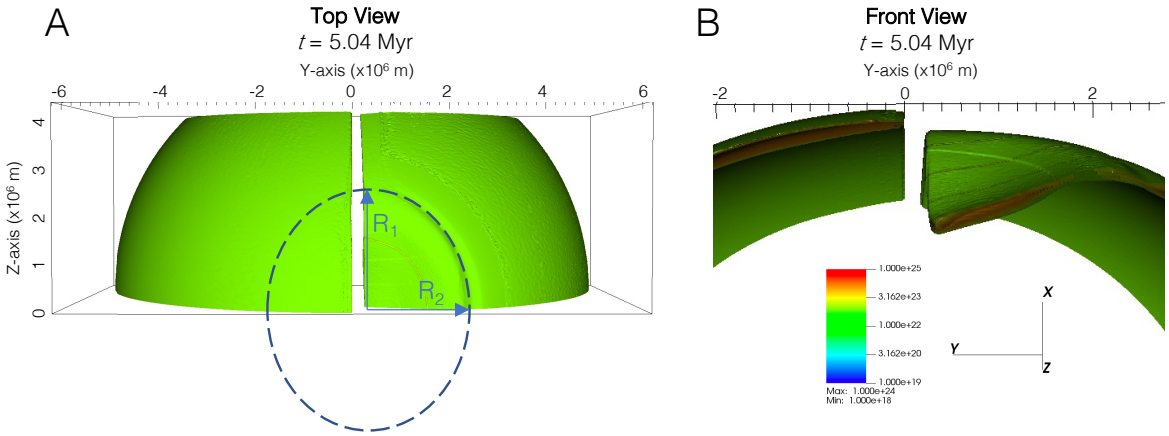

Figure 4.5. (A) Top and (B) front views of an isoviscous contour of plume-induced peel-back delamination of a 300 km lithosphere after 5.04 Myr. The surface of the contour corresponds to $\eta = 9{\cdot}10^{22}$ Pa·s. (A) The top view shows the lateral extent of delamination. An ellipse with $R_1 = 2500$ km and $R_2 = 2100$ km is fitted to the location of the trench. No delamination is observed at the opposite end of the rift zone. (B) The front view highlights the slab morphology during slab sinking. Unlike the corresponding 2D models of Chapter 2-3, no slab tip deflection is observed in 3D.

the model can be fit by an ellipse with with the shorter axis perpendicular to the rift with a length scale of 2100 km and an along-axis diameter of 5000 km when considering the symmetry across the equatorial plane (Fig. 4.5). Although this model does not reproduce the exact surface features at Artemis, a more circular retreating trench may be formed by modeling more complicated rift geometries. The current uni-axial and relatively wide rift geometry does nothing to hinder the continued expansion of the delaminated area and likely represents the uppermost limit on the width of the delamination zone. In reality, Venus' chasmata are branching and discontinuous which could limit delamination propagation. These effects will be investigated in future studies.

4.5 Conclusions

Before this study, it was unknown whether the peel-back delamination mechanism presented in 2D in Chapters 2 and 3 would be viable in three dimensions. The 3D model presented here represents an important first step in validating retrograde lithospheric

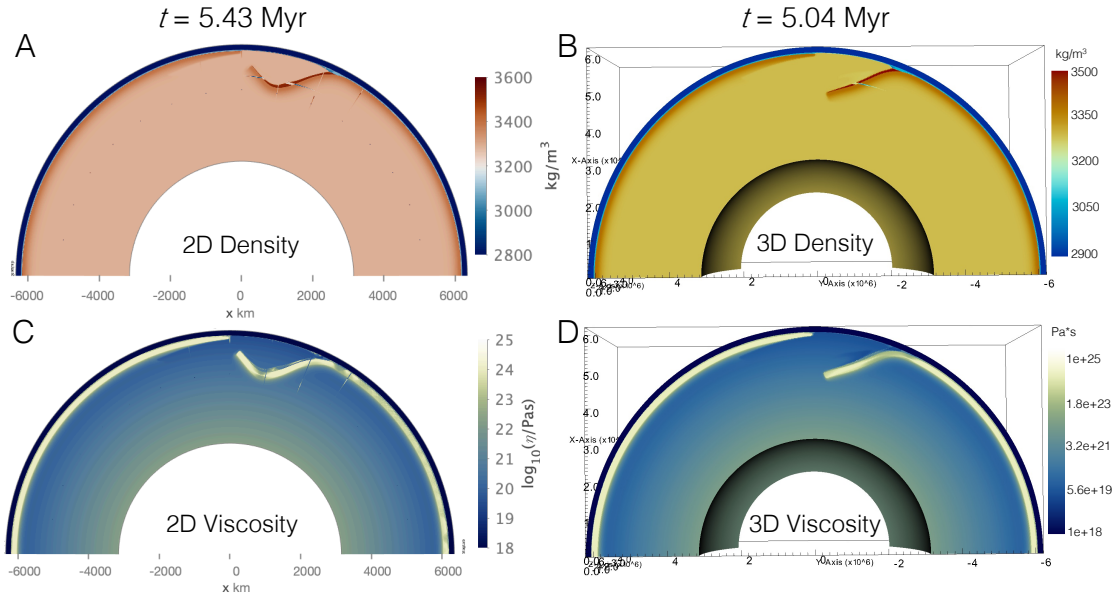

Figure 4.6. (A,B) Density and (C,D) viscosity profiles of slab rollback during a plume-induced peel-back delamination event. (A) The mid-mantle phase transitions beginning at 710 km depth (garnet trap and postspinel boundary deflection) induce strong slab tip deflection in 2D models. (B) In a comparable 3D model, the same phase transitions have a much weaker effect on slab sinking and result in no slab tip deflection. This discrepancy may be the result of the toroidal component of mantle flow expected in 3D models of retrograde subduction (Fig. 4.1). In 3D, mantle material can flow from behind the sinking slab, around the lateral plate edges, and into the space in front of the slab which may resist slab tip deflection.

delamination initiated at a rift zone on Venus using realistic crustal buoyancy. Plume-induced delamination initiates via crustal yielding similar to what was observed in 2D; however it appears that concurrent buoyancy-driven peel-back delamination of down-axis lithosphere is inhibited by 3D toroidal mantle flow effects. Slab morphology also appears to be affected by lateral mantle flow dynamics, as evidenced by the absence of slab tip deflection in the mid-mantle which was only observed in 2D.

Future work may involve using discontinuous chasmata trenches with variable width in order to investigate effects on delamination geometry. Artemis Corona was previously identified as a possible location of peel-back delamination, however the model here produced a more elliptical delamination zone centered along the rift axis. A finite

chasma weakness may limit the on-axis length scale of delamination and produce more corona-like surface features. 2D slices through the delaminating slab can be used to compare the flexural response of models to specific locations on Venus. Lithospheric flexure and delamination area in 3D models may be variable with changes in lithospheric thickness and mantle viscosity structure.

4.6 Acknowledgments

Chapter 4, in part is being prepared for submission for publication of the material as: Adams, A. C., Stegman, D. R., Smrekar, S. E., Tackley, P. J. Modeling Peel-Back Delamination on Venus in Three Dimensions. The dissertation author is the primary investigator and author of this material.

Chapter 5

Conclusions

Through this work, we have furthered our understanding about the nature of lithospheric instabilities on Venus. These findings also inform larger questions about Venus' evolution, as well as the evolution of Earth and other Earth-sized silicate planets. This work shows that the whether lithospheric instabilities form is strongly dependent on non-linear feedbacks in the lithospheric stress field. The stress field is the connection between the distribution of buoyancy sources within the lithosphere and material plasticity in its upper, coldest portion. By including a sticky-air upper boundary condition and sub-5 km model grid resolution, the lithospheric stress field can be accurately resolved to represent these complex non-linear interactions which occur during plate bending and lithospheric recycling.

The work presented in this dissertation supports the viability of an entirely new planetary tectonic regime called peel-back delamination (PBD), in which lithospheric mantle on Venus can be recycled into the interior on a regional scale while still preserving some crust at the surface. Our understanding of how planets recycle their lithosphere is strongly biased by plate tectonics on Earth, which is dominated by subduction of oceanic plates that have relatively thin (6-7 km) basaltic crust. A key reason why we observe peel-back delamination rather than subduction is the inclusion of a 30 km-thick layer of positively buoyant basaltic crust which counteracts the negative thermal buoyancy of the

lithospheric mantle. The majority of pre-existing geodynamic models studying lithospheric recycling on Venus fail to consider the compositional buoyancy of crust, which is shown here to have a strong stabilizing effect on planetary lithospheres. While plate tectonics appear to be unique to Earth, a delamination-based tectonic regime such as PBD may be more relevant for understanding the stability and dynamics of planetary lithospheres with thick basaltic crusts like Venus.

Chapter 6

Appendices

6.1 Appendix A: Supporting Information for Chapter 2

This supporting information contains figures showing a more detailed description of the viscosity profiles with depth and the topographic evolution of the reference model.

All delamination models exhibited similar changes in topographic features. For each model, we tracked the height and location of the forebulge and the depth and location of the trench over time. Initially, there was a topographic high over the surface of the gap as is expected due to the density contrast with adjacent lithosphere. Early in the model evolution (0.2 Myr), the edge of the thickest plate h_L bent downward into the mantle, creating a small trench (Appendix A; Fig 6.2A). As the slab continued to sink, a topographic low formed in association with the location of the trench and a topographic high formed on the surface of the down-going plate over the flexural bulge. The peak over the forebulge increased in height as both the forebulge and trench retreated steadily away from the initial gap zone (Appendix A; Fig 6.2B-D). The topography over the gap decreased in height compared to the initial stages and remained near zero elevation for the duration of the model evolution. A topographic high marked the edge of the non-delaminating plate with thickness h_{L-min}. The end of steady-state delamination was punctuated by the start of slab break-off at the surface. As the plate began to break-off at

the surface, the magnitude of the trench depth and forebulge height decreased sharply. The trench and forebulge movement also suddenly changed directions from moving away from the gap to being pulled back toward the site of break-off. The timings of these changes in trench depth, forebulge height, and forebulge location were used to define the end of steady-state delamination for each model (see Fig. 2.9).

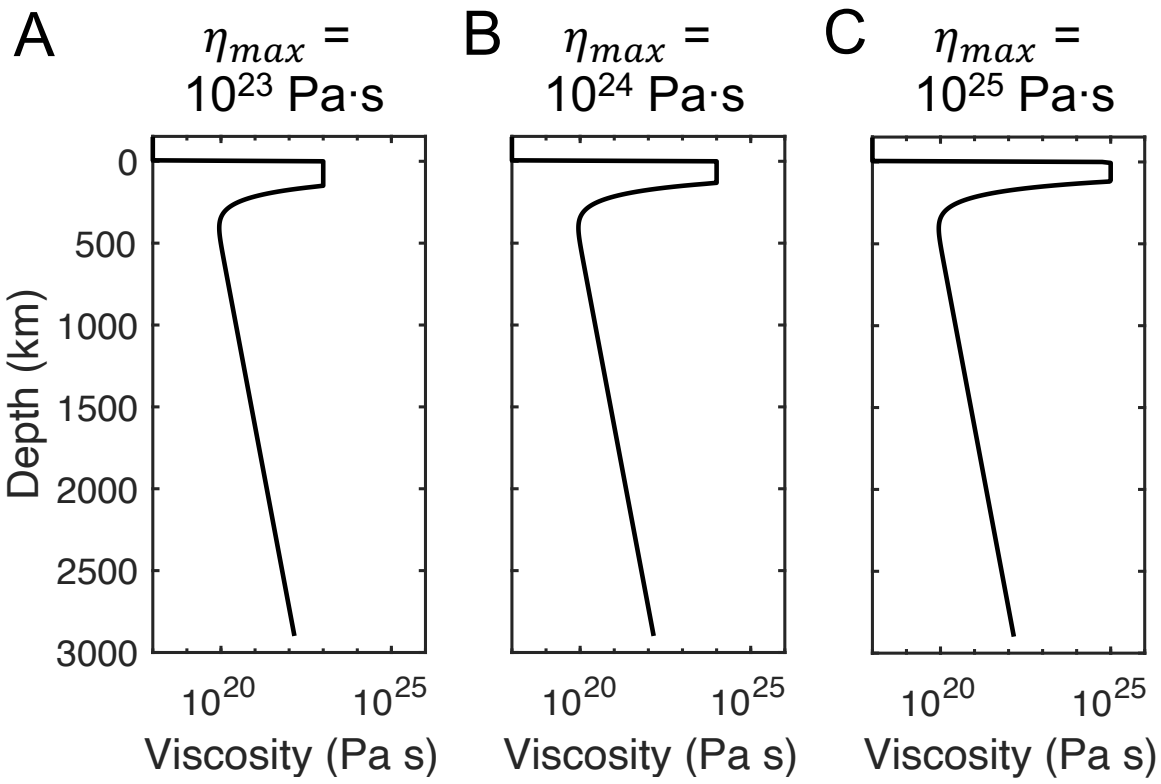

Figure 6.1. Viscosity profile with depth given for (A) $\eta_{max} = 10^{23}$ Pa·s, (B) $\eta_{max} = 10^{24}$ Pa·s, and (C) $\eta_{max} = 10^{25}$ Pa·s. The maximum viscosity cutoff is relevant for the colder lithosphere and does not affect the viscosity at depth. A three order of magnitude viscosity increase is applied over the depth of the mantle. The profiles are identical except for where the viscosity cutoff is applied in the lithosphere.

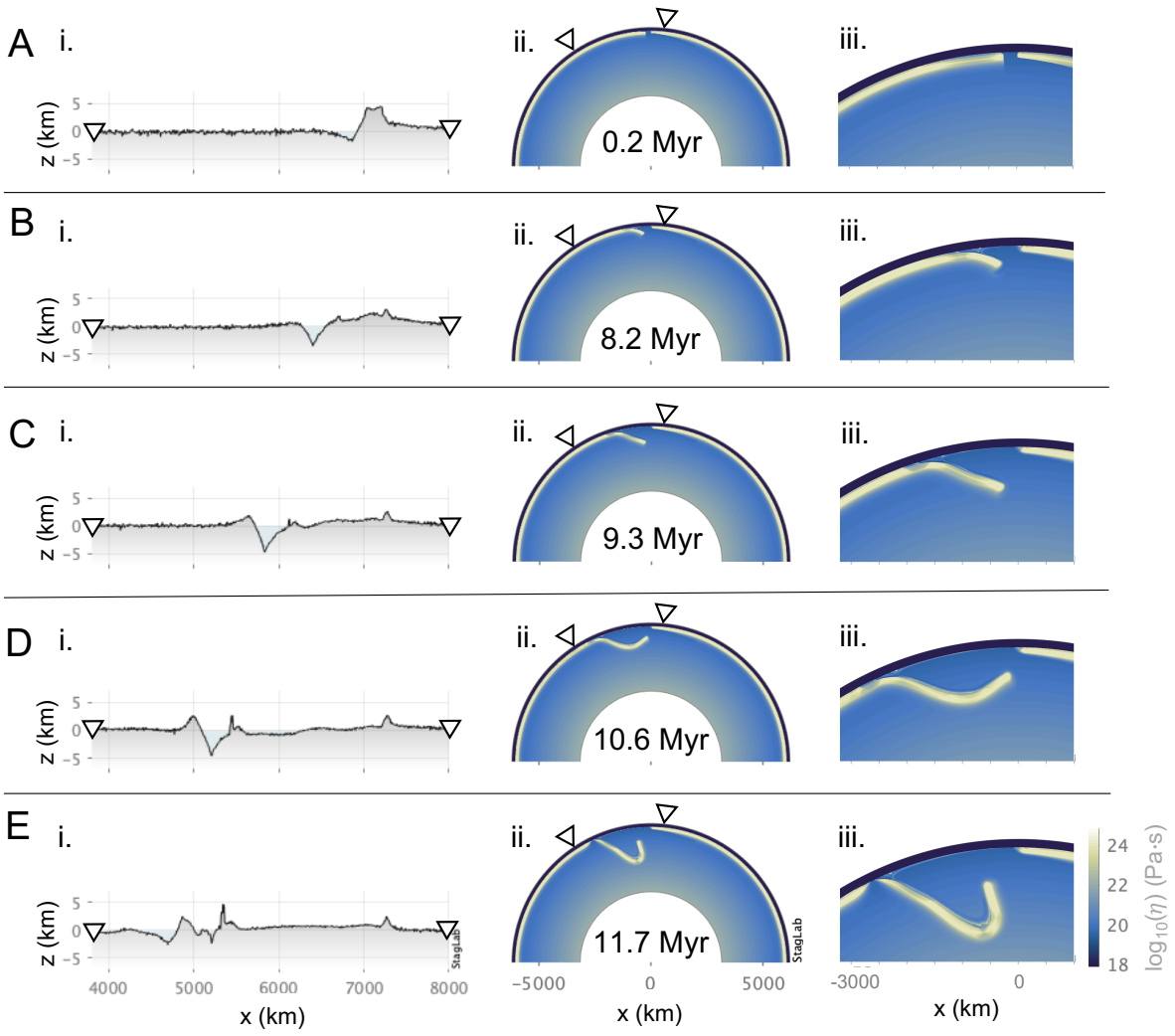

Figure 6.2. Typical evolution of a peel-back delamination event shown in the (i) topography field, (ii) global viscosity field, and (iii) local viscosity field of the reference model (B_{crust} = -300 kg/m^3, h_L = 250 km, η_{max} = 10^{24} Pa·s). Timing of model stages (A-E) correspond to Figure 2.5.

6.2 Appendix B: Supporting Information for Chapter 3

The following contains supporting figures further describing the initial model condition as well as two test cases which fall outside of the original parameter space but give further insight into the mechanism of plume-induced peel-back delamination. Two tables are provided which summarize the parameter space and model outcomes used in

this study.

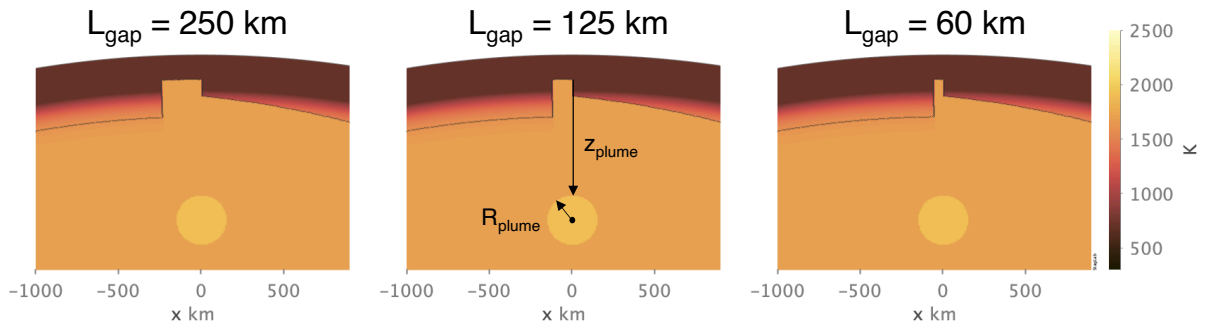

Figure 6.3. The temperature field of the initial condition is shown for variable rift zone width, L_{gap}. The starting position of the top of the plume head is fixed at a depth of $z_{plume} = 700$ km from the surface, and the radius of the plume head is varied ($R_{plume} = 150$ km shown here).

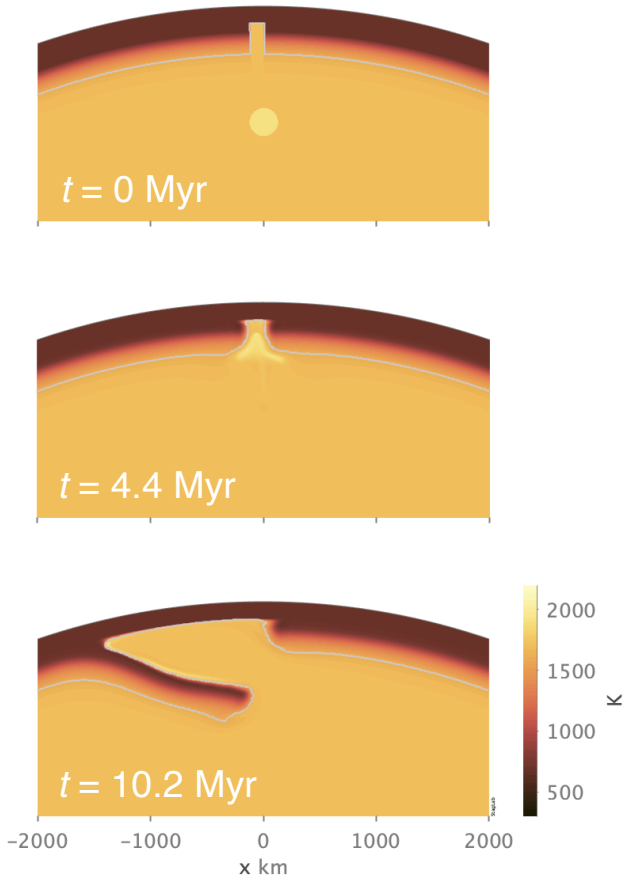

Figure 6.4. A test case of single-sided PBD initiated from a symmetric subsurface rift geometry, with two 250-km-thick plate edges separated by a 125-km-wide gap (B_{crust} = -350 kg/m^3). A 125-km-radius plume destabilizes only the left plate edge, while the right plate remains stagnant-lid. There is slightly more extensive plume underplating beneath the right plate due to the plume's initial position centered 700 km below the right plate edge; however delamination in the right plate appears to be primarily inhibited by the uplifting force of the plume rising directly beneath the plate edge. Destabilization of one side of the rift gap may be facilitated by plume uplift on the opposing side of the rift, though this will need to be further investigated in future studies.

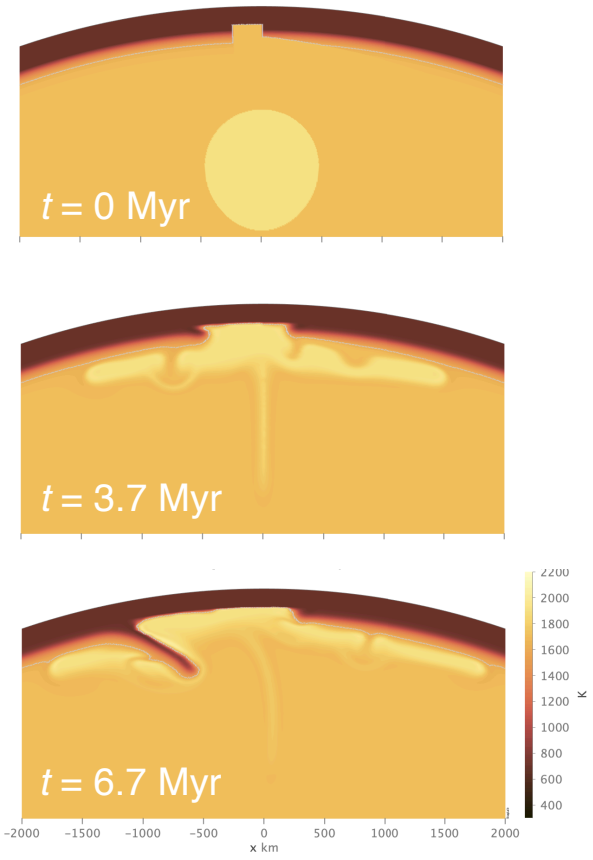

Figure 6.5. Only one case of plume-induced PBD was initiated in 150 km lithosphere (L_{gap} = 250 km, B_{crust} = -265 kg/m^3). Due to the lack of negative buoyancy in the lithospheric mantle, a relatively large plume of radius 500 km was required for destabilization. Despite the uplifting plume force beneath the plate edge, the strong plume buoyancy force in the rift gap combined with relatively low crustal buoyancy results in bending near the plate edge. PBD continues to progress due to the formation of eclogite in the slab tip. Localized downwellings from thermal erosion of the lithosphere can induce convection patterns that may precede delamination.

Table 6.1. Plume-induced PBD summary of model parameters and outcomes

Model	Lithosphere Thickness (km)	Gap Width (km)	Crustal Density Contrast (B_{crust}) (kg/m^3)	Plume Radius (km)	Outcome
1	200	250	-265	50	Stagnant-Lid
2	200	250	-300	50	Stagnant-Lid
3	200	250	-265	100	Delamination
4	200	250	-300	100	Delamination
5	200	250	-350	100	Stagnant-Lid
6	200	250	-265	150	Delamination
7	200	250	-300	150	Delamination
8	200	250	-350	150	Delamination
9	200	250	-400	150	Delamination
10	200	250	-265	250	Delamination
11	200	250	-300	250	Delamination
12	200	250	-350	250	Delamination
13	200	250	-400	250	Delamination
14	200	125	-265	100	Delamination
15	200	125	-300	100	Stagnant-Lid
16	200	125	-265	150	Delamination
17	200	125	-300	150	Delamination
18	200	125	-350	150	Stagnant-Lid
19	200	125	-265	250	Delamination
20	200	125	-300	250	Delamination
21	200	125	-350	250	Delamination
22	200	125	-400	250	Stagnant-Lid
23	200	60	-265	150	Stagnant-Lid
24	200	60	-300	150	Stagnant-Lid
25	200	60	-265	250	Delamination
26	200	60	-300	250	Stagnant-Lid

Table 6.2. Plume-induced PBD summary of model parameters and outcomes (continued)

Model	Lithosphere Thickness (km)	Gap Width (km)	Crustal Density Contrast (B_{crust}) (kg/m^3)	Plume Radius (km)	Outcome
27	250	250	-400	25	Stagnant-Lid
28	250	250	-400	75	Delamination
29	250	250	-400	100	Delamination
30	250	250	-300	150	Delamination
31	250	250	-350	150	Delamination
32	250	250	-400	150	Delamination
33	250	250	-300	250	Delamination
34	250	250	-350	250	Delamination
35	250	250	-400	250	Delamination
36	250	60	-300	100	Delamination
37	250	60	-400	100	Stagnant-Lid
38	250	60	-300	150	Delamination
39	250	60	-350	150	Delamination
40	250	60	-400	150	Stagnant-Lid
41	250	60	-300	250	Delamination
42	250	60	-350	250	Delamination
43	250	60	-400	250	Delamination
44	250	60	-265	0	Stagnant-Lid
45	150	250	-265	250	Stagnant-Lid
46	150	250	-300	250	Stagnant-Lid
47	150	250	-350	250	Stagnant-Lid
48	150	250	-265	400	Stagnant-Lid
49	150	250	-265	500	Delamination

Bibliography

[1] S. C. Solomon, S. E. Smrekar, I. L. D. Bindschadler, R. E. Grimm, W. M. Kaula, G. E. McGill, R. J. Phillips, R. S. Saunders, G. Schubert, S. W. Squyres, and E. R. Stofan, "Venus tectonics: An overview of magellan observations," *Journal of Geophysical Research*, vol. 97, no. E8, pp. 13,199–13,255, 1992.

[2] D. T. Sandwell and G. Schubert, "Evidence for retrograde lithospheric subduction on Venus," *Science*, vol. 257, pp. 766–770, 1992.

[3] G. Schubert and D. Sandwell, "A global survey of possible subduction sites on Venus," *Icarus*, vol. 117, pp. 173–196, 1995.

[4] C.-T. Lee, P. Luffi, T. Plank, H. Dalton, and W. P. Leeman, "Constraints on the depths and temperatures of basaltic magma generation on Earth and other terrestrial planets using new thermobarometers for mafic magmas," *Earth Planet. Sci. Lett.*, vol. 279, pp. 20–33, 2009.

[5] J. G. Shellnutt, "Mantle potential temperature estimates of basalt from the surface of Venus," *Icarus*, vol. 277, pp. 98–102, 2016.

[6] M. B. Weller and M. S. Duncan, "Insight into terrestrial planetary evolution via mantle potential temperatures," 2015.

[7] D. L. Kohlstedt, B. Evans, and S. J. Mackwell, "Strength of the lithosphere: constraints imposed by laboratory experiments," *Journal of Geophysical Research*, vol. 100, pp. 17587–17602, 1995.

[8] S. J. Mackwell, M. E. Zimmerman, and D. L. Kohlstedt, "High-temperature deformation of dry diabase with application to tectonics on Venus," *Journal of Geophysical Research*, vol. 103, pp. 975–984, 1998.

[9] S. ichiro Karato and S. Barbot, "Dynamics of fault motion and the origin of contrasting tectonic style between earth and venus," *Scientific Reports*, vol. 8, 12 2018.

[10] D. T. Sandwell and G. Schubert, "Flexural ridges, trenches, and outer rises around coronae on Venus," *Journal of Geophysical Research*, vol. 97, 1992.

[11] P. B. James, M. T. Zuber, and R. J. Phillips, "Crustal thickness and support of topography on Venus," *Journal of Geophysical Research E: Planets*, vol. 118, pp. 859–875, 2013.

[12] A. Jiménez-Díaz, J. Ruiz, J. F. Kirby, I. Romeo, R. Tejero, and R. Capote, "Lithospheric structure of venus from gravity and topography," *Icarus*, vol. 260, pp. 215–231, 2015.

[13] R. J. Stern, "Subduction initiation: Spontaneous and induced," *Earth and Planetary Science Letters*, vol. 226, pp. 275–292, 2004.

[14] P. F. Rey, N. Coltice, and N. Flament, "Spreading continents kick-started plate tectonics," *Nature*, vol. 513, pp. 405–408, 2014.

[15] M. Maffione, C. Thieulot, D. J. van Hinsbergen, A. Morris, O. Plümper, and W. Spakman, "Dynamics of intraoceanic subduction initiation: 1. oceanic detachment fault inversion and the formation of supra-subduction zone ophiolites," *Geochemistry, Geophysics, Geosystems*, vol. 16, pp. 1753–1770, 2015.

[16] T. V. Gerya, R. J. Stern, M. Baes, S. V. Sobolev, and S. A. Whattam, "Plate tectonics on the earth triggered by plume-induced subduction initiation," *Nature*, vol. 527, pp. 221–225, 2015.

[17] G. Lu, B. J. Kaus, L. Zhao, and T. Zheng, "Self-consistent subduction initiation induced by mantle flow," *Terra Nova*, vol. 27, pp. 130–138, 2015.

[18] A. J. Gülcher, T. V. Gerya, L. G. Montési, and J. Munch, "Corona structures driven by plume–lithosphere interactions and evidence for ongoing plume activity on Venus," *Nature Geoscience*, vol. 13, pp. 547–554, 2020.

[19] P. J. Tackley, "Modelling compressible mantle convection with large viscosity contrasts in a three-dimensional spherical shell using the yin-yang grid," *Physics of the Earth and Planetary Interiors*, vol. 171, pp. 7–18, 2008.

[20] F. Crameri, H. Schmeling, G. J. Golabek, T. Duretz, R. Orendt, S. J. H. Buiter, D. A. May, B. J. P. Kaus, T. V. Gerya, and P. J. Tackley, "A comparison of numerical surface topography calculations in geodynamic modelling: an evaluation of the 'sticky air' method," *Geophysical Journal International*, vol. 189, pp. 38–54, 2012.

[21] M. Armann and P. J. Tackley, "Simulating the thermochemical magmatic and tectonic evolution of Venus's mantle and lithosphere: Two-dimensional models," *Journal of Geophysical Research: Planets*, vol. 117, 2012.

[22] F. Crameri and P. J. Tackley, "Subduction initiation from a stagnant lid and global overturn: new insights from numerical models with a free surface," *Progress in Earth and Planetary Science*, vol. 3, 2016.

[23] T. Rolf, B. Steinberger, U. Sruthi, and S. C. Werner, "Inferences on the mantle viscosity structure and the post-overturn evolutionary state of Venus," *Icarus*, vol. 313, pp. 107–123, 2018.

[24] S. Uppalapati, T. Rolf, F. Crameri, and S. C. Werner, "Dynamics of lithospheric overturns and implications for Venus's surface," *Journal of Geophysical Research: Planets*, vol. 125, 2020.

[25] M. B. Weller and W. S. Kiefer, "The physics of changing tectonic regimes: Implications for the temporal evolution of mantle convection and the thermal history of Venus," *Journal of Geophysical Research: Planets*, vol. 125, 2020.

[26] C. C. Reese, V. S. Solomatov, and L. N. Moresi, "Non-newtonian stagnant lid convection and magmatic resurfacing on Venus," *Icarus*, vol. 139, pp. 67–80, 1999.

[27] V. S. Solomatov and L. N. Moresi, "Stagnant lid convection on Venus," *Journal of Geophysical Research*, vol. 101, pp. 4737–4753, 1996.

[28] J. T. Ratcliff, G. Schubert, and A. Zebib, "Three-dimensional variable viscosity convection of an infinite prandtl number boussinesq fluid in a spherical shell," *Geophysical Research Letters*, vol. 22, pp. 2227–2230, 1995.

[29] J. T. Ratcliff, P. J. Tackley, G. Schubert, and A. Zebib, "Transitions in thermal convection with strongly variable viscosity," *Physics of the Earth and Planetary Interiors*, vol. 102, pp. 201–212, 1997.

[30] T. Spohn, "Mantle differentiation and thermal evolution of mars, mercury, and venus," 1991.

[31] D. L. Lourenço, A. B. Rozel, T. Gerya, and P. J. Tackley, "Efficient cooling of rocky planets by intrusive magmatism," *Nature Geoscience*, vol. 11, pp. 322–327, 2018.

[32] D. L. Lourenço, A. B. Rozel, M. D. Ballmer, and P. J. Tackley, "Plutonic-squishy lid: A new global tectonic regime generated by intrusive magmatism on Earth-like planets," *Geochemistry, Geophysics, Geosystems*, vol. 21, 2020.

[33] J. W. Hernlund and P. J. Tackley, "Modeling mantle convection in the spherical annulus," *Physics of the Earth and Planetary Interiors*, vol. 171, pp. 48–54, 2008.

[34] S. Azuma, I. Katayama, and T. Nakakuki, "Rheological decoupling at the moho and implication to Venusian tectonics," *Scientific Reports*, vol. 4, pp. 1–5, 2014.

[35] I. Katayama, "Strength models of the terrestrial planets and implications for their lithospheric structure and evolution," *Progress in Earth and Planetary Science*, vol. 8, 2021.

[36] J. Tian, P. J. Tackley, and D. L. Lourenço, "The tectonics and volcanism of Venus: New modes facilitated by realistic crustal rheology and intrusive magmatism," *Icarus (in review)*, 2023.

[37] R. J. Phillips and V. L. Hansen, "Tectonic and magmatic evolution of Venus," *Annu. Rev. Earth Planet. Sci.*, vol. 22, pp. 597–654, 1994.

[38] M. L. Feuvre and M. A. Wieczorek, "Nonuniform cratering of the Moon and a revised crater chronology of the inner solar system," *Icarus*, vol. 214, pp. 1–20, 2011.

[39] W. B. McKinnon, K. J. Zahnle, B. A. Ivanov, and H. J. Melosh, "Cratering on Venus - models and observations," *Venus II : Geology, Geophysics, Atmosphere, and Solar Wind Environment*, pp. 969–1014, 1997.

[40] G. G. Schaber, R. G. Strom, H. J. Moore, L. A. Soderblom, R. L. Kirk, D. J. Chadwick, D. D. Dawson, L. R. Gaddis, J. M. Boyce, and I. Russell, "Geology and distribution of impact craters on Venus: What are they telling us?," *Journal of Geophysical Research: Planets*, vol. 97, pp. 257–270, 1992.

[41] D. L. Turcotte, "An episodic hypothesis for Venusian tectonics," *Journal of Geophysical Research*, vol. 98, pp. 61–78, 1993.

[42] R. J. Phillips, R. F. Raubertas, R. E. Arvidson, I. C. Sarkar, R. R. Herrick, N. Izenberg, and R. E. Grimm, "Impact craters and Venus resurfacing history," *Journal of Geophysical Research*, vol. 97, pp. 923–938, 1992.

[43] C. Riedel, G. G. Michael, C. Orgel, C. Baum, C. H. van der Bogert, and H. Hiesinger, "Studying the global spatial randomness of impact craters on Mercury, Venus, and the Moon with geodesic neighborhood relationships," *Journal of Geophysical Research: Planets*, vol. 126, 2021.

[44] R. G. Strom, G. G. Schaber, and D. D. Dawson, "The global resurfacing of Venus," *Journal of Geophysical Research*, vol. 99, pp. 899–909, 1994.

[45] E. M. Parmentier and P. C. Hess, "Chemical differentiation of a convecting planetary interior: Consequences for a one plate planet such as Venus," *Geophysical Research Letters*, vol. 19, pp. 2015–2018, 1992.

[46] D. L. Turcotte, "How does Venus lose heat?," *Journal of Geophysical Research*, vol. 100, pp. 16,931–16,940, 1995.

[47] D. L. Turcotte, G. Morein, D. Roberts, and B. D. Malamud, "Catastrophic resurfacing and episodic subduction on Venus," *Icarus*, vol. 139, pp. 49–54, 1999.

[48] N. Namiki and S. C. Solomon, "Impact crater densities on volcanoes and coronae on Venus: Implications for volcanic resurfacing," *Science*, vol. 265, pp. 929–933, 1994.

[49] R. R. Herrick, "Resurfacing history of Venus," *Geology*, vol. 22, pp. 703–706, 1994.

[50] L. Moresi and V. Solomatov, "Mantle convection with a brittle lithosphere: thoughts on the global tectonic styles of the Earth and Venus," *Geophysical Journal International*, vol. 133, pp. 669–682, 1998.

[51] S. King, "Venus resurfacing constrained by geoid and topography," *Journal of Geophysical Research: Planets*, vol. 123, pp. 1041–1060, 2018.

[52] A. T. Basilevsky and J. W. Head, "Venus: Timing and rates of geologic activity," *Geology*, vol. 30, p. 1015, 2002.

[53] R. R. Herrick and M. E. Rumpf, "Postimpact modification by volcanic or tectonic processes as the rule, not the exception, for Venusian craters," *Journal of Geophysical Research E: Planets*, vol. 116, 2011.

[54] N. R. Izenberg, R. E. Arvidson, and R. J. Phillips, "Impact crater degradation on Venusian plains," *Geophysical Research Letters*, vol. 21, pp. 289–292, 1994.

[55] V. L. Hansen and D. A. Young, "Venus's evolution: A synthesis," *Special Paper of the Geological Society of America*, vol. 419, pp. 255–273, 2007.

[56] R. J. Phillips and N. R. Izenberg, "Ejecta correlations with spatial crater density and venus resurfacing history," vol. 22, 1995.

[57] R. J. Phillips, R. E. Arvidson, J. M. Boyce, D. B. Campbell, J. E. Guest, G. G. Schaber, and L. A. Soderblom, "Impact craters on Venus: Initial analysis from magellan," 1991.

[58] M. A. Bullock, D. H. Grinspoon, and J. W. Head, "Venus resurfacing rates: Constraints provided by 3-D monte carlo simulations," *Geophysical Research Letters*, vol. 20, pp. 2147–2150, 1993.

[59] E. E. Bjonnes, V. L. Hansen, B. James, and J. B. Swenson, "Equilibrium resurfacing of Venus: Results from new monte carlo modeling and implications for Venus surface histories," *Icarus*, vol. 217, pp. 451–461, 2012.

[60] J. G. O'Rourke, A. S. Wolf, and B. L. Ehlmann, "Venus: Interpreting the spatial distribution of volcanically modified craters," *Geophysical Research Letters*, vol. 41, pp. 8252–8260, 2014.

[61] E. V. Shalygin, A. T. Basilevsky, W. J. Markiewicz, D. V. Titov, M. A. Kreslavsky, and T. Roatsch, "Search for ongoing volcanic activity on Venus: Case study of maat mons, sapas mons and ozza mons volcanoes," *Planetary and Space Science*, vol. 73, pp. 294–301, 2012.

[62] E. V. Shalygin, W. J. Markiewicz, A. T. Basilevsky, D.V.Titov, N. I. Ignatiev, and J. W. Head, "Active volcanism on Venus in the ganiki chasma rift zone," *Geophysical Research Letters*, vol. 42, pp. 4762–4769, 2015.

[63] S. E. Smrekar, E. R. Stofan, N. Mueller, A. Treiman, L. Elkins-Tanton, J. Helbert, G. Piccioni, and P. Drossart, "Recent hotspot volcanism on Venus from virtis emissivity data," *Science*, vol. 328, pp. 605–608, 2010.

[64] A. Davaille, S. E. Smrekar, and S. Tomlinson, "Experimental and observational evidence for plume-induced subduction on Venus," *Nature Geoscience*, vol. 10, pp. 349–355, 2017.

[65] F. S. Anderson and S. E. Smrekar, "Global mapping of crustal and lithospheric thickness on Venus," *Journal of Geophysical Research E: Planets*, vol. 111, 2006.

[66] F. Crameri, C. R. Lithgow-Bertelloni, and P. J. Tackley, "The dynamical control of subduction parameters on surface topography," *Geochemistry, Geophysics, Geosystems*, vol. 18, pp. 1661–1687, 2017.

[67] F. Crameri, "Staglab," 2021.

[68] P. Martin, E. R. Stofan, L. S. Glaze, and S. Smrekar, "Coronae of parga chasma, Venus," *Journal of Geophysical Research: Planets*, vol. 112, 2007.

[69] F. Nimmo and D. McKenzie, "Convective thermal evolution of the upper mantles of Earth and Venus," *Geophysical Research Letters*, vol. 24, pp. 1539–1542, 1997.

[70] J. Arkani-Hamed, "On the tectonics of Venus," *Physics of the Earth and Planetary Interiors*, vol. 76, pp. 75–96, 1993.

[71] W. R. Buck, "Global decoupling of crust and mantle: Implicatons for topography, geoid and mantle viscosity on Venus," *Geophysical Research Letters*, vol. 9, pp. 2111–2114, 1992.

[72] R. Ghail, "Rheological and petrological implications for a stagnant lid regime on Venus," *Planetary and Space Science*, vol. 113-114, pp. 2–9, 2015.

[73] M. Ogawa and T. Yanagisawa, "Mantle evolution in Venus due to magmatism and phase transitions: From punctuated layered convection to whole-mantle convection," *Journal of Geophysical Research: Planets*, vol. 119, pp. 867–883, 2014.

[74] M. Akaogi and E. Ito, "Refinement of enthalpy measurement of mgsio 3 perovskite and negative pressure-temperature slopes for perovskite-forming reactions," *Geophysical Research Letters*, vol. 20, pp. 1839–1842, 1993.

[75] Y. Fei, J. V. Orman, J. Li, W. van Westrenen, C. Sanloup, W. Minarik, K. Hirose, T. Komabayashi, M. Walter, and K. Funakoshi, "Experimentally determined postspinel transformation boundary in mg2sio4 using mgo as an internal pressure standard and its geophysical implications," *Journal of Geophysical Research: Solid Earth*, vol. 109, 2004.

[76] T. Irifune, N. Nishiyama, K. Kuroda, T. Inoue, M. Isshiki, W. Utsumi, K.-I. Funakoshi, S. Urakawa, T. Uchida, T. Katsura, and O. Ohtaka, "The postspinel phase boundary in mg2sio4 determined by in situ x-ray diffraction," *Science*, vol. 279, pp. 1698–1700, 1998.

[77] T. Katsura, H. Yamada, T. Shinmei, A. Kubo, S. Ono, M. Kanzaki, A. Yoneda, M. J. Walter, E. Ito, S. Urakawa, K. Funakoshi, and W. Utsumi, "Post-spinel transition in mg2sio4 determined by high p-t in situ x-ray diffractometry," *Physics of the Earth and Planetary Interiors*, vol. 136, pp. 11–24, 2003.

[78] Y. Fukao, M. Obayashi, T. Nakakuki, H. Utada, D. Suetsugu, T. Irifune, E. Ohtani, S. Yoshioka, H. Shiobara, T. Kanazawa, and K. Hirose, "Stagnant slab: A review," *Annual Review of Earth and Planetary Sciences*, vol. 37, pp. 19–46, 2009.

[79] G. F. Davies, "Episodic layering of the early mantle by the 'basalt barrier' mechanism," *Earth and Planetary Science Letters*, vol. 275, pp. 382–392, 2008.

[80] L. T. Elkins-Tanton, "Continental magmatism, volatile recycling, and a heterogeneous mantle caused by lithospheric gravitational instabilities," *Journal of Geophysical Research: Solid Earth*, vol. 112, 2007.

[81] O. H. Göğüş, R. N. Pysklywec, A. M. Şengör, and E. Gün, "Drip tectonics and the enigmatic uplift of the central anatolian plateau," *Nature Communications*, vol. 8, 2017.

[82] G. A. Houseman and P. Molnar, "Gravitational (rayleigh-taylor) instability of a layer with non-linear viscosity and convective thinning of continental lithosphere," *Geophysical Journal International*, vol. 128, pp. 125–150, 1997.

[83] T. E. Johnson, M. Brown, B. J. Kaus, and J. A. Vantongeren, "Delamination and recycling of archaean crust caused by gravitational instabilities," *Nature Geoscience*, vol. 7, pp. 47–52, 2014.

[84] R. I. Petersen, D. R. Stegman, and P. J. Tackley, "The subduction dichotomy of strong plates and weak slabs," *Solid Earth*, vol. 8, pp. 339–350, 2017.

[85] W. P. Schellart, "Evolution of subduction zone curvature and its dependence on the trench velocity and the slab to upper mantle viscosity ratio," *Journal of Geophysical Research: Solid Earth*, vol. 115, 2010.

[86] P. Bird, "Continental delamination and the colorado plateau," *Journal of Geophysical Research*, vol. 84, 1979.

[87] L. Chen, "The role of lower crustal rheology in lithospheric delamination during orogeny," *Frontiers in Earth Science*, vol. 9, 2021.

[88] O. H. Göğüş and K. Ueda, "Peeling back the lithosphere: Controlling parameters, surface expressions and the future directions in delamination modeling," *Journal of Geodynamics*, vol. 117, pp. 21–40, 2018.

[89] N. J. Krystopowicz and C. A. Currie, "Crustal eclogitization and lithosphere delamination in orogens," *Earth and Planetary Science Letters*, vol. 361, pp. 195–207, 2013.

[90] V. Magni, C. Faccenna, J. V. Hunen, and F. Funiciello, "Delamination vs. break-off: The fate of continental collision," *Geophysical Research Letters*, vol. 40, pp. 285–289, 2013.

[91] R. Meissner and W. Mooney, "Weakness of the lower continental crust: a condition for delamination, uplift, and escape," *Tectonophysics*, vol. 296, pp. 47–60, 1998.

[92] K. Ito and G. C. Kennedy, "An experimental study of the basalt-garnet granulite-eclogite transition," *Geophysical Monography Series*, vol. 14, pp. 303–314, 1971.

[93] M. T. Zuber, "Constraints on the lithospheric structure of Venus from mechanical models and tectonic surface features," *Journal of Geophysical Research*, vol. 92, pp. E541–E551, 1987.

[94] M. Faccenda, G. Minelli, and T. V. Gerya, "Coupled and decoupled regimes of continental collision: Numerical modeling," *Earth and Planetary Science Letters*, vol. 278, pp. 337–349, 2009.

[95] K. Ueda, T. V. Gerya, and J. P. Burg, "Delamination in collisional orogens: Thermomechanical modeling," *Journal of Geophysical Research: Solid Earth*, vol. 117, 2012.

[96] O. H. Göğüş and R. N. Psyklywec, "Near-surface diagnostics of dripping or delaminating lithosphere," *Journal of Geophysical Research: Solid Earth*, vol. 113, 2008b.

[97] R. W. Kay and S. M. Kay, "Delamination and delamination magmatism," *Tectonophysics*, vol. 219, pp. 177–189, 1993.

[98] P. Chowdhury, T. Gerya, and S. Chakraborty, "Emergence of silicic continents as the lower crust peels off on a hot plate-tectonic Earth," *Nature Geoscience*, vol. 10, pp. 698–703, 2017.

[99] P. Chowdhury, S. Chakraborty, T. V. Gerya, P. A. Cawood, and F. A. Capitanio, "Peel-back controlled lithospheric convergence explains the secular transitions in archean metamorphism and magmatism," *Earth and Planetary Science Letters*, vol. 538, 2020.

[100] A. L. Perchuk, O. G. Safonov, C. A. Smit, D. D. van Reenen, V. S. Zakharov, and T. V. Gerya, "Precambrian ultra-hot orogenic factory: Making and reworking of continental crust," *Tectonophysics*, vol. 746, pp. 572–586, 2018.

[101] C. Herzberg, K. Condie, and J. Korenaga, "Thermal history of the Earth and its petrological expression," *Earth and Planetary Science Letters*, vol. 292, pp. 79–88, 2010.

[102] O. H. Göğüş and R. N. Psyklywec, "Mantle lithosphere delamination driving plateau uplift and synconvergent extension in eastern anatolia," *Geology*, vol. 36, pp. 723–726, 2008a.

[103] M. Keskin, "Magma generation by slab steepening and breakoff beneath a subduction-accretion complex: An alternative model for collision-related volcanism in eastern anatolia, Turkey," *Geophysical Research Letters*, vol. 30, 2003.

[104] C. Memiş, O. H. Göğüş, E. Şengül Uluocak, R. Pysklywec, M. Keskin, A. M. Şengör, and G. Topuz, "Long wavelength progressive plateau uplift in eastern anatolia since 20 ma: Implications for the role of slab peel-back and break-off," *Geochemistry, Geophysics, Geosystems*, vol. 21, 2020.

[105] M. A. Fillerup, J. H. Knapp, C. C. Knapp, and V. Raileanu, "Mantle earthquakes in the absence of subduction? continental delamination in the romanian carpathians," *Lithosphere*, vol. 2, pp. 333–340, 2010.

[106] E. Şengül Uluocak, R. N. Pysklywec, O. H. Göğüş, and E. U. Ulugergerli, "Multidimensional geodynamic modeling in the southeast carpathians: Upper mantle flow-induced surface topography anomalies," vol. 20, pp. 3134–3149, 2019.

[107] Z. H. Li, M. Liu, and T. Gerya, "Lithosphere delamination in continental collisional orogens: A systematic numerical study," *Journal of Geophysical Research: Solid Earth*, vol. 121, pp. 5186–5211, 2016.

[108] D. R. Stegman, J. Freeman, W. P. Schellart, L. Moresi, and D. May, "Influence of trench width on subduction hinge retreat rates in 3-d models of slab rollback," *Geochemistry, Geophysics, Geosystems*, vol. 7, 2006.

[109] W. P. Schellart, J. Freeman, D. R. Stegman, L. Moresi, and D. May, "Evolution and diversity of subduction zones controlled by slab width," *Nature*, vol. 446, pp. 308–311, 2007.

[110] L. D. Ashwal, K. Burke, and V. L. Sharpton, "Lithospheric delamination on Earth and Venus," *Abstracts of the Lunar and Planetary Science Conference*, vol. 19, p. 17, 1988.

[111] S. E. Smrekar and E. R. Stofan, "Corona formation and heat loss on Venus by coupled upwelling and delamination," *Science*, vol. 277, no. 5330, pp. 1289–1294, 1997.

[112] P. K. Byrne, R. C. Ghail, M. S. Gilmore, A. M. Şengör, C. Klimczak, D. A. Senske, J. L. Whitten, S. Khawja, R. E. Ernst, and S. C. Solomon, "Venus tesserae feature layered, folded, and eroded rocks," *Geology*, vol. 49, pp. 81–85, 2020.

[113] P. K. Byrne, R. C. Ghail, A. M. Şengör, P. B. James, C. Klimczak, and S. C. Solomon, "A globally fragmented and mobile lithosphere on Venus," *Proceedings of the National Academy of Sciences*, vol. 118, 2021.

[114] A. C. Adams, "Regional-scale lithospheric recycling on venus via peel-back delamination," 2022.

[115] I. Romeo and D. L. Turcotte, "The frequency-area distribution of volcanic units on Venus: Implications for planetary resurfacing," *Icarus*, vol. 203, pp. 13–19, 2009.

[116] S. E. Smrekar, C. Ostberg, and J. G. O'Rourke, "Earth-like lithospheric thickness and heat flow on Venus consistent with active rifting," *Nature Geoscience*, 2022.

[117] M. Simons, S. C. Solomon, and B. H. Hager, "Localization of gravity and topography: Constraints on the tectonics and mantle dynamics of Venus," *Geophysical Journal International*, vol. 131, pp. 24–44, 1997.

[118] E. R. Oxburgh and E. M. Parmentier, "Compositional and density stratification in oceanic lithosphere-causes and consequences," *aTl geol. Soc. Lond*, vol. 33, pp. 343–355, 1977.

[119] J. G. O'Rourke and S. E. Smrekar, "Signatures of lithospheric flexure and elevated heat flow in stereo topography at coronae on Venus," *Journal of Geophysical Research: Planets*, vol. 123, pp. 369–389, 2018.

[120] T. Hoogenboom and G. A. Houseman, "Rayleigh-taylor instability as a mechanism for corona formation on Venus," *Icarus*, vol. 180, pp. 292–307, 2006.

[121] A. Darold and E. Humphreys, "Upper mantle seismic structure beneath the pacific northwest: A plume-triggered delamination origin for the columbia river flood basalt eruptions," *Earth and Planetary Science Letters*, vol. 365, pp. 232–242, 2013.

[122] H. Wallner and H. Schmeling, "Rift induced delamination of mantle lithosphere and crustal uplift: A new mechanism for explaining rwenzori mountains' extreme elevation?," *International Journal of Earth Sciences*, vol. 99, pp. 1511–1524, 2010.

[123] A. C. Adams, D. R. Stegman, S. E. Smrekar, and P. J. Tackley, "Regional-scale lithospheric recycling on Venus via peel-back delamination," *Journal of Geophysical Research: Planets*, vol. 127, 2022.

[124] S. E. Smrekar, T. Hoogenboom, E. R. Stofan, and P. Martin, "Gravity analysis of parga and hecate chasmata: Implications for rift and corona formation," *Journal of Geophysical Research: Planets*, vol. 115, 2010.

[125] D. T. Sandwell, C. L. Johnson, F. Bilotti, and J. Suppe, "Driving forces for limited tectonics on Venus," *Icarus*, pp. 232–244, 1997.

[126] L. S. Glaze, E. R. Stofan, S. E. Smrekar, and S. M. Baloga, "Insights into corona formation through statistical analyses," *Journal of Geophysical Research: Planets*, vol. 107, 2002.

[127] P. J. McGovern, M. E. Rumpf, and J. R. Zimbelman, "The influence of lithospheric flexure on magma ascent at large volcanoes on Venus," *Journal of Geophysical Research: Planets*, vol. 118, pp. 2423–2437, 2013.

[128] P. J. Tackley and D. J. Stevenson, "The production of small Venusian coronae by Rayleigh-Taylor instabilities in the uppermost mantle," *EOS Transactions*, vol. 72, pp. 287–287, 1991.

[129] A. J. Dombard, C. L. Johnson, M. A. Richards, and S. C. Solomon, "A magmatic loading model for coronae on venus," *Journal of Geophysical Research: Planets*, vol. 112, 2007.

[130] T. V. Gerya, "Plume-induced crustal convection: 3D thermomechanical model and implications for the origin of novae and coronae on Venus," *Earth and Planetary Science Letters*, vol. 391, pp. 183–192, 2014.

[131] D. M. Janes, "Geophysical models for the formation and evolution of coronae on Venus," *Journal of Geophysical Research*, vol. 97, 1992.

[132] D. M. Koch and M. Manga, "Neutrally buoyant diapirs: A model for Venus coronae," *Geophysical Research Letters*, vol. 23, pp. 225–228, 1996.

[133] D. Piskorz, L. T. Elkins-Tanton, and S. E. Smrekar, "Coronae formation on Venus via extension and lithospheric instability," *Journal of Geophysical Research: Planets*, vol. 119, pp. 2568–2582, 2014.

[134] S. W. Squyres, D. M. Janes, O. Baer, D. L. Bindschadler, G. Schubert, V. L. Sharpton, and E. R. Stofan, "The morphology and evolution of coronae on Venus," *Journal of Geophysical Research: Planets*, vol. 97, pp. 611–624, 1992.

[135] E. R. Stofan, D. L. Bindschadler, J. W. Head, and E. M. Parmentier, "Corona structures on Venus: models of origin," *Journal of Geophysical Research*, vol. 96, 1991.

[136] E. R. Stofan, V. L. Sharpton, G. Schubert, G. Baer, D. L. Bindschadler, D. M. Janes, and S. W. Squyres, "Global distribution and characteristics of coronae and related features on Venus: implications for origin and relation to mantle processes," *Journal of Geophysical Research*, vol. 97, 1992.

[137] F. Crameri, "Geodynamic diagnostics, scientific visualisation and staglab 3.0," *Geoscientific Model Development*, vol. 11, pp. 2541–2562, 2018.

[138] M. Thiriet, D. Breuer, C. Michaut, and A. C. Plesa, "Scaling laws of convection for cooling planets in a stagnant lid regime," *Physics of the Earth and Planetary Interiors*, vol. 286, pp. 138–153, 1 2019.

[139] M. B. Russell and C. L. Johnson, "Evidence for a locally thinned lithosphere associated with recent volcanism at aramaiti corona, Venus," *Journal of Geophysical Research: Planets*, vol. 126, 2021.

[140] V. L. Hansen, "Artemis: Surface expression of a deep mantle plume on venus," *GSA Bulletin*, vol. 7, pp. 839–848, 2002.

[141] J. E. Spencer, "Possible giant metamorphic core complex at the center of artemis corona, venus," *GSA Bulletin*, vol. 10, pp. 333–345, 2001.

[142] A. T. Basilevsky and J. W. Head, "The geologic history of venus: A stratigraphic view," *Journal of Geophysical Research: Planets*, vol. 103, pp. 8531–8544, 1998.

[143] R. C. Ghail, "Structure and evolution of southeast thetis regio," *Journal of Geophysical Research: Planets*, vol. 107, pp. 1–7, 2002.

[144] M. A. Ivanov and J. W. Head, "Global geological map of venus," *Planetary and Space Science*, vol. 59, pp. 1559–1600, 2011.

[145] L. Dupeyrat and C. Sotin, "The effect of the transformation of basalt to eclogite on the internal dynamics of Venus," *Planet. Space Sci*, vol. 43, pp. 909–921, 1995.

[146] J. S. Kargel, G. Komatsu, V. R. Baker, and R. G. Strom, "The volcanology of Venera and VEGA landing sites and the geochemistry of Venus," *Icarus*, vol. 103, pp. 253–275, 1993.

[147] Y. A. Surkov, V. L. Barsukov, L. P. Moskalyeva, V. P. Kharyukova, and A. L. Kemurdzhian, "New data on the composition, structure, and properties of Venus rock obtained by Venera 13 and Venera 14," *Journal of Geophysical Research*, vol. 89 Suppl, pp. 393–402, 1984.

[148] Y. A. Surkov, L. P. Moskalyova, V. P. Kharyukova, A. D. Dudin, G. G. Smirnov, and S. Y. Zaitseva, "Venus rock composition at the Vega 2 landing site," *Journal of Geophysical Research*, vol. 91, p. E215, 1986.

[149] J. Chen, H. Jiang, M. Tang, J. Hao, M. Tian, and X. Chu, "Venus' light slab hinders its development of planetary-scale subduction," *Nature Communications*, vol. 13, 2022.

[150] A. Regorda, C. Thieulot, I. V. Zelst, Z. Erdos, and S. Buiter, "Rifting Venus: Insights from numerical modeling," *JGR: Planets*, 2023.

[151] J. Schools and S. E. Smrekar, "High resolution numerical models of corona formation integrating magmatic processes, surface fracturing, and eclogitization," *Proceedings of the 54th Lunar and Planetary Science Conference*, 2023.

[152] A. C. Adams, "Plume-induced destabilization of rift zones on Venus," 2023.

[153] A. C. Adams, D. R. Stegman, H. Mohammadzadeh, S. E. Smrekar, and P. J. Tackley, "Plume-induced delamination initiated at rift zones on venus," *Journal of Geophysical Research: Planets*, vol. 128, 2023.

[154] F. Funiciello, M. Moroni, C. Piromallo, C. Faccenna, A. Cenedese, and H. A. Bui, "Mapping mantle flow during retreating subduction: Laboratory models analyzed by feature tracking," *Journal of Geophysical Research: Solid Earth*, vol. 111, 2006.

[155] V. Strak and W. P. Schellart, "Evolution of 3-d subduction-induced mantle flow around lateral slab edges in analogue models of free subduction analysed by stereoscopic particle image velocimetry technique," *Earth and Planetary Science Letters*, vol. 403, pp. 368–379, 2014.

[156] G. Morra and K. Regenauer-Lieb, "A coupled solid-fluid method for modelling subduction," *Philosophical Magazine*, vol. 86, pp. 3307–3323, 2006.

[157] W. P. Schellart, "Kinematics of subduction and subduction-induced flow in the upper mantle," *Journal of Geophysical Research: Solid Earth*, vol. 109, 2004.